REPORT DOCUMENTATION PAGE

Form Approved
OMB No. 0704-0188

1. AGENCY USE ONLY (Leave blank)	2. REPORT DATE	3. REPORT TYPE AND DATES COVERED
	September 23, 1996	Final Report 9/1/92 - 8/31/96

4. TITLE AND SUBTITLE

Mechanics of Localized Deformation of Solids
Under Cyclic and Thermal Loadings

5. FUNDING NUMBERS

Grant No.
F49620-92-J-0371

6. AUTHOR(S)

T. H. Lin

7. PERFORMING ORGANIZATION NAME(S) AND ADDRESS(ES)

Univ of California, Los Angeles
405 Hilgard Avenue
Los Angeles, CA 90024-1406

AFOSR-TR-97

0055

9. SPONSORING/MONITORING AGENCY NAME(S) AND ADDRESS(ES)

AFOSR/NA
Building 410, Bolling AFB DC
20332-6448

10. SPONSORING/MONITORING AGENCY REPORT NUMBER

F49620-92-J-0371

11. SUPPLEMENTARY NOTES

12a. DISTRIBUTION/AVAILABILITY STATEMENT

APPROVED FOR PUBLIC RELEASE; DISTRIBUTION IS UNLIMITED.

12b. DISTRIBUTION CODE

13. ABSTRACT *(Maximum 200 words)*

Since 1950's, many metallurgical researches on fatigue crack initiation were undertaken. Now, the difficulty is to see these multitudinous facts as a related and connected whole, largely because of the lack of a sound general theory. This present research is an attempt to develop such a general theory. It is essential in estimating (interpolating and extrapolating) fatigue lives under different design conditions. Fatigue failure has been observed at temperatures as low as 1.7°K. This indicates that although corrosion and diffusion may have important influence on but not necessary to fatigue failure. This leaves the local stress and strain to provide the basic mechanism of fatigue.

Based on the hint of intrusions and extrusions of fatigue specimens, a micromechanic theory of high-cycle fatigue crack initiation has been developed. This theory has been found to have extensive metallurgical verifications. This theory has been applied to study the interaction of multiple fatigue bands and the propagation of fatigue bands across the grain boundary. This propagation of fatigue bands has been found to depend greatly on the misorientation of the neighboring crystal. The effect of the elastic anisotropy of the component crystals of a polycrystal is analyzed.

14. SUBJECT TERMS

15. NUMBER OF PAGES
18

16. PRICE CODE

17. SECURITY CLASSIFICATION OF REPORT	18. SECURITY CLASSIFICATION OF THIS PAGE	19. SECURITY CLASSIFICATION OF ABSTRACT	20. LIMITATION OF ABSTRACT
UNCLASSIFIED	UNCLASSIFIED	UNCLASSIFIED	U

Final Technical Report

Mechanics of Localized Deformation of Solids under Cyclic Mechanical and Thermal Loadings

Grant No. F49620-92-J-0171
February 15, 1992 - June 30, 1996

Department of Civil & Environmental Engineering
School of Engineering and Applied Sciences
University of California, Los Angeles

Principal Investigator
T. H. Lin
Professor of Civil & Environmental Engineering

August, 1996

Outline

Abstract

Since 1950's, many metallurgical researches on fatigue crack initiation were undertaken. Now, the difficulty is to see these multitudinous facts as a related and connected whole, largely because of the lack of a sound general theory. This present research is an attempt to develop such a general theory. It is essential in estimating (interpolating and extrapolating) fatigue lives under different design conditions. Fatigue failure has been observed at temperatures as low as 1.7°K. this indicates that although corrosion and diffusion may have important influence on but not necessary to fatigue failure. This leaves the local stress and strain to provide the basic mechanism of fatigue.

Based on the hint of intrusions and extrusions of fatigue specimens, a micromechanic theory of high-cycle fatigue crack initiation has been developed. This theory has been found to have extensive metallurgical verifications. This theory has been applied to study the interaction of multiple fatigue bands and the propagation of fatigue bands across the grain boundary. This propagation of fatigue bands has been found to depend greatly on the misorientation of the neighboring crystal. The effect of the elastic anisotropy of the component crystals of a polycrystal is analyzed.

I. Introduction

Stresses in polycrystal under thermal or mechanical loadings are highly heterogeneous. These stresses causes localized plastic deformation, which often appears on the free surface as slip bands. These bands developed under monotonic loadings are known as shear band and those developed under cyclic loadings are known as fatigue bands. This analysis of slip bands, is applicable to those developed under both thermal and mechanical loadings.

In Section II, the mechanics of shear band formation is given. In Section III, the micromechanism of fatigue band is shown. This gives a physical model of high-cycle fatigue (HCF) crack initiation (Lin, 1992). The interaction of multiple fatigue bands in the most favorably oriented crystal at a free surface is shown in Section IV (Lin and Chen, 1989). Propagation of fatigue bands across grain boundaries is given in Section V. HCF crack initiation of intermetallic compounds is shown in Section VI. Anisotropy of elastic constants of crystal of aluminum and its alloys is small and was neglected. But this anisotropy of other metals like titanium and Ni_3Al intermetallic alloys are not small. Hence, the effect of this anisotropy on polycrystal fatigue bands is analyzed in Section VII.

II. Shear Band Formation

A long thin slice of metal of uniform rectangular cross-section is shown in Figure 1, embedded in an infinite isotropic elastic medium. The shear stress field τ_{12} caused by a uniform plastic shear strain e_{12}^p has been calculated (Lin, 1972, 1992).

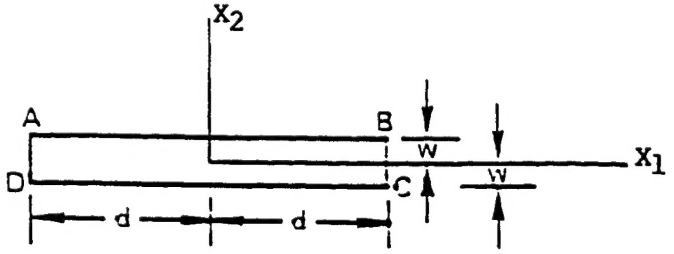

Figure 1
Thin slice cross-section.

and is given (with the subscript "12" dropped) as

$$\tau^r = \frac{2\mu e^p w}{\pi(1-\nu)}\left\{\frac{(x_1+d)\left[(x_2^2-w^2)-(x_1+d)^2\right]}{\left[(x_1+d)^2+(x_2-w)^2\right]\left[(x_1+d)^2+(x_2+w)^2\right]}\right.$$
$$\left. + \frac{(x_1-d)\left[(x_1-d)^2-(x_2^2-w^2)\right]}{\left[(x_1-d)^2+(x_2+w)^2\right]\left[(x_1-d)^2+(x_2-w)^2\right]}\right\} \tag{1}$$

Let $e^p w$ be kept constant, let e^p increase and let w decrease to zero, then

$$\tau^r = \frac{2\mu e^p w}{\pi(1-\nu)}\left\{\frac{(x_1-d)\left[(x_1-d)^2-x_2^2\right]}{\left[(x_1-d)^2+x_2^2\right]^2} - \frac{(x_1+d)\left[(x_1+d)^2-x_2^2\right]}{\left[(x_1+d)^2+x_2^2\right]^2}\right\} \tag{2}$$

The resolved shear stress due to the presence of an edge dislocation along the x_3-axis $(0,0,x_3)$ with a Burger's vector pointing in the x_1-direction, is given by Hirth and Lothe (1968) as

$$\tau^r = \frac{\mu b}{2\pi(1-\nu)}\frac{x_1(x_1^2-x_2^2)}{(x_1^2+x_2^2)^2} \tag{3}$$

Substituting $4e^p w$ in Eq. (1) by the magnitude of the Burger's vector b, it is seen that this resolved shear stress caused by the displacement of an edge dislocation of this Burger's vector from $(-d,0)$ to $(d,0)$ is exactly the same as given be Eq. (3). Hence, this plastic strain in this thin slice can be caused by the displacement of dislocations. This can also be interpreted as having a positive dislocation at $(d,0)$ and a negative one at $(-d,0)$.

Consider a most favorably oriented crystal located at a free surface of an aluminum polycrystal loaded in tension. All crystals are taken to have the same critical shear stress. The crystal with the highest resolved shear stress, known as the most favorably oriented crystal will first reach the critical shear stress and slides. Under uniaxial tension, this crystal has a slip direction α and a normal β to the slip plane making 45° with the loading axis. A small uniform initial resolved shear stress $\tau^i_{\alpha\beta}$ is assumed to exist in a thin slice, which will slide first. This slice is divided along the width into N-parallelogram grids S_n, $n = 1, 2, \ldots, N$, within each of which this plastic strain $e^p_{\alpha\beta_n}$ is taken to be uniform. From the condition that the resolved shear stress $\tau_{\alpha\beta}$ in each sliding grid equals the critical shear stress τ^c, the slip distribution in this slice has been determined (Lin, 1972, 1992). The polycrystal is of fine-grain and the equivalent force may be considered as acting in a semi-infinite solid. The thickness of the slice is much smaller than its

length. The plastic strain due to slip is assumed to be constant along the length, so the deformation caused by the equivalent forces are taken to be of plane strain. The plane stress solution of the stress field due to a point force applied in a semi-infinite plate has been given by Melan (Tung and Lin, 1966). His solution was modified by Tung and Lin (1966) for plane strain.

Using the plane strain solution, we calculate the average resolved shear stress $\tau_{\alpha\beta}$ in the m^{th} grid caused by a unit uniform plastic strain $e^p_{\alpha\beta_n}$ in the n^{th} grid. Denoting this average stress by G_{mn}, we can express the residual resolved shear stress $\tau^r_{\alpha\beta_m}$ in the m^{th} grid caused by plastic strain in all grids as

$$\tau^r_{\alpha\beta_m} = \sum_n G_{mn} e^p_{\alpha\beta_n}$$

where n is summed over all grids with plastic strain. The resolved shear stress and strain in this section refer to the $\alpha\beta$-slip system only, hence the subscripts $\alpha\beta$ are dropped, giving

$$\tau^r_m = \sum_n G_{mn} e^p_n \tag{4}$$

After plastic strain occurs, the total resolved shear stress is given by

$$\tau = \tau^i + \tau^r + \tau^a$$

where τ^a is the resolved shear stress caused by the applied load. For a grid to start or continue sliding, this total resolved shear stress must be equal to the critical shear stress

$$\tau = \tau^i + \tau^r + \tau^a = \tau^c \tag{5}$$

Writing this in incremental form,

$$\Delta\tau^r + \Delta\tau^a = \Delta\tau^c \tag{6}$$

Plastic deformation in metals is highly localized. The microscopic plastic strain in the thin slice is much larger than the macroscopic plastic strain in the metal. Hence, the strain hardening of the thin slice is much less than that of the metal and is neglected. This gives a constant critical resolved shear stress τ^c. Since the initial shear stress does not change with loading, with $\Delta\tau^c = 0$, we have in any sliding grid

$$\sum_n G_{mn}\Delta e_n^p + \Delta\tau_m^a = 0 \qquad (7)$$

This equation is applied to all grids with incremental plastic strain. We have as many equations as the unknowns. Thus the plastic strain in all grids were solved (Lin, 1972). Multiple slip bands have been observed in the most favorably oriented crystal at free surface. For numerical study, we consider ten slip bands spaced at 3 μm apart and with initial shear stress in different bands indicated in Figure 2. The polycrystal is taken to be of pure aluminum with a critical shear stress of 53.5 psi. The polycrystal is subject to a tension along x_2-direction. The calculated plastic strain distributions of the different bands at different applied loads τ_{22} are shown in Figure 3. This gives the occurrence of shear bands.

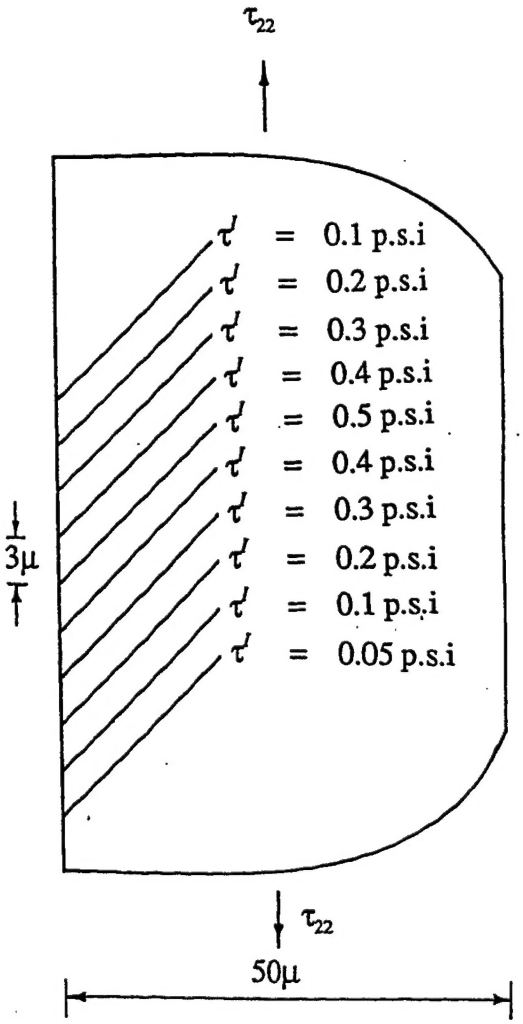

Figure 2
Most favorably oriented crystal with ten bands and initial stress.

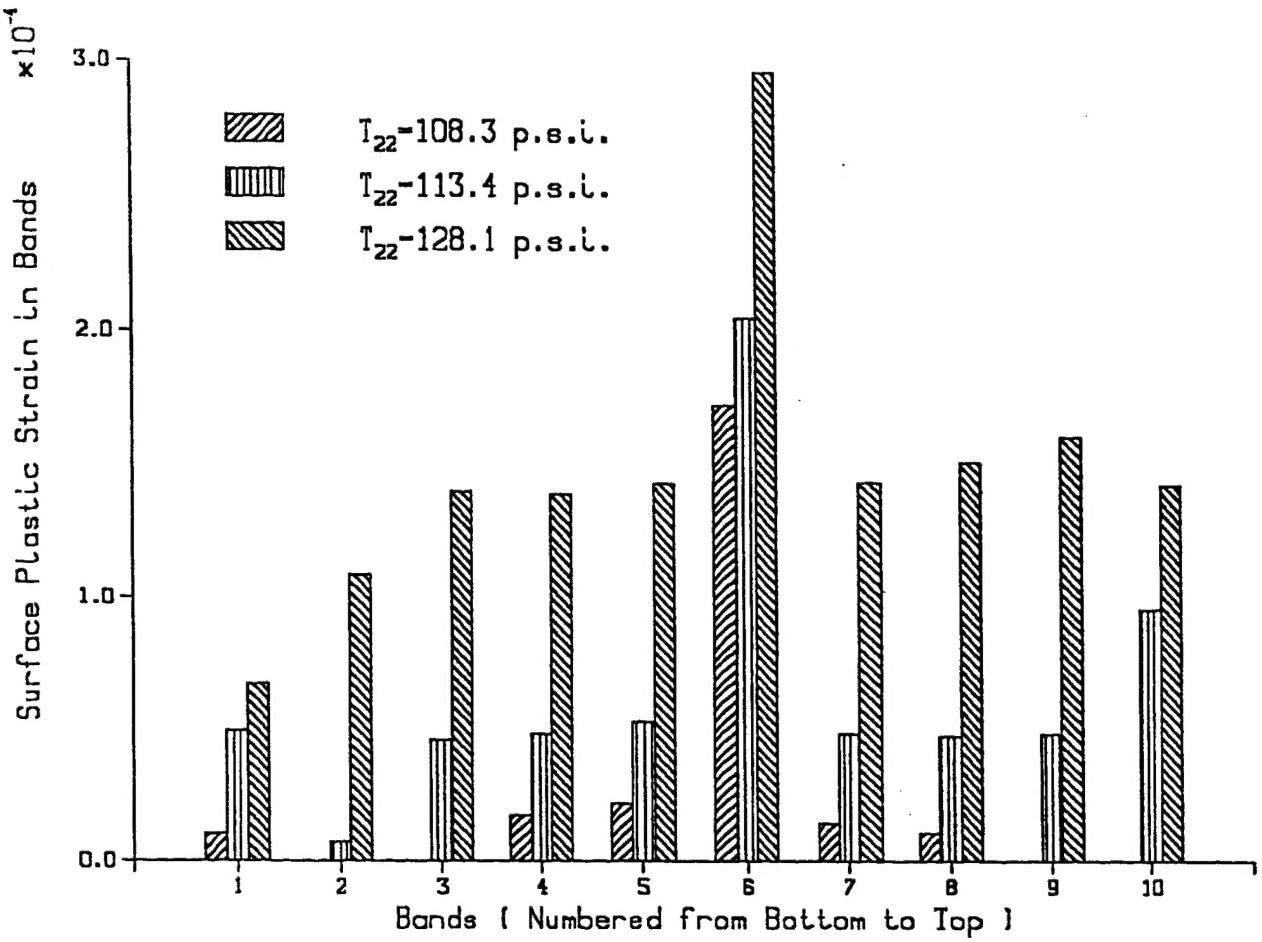

Figure 3
Surface plastic strains in different slip bands.

III. Fatigue Band Formation

More than 90% of all catastrophic failures of machines, vehicles, and other structures occurring in practice are caused by fatigue of materials. Fatigue failures occur under loadings substantially lower than the yield strength of the material. Fatigue cracks occur in two stages: crack initiation and crack propagation. Crack propagation predominates fatigue life in low-cycle fatigue, while crack initiation predominates the life in high-cycle fatigue and is also a necessary stage prior to crack propagation. Hence, fatigue crack initiation is of both scientific interest and practical importance.

MacCammon and Rosenberg (1957) and MacCrone *et al.* (1959) showed that metals are subject to failure at temperatures as low as 1.7°K. This indicates that although surface corrosion,

gas adsorption, gas diffusion into the metal, and vacancy diffusion to form voids can have an important effect on fatigue deformation, they are not necessary for fatigue failure. This seems to leave mechanics (i.e., the local stress and strain), as the basic mechanism of fatigue.

When a cyclic loading is applied to a metal, the individual grains begin to show fine slip markings after certain cycles. As loading continues, some of the lines intensify and become dark. These intense slip bands appear to be the source of fatigue cracks. If the surface of the fatigued metal is electro-polished, the fainter slip markings can be removed but not the darker bands. These are known as the persistent slip bands. The life of a specimen can be prolonged greatly by removing the surface layer periodically. A microscopic study of the development of cracks in copper by Thompson *et al.* (1956) verified the initiation of fatigue cracks in these bands.

(a) Intrusions and Extrusions

Forsyth and Stubbington (1955), and Hull (1958) found thin ribbons of metals extruded from the slip bands during fatigue loading. Extrusions of about 0.1 μm thick sometimes reached a height of 10 μm and varied in width from about 1 μm to a substantial fraction of the grain dimension. This formation of extrusions clearly are associated with shears of opposite signs on the opposite sides of an extrusion. The reverse of extrusion (i.e., intrusion) has also been observed. Both extrusions and intrusions grow monotonically in depth and width with cycles of loading. These observations are pertinent in developing the theory of fatigue crack initiation.

Fatigue cracks generally initiate at a free surface. We consider a thin slice of metal in a most favorably oriented crystal at a free surface of a polycrystal subject to a cyclic tension and compression. The slip plane and slip direction of this crystal form 45° with the specimen axis. We consider the loading to be of low amplitude. Then the plastic deformation mainly occurs in this most favorably oriented crystal.

(b) A Polycrystal Fatigue Crack Initiation Model

Most fatigue cracks initiate at a free surface. To relieve the same amount of resolved shear stress in a thin slice, a greater amount of slip (plastic shear strain) is required near the free surface than at the interior of metals (Lin and Ito, 1967). Hence, the thin slice subject to alternate forward and reversed loadings of this model is taken to be in the most favorably oriented crystal at a free surface of a polycrystal, as shown in Figure 4. This polycrystal is loaded in cyclic tension and compression of low amplitude. Plastic deformation occurring in this most favorably oriented

crystal in the polycrystal causes slip to occur in the most favorable slip system to form a persistent slip band.

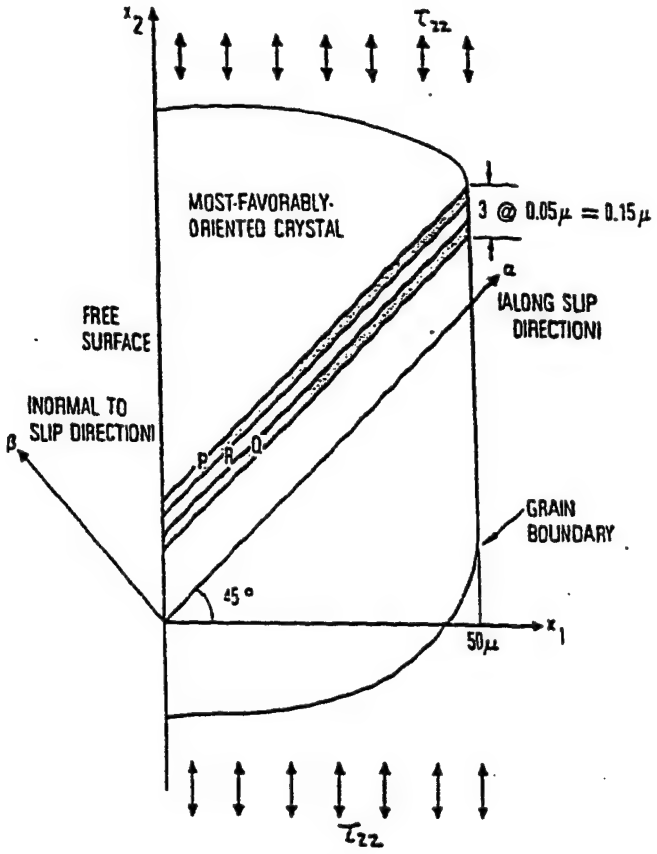

Figure 4
Most favorably oriented crystal at free surface.

The thickness of the slices P, Q, and R is much smaller than the length (dimension along x_3-axis). The plastic strain caused by slip is assumed to be constant along this length. Hence, the equivalent forces caused by this plastic strain are considered to act in a semi-infinite elastic medium under plane deformation.

(c) Initial Resolved Shear Stress

Initial defects always exist in metals and cause an initial stress field τ^i. During loading, when the resolved shear stress in some region reaches the critical shear stress τ^c, slip occurs. After unloading, this slip remains and induces a residual resolved shear stress τ^r. The resolved

shear stress caused by loading is denoted by τ^a. Hence, the total resolved shear stress is the sum of these three stresses.

$$\tau = \tau^i + \tau^r + \tau^a \tag{8}$$

For an extrusion to initiate, positive shear has to occur in a thin slice P and negative shear in a closely located slice Q (see Figure 4). The initial shear stress field τ^i favorable to this sequence of slip, clearly is one having positive shear stress in P and negative in Q. Such an initial stress field can be provided by an initial tensile strain $e^i_{\alpha\alpha}$ in R. (The repetition of Greek subscripts does not denote summation.) This positive $e^i_{\alpha\alpha}$ can be provided by a row of interstitial dislocation dipoles and a negative $e^i_{\alpha\alpha}$ by vacancy dipoles as suggested by Lin and Ito (1969a). Recently, Antonopoulos *et al.* (1967) and Mughrabi *et al.* (1983) have shown that the ladder structure in a persistent slip band (PSB) can be represented by an array of dislocation dipoles, causing initial resolved shear stresses at the interface between the PSB and the matrix.

(d) Gating Mechanism Provided by Microstresses

A tensile loading τ_{22} on the polycrystal (Figure 4) produces a positive τ^a in the whole crystal. Taking τ^i to be positive in P and negative in Q, we have $\tau^i + \tau^a$ in P reaching the critical shear stress τ^c first, and hence P slides. The plastic strain caused by slip is taken to be constant along x_3-axis, hence $\partial\tau_{\alpha 3}/\partial x_3 = 0$. The equilibrium condition with no body force, gives

$$\frac{\partial\tau_{\alpha\alpha}}{\partial\alpha} + \frac{\partial\tau_{\alpha\beta}}{\partial\beta} = 0 \tag{9}$$

Since $\partial\tau_{\alpha\alpha}/\partial\alpha$ is finite, $\partial\tau_{\alpha\beta}/\partial\beta$ must be also finite, and the changes in $\tau_{\alpha\beta}$ across the small distance between P and Q is very small. Therefore, the slip in P relieves not only the positive shear stress in P, but also in its neighboring region, including Q. The relief of positive shear stress is the same as the increase of negative resolved shear stress in Q to cause Q to slide more readily in the reverse loading. The negative slip in Q during the reverse loading relieves the negative shear stress not only in Q, but also in P, thus causing P more readily to slide in the next forward loading. This process is repeated for every cycle thus providing a gating mechanism for a monotonic buildup of local slip strain $e''_{\alpha\beta}$ in P and Q, pushing R out of the free surface and starts an extrusion. Interchanging the signs of the initial stresses in P and Q initiates an intrusion instead of an extrusion. This theory is extensively supported by metallurgical observations (Lin, 1977).

This gating mechanism was introduced by Lin and Ito (1969b) and was given in dislocation arrays by Tanaka and Mura (1981) and is also discussed in Suresh's *Fatigue of Materials* (1991).

(e) Activation of Second Slip System

The buildup of this local slip strain $e''_{\alpha\beta}$ in P and Q is caused by the positive and negative initial shear stress $\tau^i_{\alpha\beta}$ which, in turn, is caused by $e^i_{\alpha\alpha}$ in R. If R were cut out, this free length of R would be longer than the slot cut, by an amount referred to as the "static extrusion" (Antonopoulos *et al.*, 1967; Mughrabi *et al.*, 1983). This $e^i_{\alpha\alpha}$ causes an initial compression $\tau^i_{\alpha\alpha}$ in R. As the extrusion grows under cyclic loading, the slice R increases in length. This elongation causes the compression to decrease. A question has been raised as to whether the extrusion growth will cease after extrusion has reached the static extrusion. For aluminum and its alloys, the residual tensile stress $\tau^r_{\alpha\alpha}$ caused by elongation in R due to extrusion can cause changes of resolved shear stresses in all 12 slip systems of the face-centered cubic crystal. The resolved shear stress in one slip system may reach the critical shear stress and slide. The plastic strain $e''_{\xi\eta}$ caused by slip in this system has a tensor component $e''_{\alpha\alpha}$ just like $e^i_{\alpha\alpha}$ in causing the positive and negative $\tau^i_{\alpha\beta}$, respectively, in P and Q. This secondary slip has been shown by Lin *et al.* (1989) to increase greatly the extent of extrusion and intrusion. This $e''_{\xi\eta}$ causes equivalent forces $\bar{F}_3$ in addition to $\bar{F}_1$ and $\bar{F}_2$. With $\bar{F}_3$, the strains in the slices are no longer of plane strain and hence are taken to be of generalized plane strain; i.e.,

$$u_i = u_i(x_1, x_2) \qquad i = 1,2,3 \tag{10}$$

The solution of a similar problem was shown in the analysis of prismatic anisotropic bars by Lekhnitski (1963). The stress-strain relation gives

$$\tau_{ij} = 2\mu\left[\frac{\nu}{1-\nu}\delta_{ij}\theta + \frac{1}{2}\left(\frac{\partial u_i}{\partial x_j} + \frac{\partial u_j}{\partial x_i}\right)\right] \tag{11}$$

where

$$\theta = \frac{\partial u_1}{\partial x_1} + \frac{\partial u_2}{\partial x_2}$$

and ν is the Poisson's ratio. Substitution of the expression into the conditions of equilibrium yields

$$\nabla^2 u_i + \frac{1}{1-2\nu}\frac{\partial \theta}{\partial x_i} + \frac{F_i}{\mu} = 0, \qquad i = 1,2 \tag{12}$$

and

$$\nabla^2 u_3 + \frac{F_3}{\mu} = 0 \tag{13}$$

where

$$\nabla^2 = \frac{\partial^2}{\partial x_1^2} + \frac{\partial^2}{\partial x_2^2}$$

and F_i and F_3 can be either the applied forces or the equivalent forces.

Equations (12) and (13) are not coupled and can be solved separately. Lin and Lin (1983) have shown the solution of this stress field caused by F_i in Eq. (12) by using Airy's stress functions. An initial shear stress field in three thin slices P, Q, and R in Figure 1 caused by $e^i_{\alpha\alpha}$ varying linearly from zero at the free surface to a maximum at the interior boundary in the outer two slices, P and Q, and by an $e^i_{\alpha\alpha}$ of opposite sign and of double magnitude in the center slice R was numerically calculated by Lin and Lin (1983). These calculated initial shear stresses were found to be uniform in the two outer slices, one is positive and the other is negative. The regions outside of these two slices have a negligible small amount of resolve shear stresses. This initial stress field so derived from an initial strain clearly is favorable to the initiation of extrusion and satisfies both the equilibrium and compatibility conditions. This shows that initial resolved shear stresses in P and Q can be provided by an initial strain $e^i_{\alpha\alpha}$ and satisfy equilibrium conditions (Lin and Lin, 1983). To solve Eq. (13) for F_3, we write $\Phi_3(x,\bar{x})$ as $\mu u_3(x,\bar{x})$. $u_3(x,\bar{x})$ represents the displacement u_3 at point x due to force applied at $\bar{x}$. The stress is then

$$\tau_{13}(x,\bar{x}) = \frac{\partial \Phi_3}{\partial x_1}, \qquad \tau_{23}(x,\bar{x}) = \frac{\partial \Phi_3}{\partial x_2} \tag{14}$$

For a unit concentrated force F_3 at $\bar{x}$, Eq. (13) gives

$$\nabla^3 \Phi_3 + \delta(x-\bar{x}) = 0 \tag{15}$$

where $\delta(x-\bar{x})$ is the Dirac Delta function. With the boundary conditions of

$$\frac{\partial \Phi_3}{\partial x_1} = 0 \text{ at } x_1 = 0 \quad \text{and} \quad \frac{\partial \Phi_3}{\partial x_2} \to 0 \text{ as } \sqrt{x_1^2 + x_2^2} \to \infty$$

we have

$$\Phi_3(x, \bar{x}) = -\frac{1}{4\pi}(\ln X_1 + \ln X_2) \tag{16}$$

where

$$X_1 = (x_1 - \bar{x}_1)^2 + (x_2 - \bar{x}_2)^2$$
$$X_2 = (x_1 + \bar{x}_1)^2 + (x_2 - \bar{x}_2)^2$$

Hence the stress fields caused by the equivalent forces due to slip strain can be readily be calculated. This micromechanic theory of high-cycle fatigue crack initiation has extensive metallurgical verifications (Lin, 1992).

IV. Interaction of Multiple Fatigue Bands

In the early stages of high-cycle fatigue, the fatigue bands are widely spaced as light slip markings (Kennedy, 1963) in the most favorably oriented crystal at a free surface of a polycrystal. The interaction of these bands is small, so the slip distributions in the band can be analyzed as a single fatigue band in the crystal. As the fatigue loading proceeds, more slip lines appear and the interaction of neighboring fatigue bands in the crystal needs to be considered. Since the crystals surrounding this most favorable one are less favorably oriented, these multiple fatigue bands can occur in this most favorable crystal, while no fatigue band in the surrounding crystals.

One case of the interaction of slip bands in HCF crack initiation was analyzed by Lin and Chen (1989). These bands were assumed to exist in a most favorably oriented crystal at a free surface of a polycrystal. Each band is taken to consist of 3 thin slices P, Q, and R as shown in Figure 4. P and Q in each band are assumed to have equal and opposite initial resolved shear stresses. These initial stresses are different in different bands. Plastic strain distributions in these bands under cyclic loadings were calculated. The maximum shear strain at the free surface is an indication of extrusion height and/or intrusion depth, which is taken as a measure of crack initiation. This indicates the level of fatigue damage. The applied cyclic shear stress versus the number of cycles to yield different amount of surface shear strains were calculated. The shape of these curves is similar to that of Wöhler's diagrams and that of Coffin-Mansan equation. The results seem to give good physical explanations to these diagrams and equations.

V. Propagation of Fatigue Bands across Grain Boundaries

Grain boundaries are only few atomic spacings. These boundaries are assumed to have zero thickness. Fatigue fracture of a polycrystal is either transgranular or intergranular. This mode of fracture affects the ductility of the metal. It is expected that the propagation of fatigue band across the grain boundary more likely yields transgranular crack initiation and the stopping of the propagation at the grain boundary tends to cause an intergranular crack. A single fatigue band in the most favorably oriented crystal at a free surface of a polycrystal has been analyzed. The dimensions of this fatigue band in surface crystal and its neighboring crystal is shown in Figure 5. This polycrystal is a pure aluminum with a critical shear stress of 53.3 psi. An initial shear stress τ^i of 0.5 psi in P and Q was assumed. The polycrystal was subjected to a cyclic tension and compression of 107.7 psi.

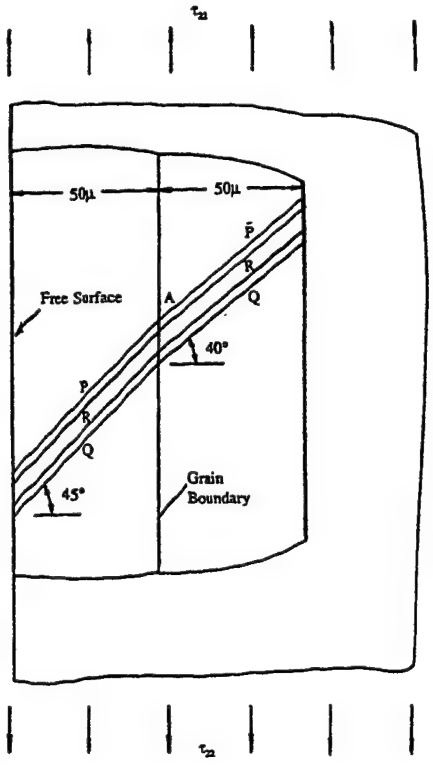

Figure 5
Fatigue band across the grain boundary.

The slip directions and slip planes of a f.c.c. crystal are shown in Figure 6. Let a_2 correspond to the $\alpha\beta$ slip system in Figure 4, which is referred to as the primary slip system. The

extrusion growth causes the tensile stress $\tau_{\alpha\alpha}$ in R. There are four slip system c_1, c_3, d_1, and d_2 equally favorable under $\tau_{\alpha\alpha}$. Of these four, c_3 is most favorable under τ_{22}, and hence will be activated next and is referred to as the second active slip system (Lin, 1992). The calculated plastic strain distribution of the primary slip system versus the distance from the free surface at different cycles of loading are shown in Figure 7. The plastic strain distributions of the second slip system, c_3, in R are shown in Figure 8. The surface plastic strain approaches a saturated value at about 650 cycles. It is seen that very little second slip in the neighboring crystal. This propagation mainly depends on the difference of orientation of the two crystals.

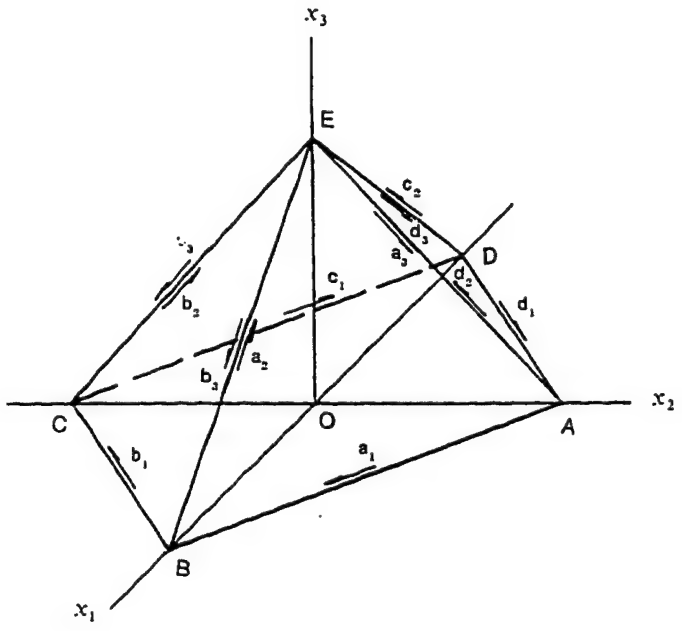

Figure 6
Crystallographic directions of a f.c.c. crystal.

Multiple fatigue bands have been observed on the surface crystal. As the magnitude of the alternate loading increases, those crystals surrounding the surface crystal will also plastically deform and give residual stress fields, which will interact with fatigue bands of the surface crystal. The resultant slip distributions in these bands have been analyzed by Lin and Chen (1989).

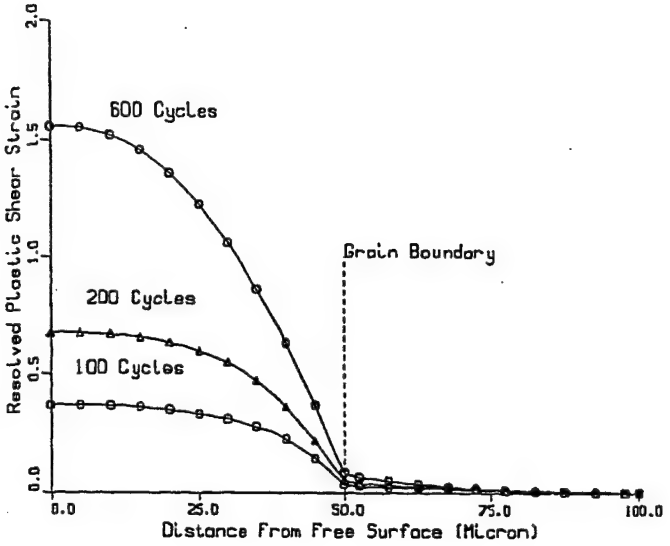

Figure 7
Plastic strain distribution of the primary slip system in P.

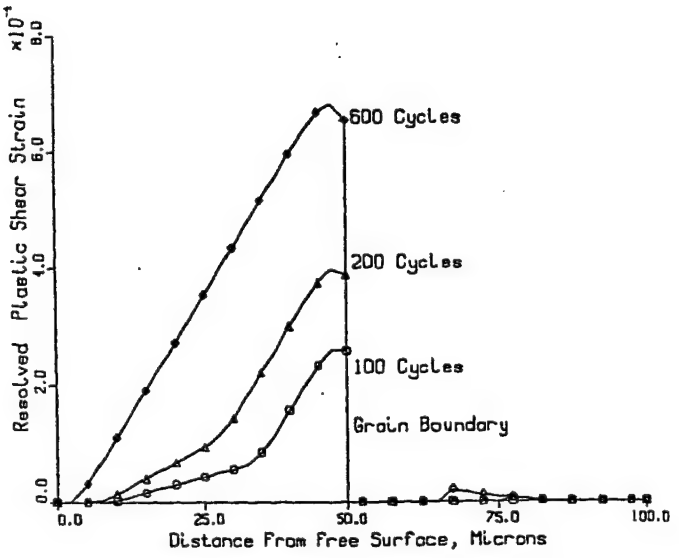

Figure 8
Plastic strain distribution of the second slip system in R.

VI. HCF Crack Initiation of Intermetallic Compounds

Ordered intermetallic compounds favor planar slip and tend to have no cross-slip or multiple slip. This is due to the long Burger's vector of these intermetallics. Test results show that long-rang order in intermetallic compounds substantially increase their fatigue lives in stress-controlled cycling but decreases in the strain-controlled fatigue resistance. Stoloff *et al.* (1986) indicated that the least understood aspects of the cyclic behavior of intermetallic compounds are the processes leading to crack initiation. Using the inhibition of cross or multiple slip in the ordered compounds, the present micromechanic model has been found to satisfactorily explain the cyclic behavior of the intermetallic compounds (Lin and Chen, 1992, 1993).

VII. Effect of Crystal Elastic Anisotropy on Polycrystal Fatigue Band

Previous studies on fatigue bands were for aluminum and its alloys. The anisotropy of their elastic constants is small and accordingly neglected. However, this anisotropy of other metals such as titanium and some intermetallic alloys is not small. Hence, in this section, anisotropy is here analyzed.

In an earlier study, the anisotropy of the most favorably oriented crystal at a free surface is considered. The metal exterior to the surface is assumed to be elastically isotropic and homogeneous. Thus, it is reduced to an inclusion problem. This heterogeneous solid is transformed into a homogeneous one by using Eshelby's Equivalent Inclusion Method (Eshelby, 1957, 1961, Mura, 1982). In this method, an extra set of eigenstrains, which behave the same as the inelastic strains, is introduced. The eigenstrains explicitly depend on the applied stresses and plastic strains and thus can be implicitly incorporated in the formulation of solutions. The surface crystal is assumed to have the anisotropic elastic constants of Ni_3Al monocrystalline intermetallic compound (Yang, 1985). The surrounding crystals are assumed to have isotropic elastic constants. The plastic strain distributions and the cumulative surface plastic strain in the fatigue band versus the number of loading cycles are calculated, and the effect of elastic anisotropy on the formation of extrusions and intrusions is shown. The details of the analysis are shown in the paper published in AMD-Vol. 204, *Numerical Methods in Structural Mechanics, ASME*, 1995. A copy of this paper is given in the appendix.

In the above study, the crystals surrounding the surface crystal were assumed to be isotropic. In a later refined study, the orientations of the surrounding crystal were considered. This introduces different anisotropic elastic constants to different crystal referring to the specimen axes. This model is more realistic. The plastic shear strain distribution in the fatigue bands were calculated. This cumulative surface plastic shear strains versus the number of loading cycles for the case with the consideration of crystal anisotropy and for the case without, were calculated and shown. It is shown that the neglect of this crystal anisotropy may cause significant error in calculating the slip distribution and in estimating the fatigue crack initiation. The analysis is published in the *Journal of Engineering Materials and Technology* (Teng and Lin, 1995). A copy of the paper is given in the appendix.

VIII. References

Antonopoulos J.G., Brown L.M., and Winter A.T. (1967), "Vacancy Dipoles in Fatigued Copper", *Phil. Mag.*, Vol. 34, p. 549.

Eshelby J.D. (1957), "The Dtermination of the Elastic Field of an Ellipsoidal Inclusion and Related Problems", *Proc. Roy. Soc. A*, Vol. 241, pp. 376-396.

Eshelby J.D. (1961), "Elastic Inclusions and Inhomogeneities", *Progress in Solid Mechanics*, Vol. II, edited by I.N. Sneddon and R. Hill, North Holland Rublishing Company, pp. 89-139.

Forsyth P.J.E. and Stubbington C.A. (1955), "The Slip Band Extrusion Effect Observed in some Aluminum Alloys Subjected to Cyclic Stresses", *J. Inst. Metals*, Vol. 83, p. 395.

Hirth J.P. and Lothe J. (1968), *Theory of Dislocations*, MaCraw-Hill.

Hull D. (1958), "Surface Structure of Slip Bands on Copper Fatigued at 293°, 90°, 4.2°K", *J. Inst. Metals*, Vol. 86, p. 425.

Kennedy A.J. (1963), Process of Creep and Fatigue of Metals, *John Wiley & Sons, Inc.*, pp. 2, 331-343.

Lekhnitski S.G. (1963), *Theory of Elasticity of an Anisotropic Body*, Holden-Day, San Francisco, pp. 129-134.

Lin S.R. and Lin T.H. (1983), "Initial Strain Field and Fatigue Crack Initiation Mechanics", *J. Appl. Mech.*, Vol. 50, pp. 367-372.

Lin T.H. and Ito Y.M. (1967), "Slip Distribution in Thin Slice of a Crystal at a Free Surface", *J. Appl. Phys.*, Vol. 3, pp. 775-780.

Lin T.H. and Ito Y.M. (1969a), "Fatigue Crack Nucleation in Metals", *Proc. U.S. Natl. Acad. Sci.*, Vol. 64, pp. 631-635.

Lin T.H. and Ito Y.M. (1969b), "Micromechanics of Fatigue Crack Nucleation Mechanism", *J. Mech. Phys. Solid*, Vol. 17, pp. 511-523.

Lin T.H. (1972), "Microstress Fields of Slip Bands and the Inhomogeneity of Plastic Deformation of Metals", *Proc. International Symposium of Foundations of Plasticity*.

Lin T.H. (1977), "Micromechanics of Deformation of Slip Bands Under Monotonic and Cyclic Loadings", *Reviews of the Deformation Behavior of Materials*, edited by P. Felham, Freund Publishing House, Tel-Aviv, Israel, pp. 317-351.

Lin T.H., Lin S.R., and Wu X.Q. (1989), "Micromechanics of an Extrusion in High-Cycle Fatigue", *Phil. Mag. A*, Vol. 59, pp. 1263-1276.

Lin T.H. and Chen Q.Y. (1989), "Interaction of Slip Bands in High-Cycle Fatigue Crack Initiation", *Micromechanics and Inhomogeneity, The Toshio Mura Anniversary Volume*, Springer Verlag, pp. 231-241.

Lin T.H. (1992), "Micromechanics of Crack Initiation in High-Cycle Fatigue", *Advances in Applied Mechanics*, Vol. 29, pp. 1-68.

Lin T.H. and Chen Q.Y. (1993), "Micromechanics of Stress and Strain-Controlled, High-Cycle Fatigue Crack Initiation of Intermetallic Compounds", *Mat. Sci. & Eng.*, A170, pp. 103-110.

Teng N.J., Lin T.H., and Wong K.F. (1995), "Effect of Elastic Anisotropy on Fatigue Band in Polycrystalline Solids", AMD-Vol. 204, *Numerical Methods in Structural Mechanics, ASME*, pp. 151-160.

Teng N.J. and Lin T.H. (1995), "Elastic Anisotropy Effect of Crystals on Polycrystal Fatigue Crack Initiation", *J. Eng. Materials and Technology, Trans. ASME*, pp. 470-477.

Tung T.K. and Lin T.H. (1966), "Slip Strains and Stress in Polycrystalline Aggregate under Cyclic Load", *J. Appl. Mech.*, Vol. 33, pp. 363-370.

McCammon R.D. and Rosenberg H.M. (1957), "The Fatigue and Ultimate Tensile Strengths of Metals between 4.2° and 293°K", *Proc. Roy. Soc. A*, Vol. 242, pp. 203-211.

MacCrone R.K., McCammon R.D., and Rosenberg H.M. (1959), "The Fatigue of Metal at 1.7°K", *Phil. Mag.*, Vol. 4, pp. 267-272.

Mughrabi H., Wang R., Differt K., and Essmann U. (1983), "Fatigue Crack Initiation by Cyclic Slip Irreversibilities in High-Cycle Fatigue", *Fatigue Mechanism*, ASTM-STP-811, pp. 5-45.

Mura T. (1982), "Micromechanics of Defects in Solids", *Martinus Nijhoff Publishers*, pp. 1-6, 151-159.

Stoloff N.S., Fuchs G.E., Kuruvilla K.A., and Choe S.J. (1986), "Fatigue of Intermetallic Compounds", *High-Temperature Ordered Intermetallic Alloys II*, edited by N.S. Stoloff, C.C. Koch, C.T. Liu, and O. Izumi, Materials Research Society, Vol. 81, p. 247.

Suresh S. (1991) "Fatigue of Materials", *Cambridge University Press*, Chapter 3, p. 119.

Tanaka K. and Mura T. (1981), "A Dislocation Model for Fatigue Crack Initiation", *J. Appl. Mech.*, Vol. 48, pp. 97-102.

Thompson N., Wadsworth N., and Louas N. (1956), "The Origin of Fatigue Fracture in Copper", *Phil. Mag.*, Vol. 1, pp. 113-126.

Yang S.W. (1985), "Elastic Constants of a Monocrystalline Nickel-Base Superalloy", *Mectalurgical Transactions A*, Vol. 16A, pp. 661-665.

IX. Appendix: Reprints

1. Lin T.H. and Chen Q.Y., "Micromechanics of High-Cycle Initiation of Fatigue Cracking Intermetallic Compounds", *ACTA Metall. Mater.*, Vol. 40, No. 12, pp. 3255-3263, 1992.
2. Lin T.H. and Chen Q.Y., "Micromechanics of Stress and Strain-Controlled, High-Cycle Fatigue Crack Initiation of Intermetallic Compounds", *Mat. Sci. & Eng.*, A170, pp. 103-110, 1993.
3. Chen Q.Y. and Lin T.H., "High-Cycle Fatigue Crack Initiation of Intermetallic Compounds", *Proc. 5th Int. Conf. on Fatigue and Fatigue Thresholds*, 5/3-7/93, pp. 1043-1050, 1993.
4. Teng N.J., Lin T.H., and Wong K.F., "Effect of Elastic Anisotropy on Fatigue Band in Polycrystalline Solids", *AMD-Vol. 204, Numerical Methods in Structural Mechanics, ASME*, pp. 151-160, 1995.
5. Teng N.J. and Lin T.H., "Elastic Anisotropy Effect of Crystals on Polycrystal Fatigue Crack Initiation", *J. Eng. Materials and Technology, Trans. ASME*, pp. 470-477, 1995.

Acta metall. mater. Vol. 40, No. 12, pp. 3255–3263, 1992
Printed in Great Britain.

0956-7151/92 $5.00 + 0.00

MICROMECHANICS OF HIGH-CYCLE INITIATION OF FATIGUE CRACKING INTERMETALLIC COMPOUNDS

T. H. LIN and Q. Y. CHEN

Department of Civil Engineering, University of California, Los Angeles, CA 90024, U.S.A.

(Received 2 December 1991; in revised form 8 June 1992)

Abstract—Tests have shown that ordered intermetallic compounds favor planar slip and tend to have no cross-slip or multi-slip. This was explained by the long Burger's vector in these ordered compounds. The flow stress of the ordered has been found to be less than that of the disordered ones. However the high-cycle fatigue life of the ordered was found to be significantly more than that of the disordered. This is believed to be due to low rate of crack initiation. Cracks have been found to initiate exclusively at slip bands extrusions and intrusions in intermetallic compounds. This paper shows a micromechanic fatigue model. This model was used to calculate the extrusion growth of a single fatigue band and then multiple fatigue bands in the most favorably oriented crystal. It was found that extrusion growth in the ordered alloy is significantly less than that in the disordered ones. The S–N curves to give given plastic shear strains of the extrusion at the free surface were calculated for both the ordered and disordered alloys. It was found that the ordered alloy has significantly higher S–N curves as observed in experiments.

Résumé—Des essais montrent que les composés intermétalliques ordonnés favorisent un glissement plan et tendent à ne pas opérer de glissements déviés simple ou multiple. Ceci s'explique par le long vecteur de Burgers des ces composés ordonnés. On trouve que la contrainte d'écoulement plastique des matériaux ordonnés est inférieure à celle des matériaux désordonnés. Cependent, on trouve que la durée de vie en cyclage à fréquence élevée des matériaux ordonnés est beaucoup plus grande que celle des matériaux déordonnés. On pense que ceci est dû à la faible vitesse d'initiation des fissures. On trouve, dans les composés intermétalliques, que les fissures commencent exclusivement aux extrusions et intrusions des bandes de glissement. Cet article donne un modèle de fatigue micromécanique. Ce modèle est utilisé pour calculer la croissance de l'extrusion d'une bande unique de fatigue, puis de bandes multiples dans un cristal orienté de la manière la plus favorable. On trouve que la croissance d'une extrusion dans un alliage ordonné est beaucoup moins importante que dans des alliages désordonnés. Les courbes S–N, destinées à donner des déformations plastiques donnees par cisaillement de l'extrusion sur la surface libre sont calculées à la fois pour des alliages ordonné et désordonné. On trouve que l'alliage ordonné à des courbes S–N beaucoup plus hautes que celles que l'on observe expérimentalement.

Zusammenfassung—Versuche haben gezeigt, daß geordnete intermetallische Verbindungen ebene Gleitung bevorzugen, also Quergleitung und Vielfachgleitung vermeiden. Dieses Verhalten wird mit dem langen Burgersvektor erklärt. Die Fließspannung der geordneten Legierungen ist kleiner als die der entordneten. Allerdings ist die Ermüdungslebensdauer der geordneten Legierungen beträchtlich größer als die der entordneten. Das wird einer niedrigen Rißbildungsrate zugeschrieben. Die Risse entstehen ausschließlich an Gleitbandextrusionen und -intrusionen. Diese Arbeit baut ein mikromechanisches Ermüdungsmodell auf. Mit diesem Modell wird das Extrusionswachstum eines einzelnen Ermüdungsbandes und dann vieler Ermüdungsbänder in den am günstigsten orientierten Körnern berechnet. Es ergibt sich, daß das Extrusionswachstum in den geordneten Legierungen bedeutend geringer ist als in den entordneten. Die S–N-Kurven, welche die plastischen Scherungen der Extrusionen an der freien Oberfläche angeben, werden für geordnete und ungeordnete Legierungen berechnet. Das Ergebnis ist, daß die geordnete Legierung beträchtlich höhere S–N-Kurven aufweist als gemessen im Experiment.

1. INTRODUCTION

The ordered structure of intermetallic compounds gives a dislocation Burgers vector quite long compared to that of disordered alloys. The dislocation with this long Burger's vector is known as a superdislocation. In a f.c.c. material, the Burger's vector is $\frac{1}{2}[110]$, while in an ordered intermetallic compounds such as Ni_3Al, the Burger's vector is [110]. The increased length of the Burger's vector in intermetallic compounds favors planar slip and tends to inhibit cross-slip and/or multiple slip.

Fatigue tests of FeCo–V show that slip along (110) occurs for both ordered and disordered alloy samples. Cracks initiated almost exclusively at slip bands, intrusions and extrusions. Tests carried out in high vacuum (5×10^{-7} torr) also have shown that slip bands are preferred sites for crack initiation and propagation for both ordered and disordered conditions. Similar tests on Ni_3Al show the development of extrusions and intrusions into cracks. Hence the height of the extrusion or the depth of the intrusion is here taken as a measure of fatigue damage.

This influence of long range order on stress-controlled high cycle fatigue tested at 25°C was first reported for Ni_3Mn and FeCo–V. In both cases high-cycle fatigue lives were substantially increased, in spite of a decrease in yield stress with order for FeCo–V [2, 3]. Later, high cycle fatigue tests were extended to $FeNi_3$–V polycrystals, Ni_3Al single crystals etc. [4]. In both cases, fatigue lives were substantially increased in spite of a decrease in flow stress with order for FeCo–V. It was found that the ratio of the fatigue limit to yield strength exceeds 0.5 for most of the ordered alloys, while in the disordered condition, the ratio decreases significantly, [5]. Since crack propagation is much more rapid in ordered conditions as indicated by Stoloff *et al.* [5] it has been concluded that ordering substantially delays crack initiation while not changing the location of the earliest crack [5]. They further indicated that the least understood aspects of cyclic behavior of intermetallic compounds are the processes leading to crack initiation. The present paper is an attempt to give the mechanism of high-cycle fatigue crack initiation of some long range ordered intermetallic compounds. The present study analyzes the micro stress and strain fields of the fatigue bands. These stress and strain fields show analytically the long range order effect on fatigue crack initiation. This analysis is not for low cycle fatigue. As indicated by Stoloff *et al.* [5], there is no evidence that ordering is beneficial under strain-controlled low cycle fatigue conditions.

Flow stress of many intermetallic alloys increase with quenched temperature to a peak temperature [2]. Octahedral slip was found to be predominant at temperatures below the peak temperature, while primary cube slip is prevalent above the peak temperature [4]. The present calculated results are to be compared to the test results conducted at 25°C, hence octahedral slip is considered. In the present analysis, the intermetallic compounds are assumed to follow Schmids law.

2. A POLYCRYSTAL FATIGUE MODEL

Extrusions and intrusions in fatigue specimens were first discovered by Forsyth and Stubbington [6] and later found by a number of other physicists and material scientists. These extrusions and intrusions are favourable sites for fatigue cracks. Following the clue provided by the observation on extrusion and intrusions, a number of theories of fatigue crack initiation were proposed by different investigators [7]. One theory considered a column of metal containing a single screw dislocation traveling a complete circuit and the volume contained in the circuit is translated parallel to the dislocation. this causes the metal to extrude. This mechanism does not explain why the dislocation under cyclic stressing, does not oscillate back and forth along the same path rather than traversing a closed circuit. Drawbacks of this and other theories are discussed by Kennedy [7]. Clearly,

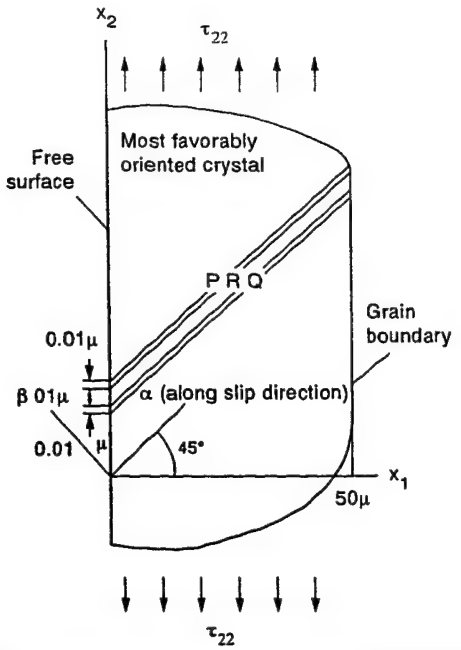

Fig. 1. Most favorably oriented crystal at free surface.

some gating mechanism is needed to convert the back and forth oscillation of the dislocation into a unidirectional circuit.

Most fatigue cracks initiate at a free surface. To relieve the same amount of resolved shear stress in a thin slice, a greater amount of slip (plastic shear strain) is required near the free surface than at the interior of metals [8]. Hence, the thin slice subject to alternate forward and reversed loadings of this model is taken to be in the most favorably oriented crystal at a free surface of a polycrystal, as shown in Fig. 1. This polycrystal is loaded in cyclic tension and compression of low amplitude and plastic deformation essentially occurs only in the most favourably oriented crystal. Figure 1 corresponds to a persistent slip band, which was formed after slip had occurred in the most favourable slip system in the whole crystal.

(a) Initial resolved shear stress

Initial defects always exist in metals and cause an initial stress field τ^i. During loading, when the resolved shear stress in some region reaches the critical shear stress τ^c, slip occurs. After unloading, this slip remains and induces a residual resolved shear stress τ^r. The resolved shear stress caused by loading is denoted by τ^a. Hence the total resolved shear stress is the sum of these three stresses

$$\tau = \tau^i + \tau^r + \tau^a. \tag{1}$$

For an extrusion to initiate, positive shear has to occur in a thin slice P and negative shear in a closely located slice Q (Fig. 1). The initial shear stress field τ^i favorable to this sequence of slip, clearly is one having positive shear stress in P and negative in Q. Such an initial stress field can be provided by an initial tensile strain $e^i_{\alpha\alpha}$ in R. (The repetition of

Greek superscripts does not denote summation.) This positive $e^{i}_{\alpha\alpha}$ can be provided by a row of interstitial dislocation dipoles and a negative $e^{i}_{\alpha\alpha}$ by vacancy dipoles as suggested by Lin and Ito [10]. Recently, Antonopoulos *et al.* [11] and Mughrabi *et al.* [12] have shown that the ladder structure in a persistent slip band (PSB) can be represented by an array of dislocation dipoles, causing initial resolved shear stresses at the interface between the PSB and the matrix.

(b) Gating mechanism

A tensile loading τ_{22} on the polycrystal (Fig. 1) produces a positive τ^{a} in the whole crystal. Taking τ^{i} to be positive in P and negative in Q, we have $\tau^{i}+\tau^{a}$ in P reaching the critical shear stress τ^{c} first; and hence, P slides. The plastic strain caused by slip is taken to be constant along x_3-axis, hence $\partial\tau_{\alpha 3}/\partial x_3 = 0$. The equilibrium condition with no body force, gives

$$\frac{\partial\tau_{\alpha\alpha}}{\partial\alpha}+\frac{\partial\tau_{\alpha\beta}}{\partial\beta}=0.$$

Since $\partial\tau_{\alpha\alpha}/\partial\alpha$ is finite, $\partial\tau_{\alpha\beta}/\partial\beta$ must be also finite, and the change in $\tau_{\alpha\beta}$ across the small distance between P and Q is very small. Therefore the slip in P relieves not only the positive shear stress in P, but also in its neighboring region including Q. The relief of positive shear stress is the same as the increase of negative shear stress. Hence this slip increases the negative resolved shear stress in Q to cause Q to slide more readily in the reverse loading. The negative slip in Q relieves the negative shear stress not only in Q, but also in P, thus causing P more readily to slide in the next forward loading. This process is repeated for every cycle thus providing a natural gating mechanism for a monotonic buildup of local slip strain $e''_{\alpha\beta}$ in P and Q, pushing R out of the free surface and starts an extrusion. Interchanging the signs of the initial stresses in P and Q initiates an intrusion instead of an extrusion. This theory is extensively supported by metallurgical observations [8].

3. CALCULATION OF RESIDUAL STRESS FIELD

The resolved shear stress is the sum of the initial, applied and residual shear stresses [equation (1)]. To calculate the residual stress, the analogy between plastic strain and applied force [13] is applied. It has been shown that the equivalent body force per unit volume along the x_i-axis due to plastic strain e''_{ij} in a body with isotropic elastic constants is

$$F_i = -(\lambda e''_{kk,i}+2Ge''_{ij,j}) \tag{2}$$

where λ and G are Lame's constants. The repetition of an italic subscript denotes summation and the subscript after a comma denotes differentiation, with respect to the coordinate variable. The equivalent surface force per unit area along the x_i-axis has been shown as

$$S_i = (\lambda\delta_{ij}e''_{kk}+2Ge''_{ij})\nu_j \tag{3}$$

where ν_j is the cosine of the angle between the exterior normal to the surface and the x_j-axis.

From a given e''_{ij}, we obtain F_i and S_i from equations (2) and (3). Then we apply this F_i and S_i to the body and obtain the strain distribution e_{ij} in this body by elastic solution. The residual stress field in this body is then

$$\tau^{r}_{ij} = (\lambda\,\delta_{ij}e_{kk}+2Ge_{ij}-\lambda\,\delta_{ij}e''_{kk}-2Ge''_{ij}) \tag{4}$$

where δ_{ij} is the Kronecker delta. This analogy reduces to Duhamel's analogy for thermal stress [12], if the plastic strain e''_{ij} is replaced by thermal strain e^{T}_{ij}.

The lengths of slices P, Q and R along the x_3-direction are much larger than the thickness and their inclined lengths as shown in Fig. 1. Hence, strains in the major central portion of the slices are taken to be of generalized plane strain, i.e.

$$u_i = u_i(x_1, x_2) \quad i = 1, 2, 3. \tag{5}$$

The solution of a similar problem was shown in the analysis of prismatic anisotropic bars by Lekhnitski [14]. The stress–strain relation gives

$$\tau_{ij} = 2G\left[\frac{\nu}{1-2\nu}\delta_{ij}\theta+\tfrac{1}{2}(u_{i,j}+u_{j,i})\right] \tag{6}$$

where $\theta = u_{1,1}+u_{2,2}$ and ν is Poisson's ratio. Substitution of the expression into the conditions of equilibrium yields

$$\nabla^2 u_i+\frac{1}{1-2\nu}\frac{\partial\theta}{\partial x_i}+\frac{F_i}{G}=0, \quad i=1,2 \tag{7}$$

and

$$\nabla^2 u_3+\frac{F_3}{G}=0 \tag{8}$$

where

$$\nabla^2=\frac{\partial^2}{\partial x_1^2}+\frac{\partial^2}{\partial x_2^2}.$$

F_i and F_3 can be either the applied forces or the equivalent forces.

Equations (7) and (8) are not coupled and can be solved separately. Lin [13] have shown the solution of this stress field caused by F_i in equation (7), by using Airy's stress functions. Let $\tau^{k}_{ij}(\mathbf{x}, \bar{\mathbf{x}})$ be the stress at x due to a unit force along x_k-axis applied at $\bar{x}$ of this semi-infinite medium and $\phi_k(\mathbf{x}, \bar{\mathbf{x}})$ be the corresponding Airy stress function, where x denotes (x_1, x_2, x_3). Lin and Lin [15] have expressed the stress components in terms of the stress function as

$$\tau^{k}_{11}(\mathbf{x},\bar{\mathbf{x}})=\frac{\partial^2\phi_k}{\partial x_2^2}, \quad \tau^{k}_{22}(\mathbf{x},\bar{\mathbf{x}})=\frac{\partial^2\phi_k}{\partial x_1^2},$$

$$\tau^{k}_{22}(\mathbf{x},\bar{\mathbf{x}})=-\frac{\partial^2\phi_k}{\partial x_1\,\partial x_2}, \quad k=1,2 \tag{9}$$

$$\left\{\begin{aligned}\phi_1(\mathbf{x},\bar{\mathbf{x}}) &= -(p+q)(x_2-\bar{x}_2)(\theta_1+\theta_2)\\ &\quad +\tfrac{1}{2}q(x_1-\bar{x}_1)\ln(X_1/X_2)\\ &\quad +2p\frac{x_1\bar{x}_1(x_1+\bar{x}_1)}{X_2}\\ \phi_2(\mathbf{x},\bar{\mathbf{x}}) &= (p+q)(x_2-\bar{x}_2)(\theta_1+\theta_2)\\ &\quad +\tfrac{1}{2}q(x_2-\bar{x}_2)\ln(X_1/X_2)\\ &\quad -2p\frac{x_1\bar{x}_1(x_2-\bar{x}_2)}{X_2}\end{aligned}\right\} \quad (10)$$

$$\left\{\begin{aligned}&p=\frac{1}{4\pi(1-\nu)},\quad q=p(1-2\nu),\\ &\theta_1=\arctan\left\{\frac{x_2-\bar{x}_2}{x_1-\bar{x}_1}\right\},\quad -\pi\leqslant\theta_1<\pi\\ &\theta_2=\arctan\left\{\frac{x_2-\bar{x}_2}{x_1+\bar{x}_1}\right\},\quad -\frac{\pi}{2}\leqslant\theta_2<\frac{\pi}{2}\\ &X_1=(x_1-\bar{x}_1)^2+(x_2-\bar{x}_2)^2,\\ &X_2=(x_1+\bar{x}_1)^2+(x_2-\bar{x}_2)^2\end{aligned}\right\}. \quad (11)$$

To solve equation (8) for F_3, we write $\phi_3(\mathbf{x},\bar{\mathbf{x}})$ as $Gu_3(\mathbf{x},\bar{\mathbf{x}})$.The stress is then

$$\tau^3_{13}(\mathbf{x},\bar{\mathbf{x}})=\frac{\partial\phi_3}{\partial x_1};\quad \tau^3_{23}(\mathbf{x},\bar{\mathbf{x}})=\frac{\partial\phi_3}{\partial x_2}. \quad (12)$$

All other stress components are zero. For a unit concentrated force F_3 at $\bar{\mathbf{x}}$, equation (8) gives

$$\nabla^2\phi_3+\delta(\mathbf{x}-\bar{\mathbf{x}})=0 \quad (13)$$

where $\delta(\mathbf{x},\bar{\mathbf{x}})$ is the Dirac Delta function. With the boundary conditions of

$$\frac{\partial\phi_3}{\partial x_1}=0 \quad \text{at } x_1=0 \quad \text{and}$$
$$\frac{\partial\phi_3}{\partial x_1}=0 \quad \text{and} \quad \frac{\partial\phi_3}{\partial x_2}\to 0 \text{ as } \sqrt{x_1^2+x_2^2}\to\infty \quad (14)$$

we have

$$\phi_3(\mathbf{x},\bar{\mathbf{x}})=-\frac{1}{4\pi}(\ln X_1+\ln X_2) \quad (15)$$

where X_1, X_2 are given in equation (11). Hence the stress fields caused by the equivalent forces due to slip strain can readily be calculated.

4. EFFECT OF THE INHIBITION OF CROSS-SLIP OR MULTIPLE SLIP IN INTERMETALLIC COMPOUNDS ON HIGH-CYCLE FATIGUE

The above gives a method of calculation of the growth of an extrusion or an intrusion due to a single slip system. To understand the effect of the inhibition of cross or multiple slip of ordered intermetallic alloys on fatigue crack initiation, we need to study the effect of secondary slip on the extent of extrusion.

The buildup of this local slip strain $e''_{\alpha\beta}$ in P and Q is caused by the positive and negative initial shear stress $\tau^i_{\alpha\beta}$ which, in turn, is caused by $e^i_{\alpha\alpha}$ in R. If R were cut out, this free length of R would be longer than the slot cut, by an amount referred to as the "static extrusion" [11]. This $e^i_{\alpha\alpha}$ causes an initial compression $\tau^i_{\alpha\alpha}$ in R. As the extrusion grows under cyclic loading, the slice R increases in length. This elongation causes the compression to decrease. A question has been raised as to whether the extrusion growth will cease after the extrusion has reached the static extrusion. The residual tensile stress $\tau^i_{\alpha\alpha}$ caused by elongation in R due to extrusion can cause changes of resolved shear stresses in all 12 slip systems. The resolved shear stress in one slip system may reach the critical shear stress and slide. The plastic strain $e''_{\xi\eta}$ caused by slip in this system has a tensor component $e''_{\alpha\alpha}$ just like $e^i_\alpha\alpha$ in causing the positive and negative $\tau^i_{\alpha\beta}$, respectively, in P and Q. This secondary slip has been shown [16, 17] to increase greatly the extent of extrusion and intrusion. This method is here used to calculate the fatigue damage for the case with second slip and that without second slip. These two cases correspond to disordered and ordered superalloys respectively.

5. NUMERICAL CALCULATION

The mechanical properties used in the calculation were taken to correspond to Ni_3Al. The critical resolved shear stress τ^c was taken to be 200 MPa, Pope and Ezz [18]. The shear modulus G was calculated from the elastic compliance S_{1212} [18]. This S_{1212} is 0.848×10^{-2} (1/GPa), gives

$$G=\frac{1}{4S_{1212}}=\frac{10^3\text{ MPa}}{4\times0.848\times10^{-2}}=29{,}400\text{ MPa}.$$

The Possion's ratio was taken to be 0.3. Calculations have been made for a single fatigue band and then multiple fatigue bands. Since the local plastic strain in the band is much larger than the average plastic strain in the crystal, the strain-hardening rate in the band is much less than that of the crystal. The strain-hardening in the slip band is here neglected.

(a) A single fatigue band

The dimensions of this single fatigue band in the most favorably oriented crystal at the free surface of an intermetallic compound polycrystal are shown in Fig. 1. The initial resolved shear stress τ^i was taken to be 0.46 MPa. $\tau^a=200.0$ MPa. This gives an excessive shear stress τ^E, defined as $\tau^a+\tau^i-\tau^c$, of 0.46 MPa. The three slip directions of each of the four slip planes of a f.c.c. crystal are shown in Fig. 2. The most favorably oriented crystal of a polycrystal loaded under alternate tension and compression along the x_2-axis (Fig. 1) has a slip plane and a slip direction making an angle of 45° with the direction of loading. The slip system is referred to as the primary slip system. Let a_2 in Fig. 2, correspond to this system.

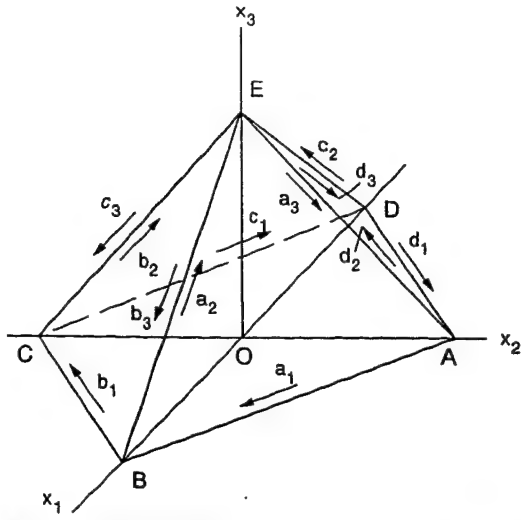

Fig. 2. Crystallographic direction of a f.c.c. crystal.

During fatigue loading, the build-up of large local plastic shear strain in the primary slip system, positive in P and negative in Q, tends to start an extrusion or an intrusion. Consequently an appreciable direct stress τ_{zz} will be built up in R. The Schmid factors of all the 12 slip systems for the stress τ_{ij} and those for τ_{zz} have been calculated [16] as shown in Table 1. It was found that there are four slip systems c_1, c_3, d_1 and d_2 equally favorably under τ_{zz}. Of these four, c_3 is most favorably under τ_{22}, where τ_{22} is the alternate loading. Hence c_3 is considered to be the active second slip system in R.

For numerical calculations, the slices P, Q, R are divided into a number of parallelogram grids along the length in the α-direction. Each grid is taken to have constant plastic strain. The average stress in the grid is taken as the corresponding grid stress. From the plane strain solution of a semi-infinite medium the stress field caused by a uniform plastic strain $e''_{\alpha\beta_n}$ in the nth grid was calculated. The average relieved stress $\tau^{r}_{\alpha\beta}(x)$ over the mth grid denoted by $\tau^{r}_{\alpha\beta_m}$ is written as

$$\tau^{r}_{\alpha\beta_m} = -C(m, \alpha\beta; n, \alpha\beta)e''_{\alpha\beta_n}.$$

As a cyclic loading proceeds, slips occur in P and Q and cause a residual stress field. The total resolved shear stress in the mth grid of $\alpha\beta$ slip system is the sum of the initial, residual and applied stresses

$$\tau_{\alpha\beta_m} = \tau^{i}_{\alpha\beta_m} + \tau^{a}_{\alpha\beta_m} - \sum_{n} C(m, \alpha\beta; n, \alpha\beta)e''_{\alpha\beta_n} \qquad (16)$$

where n is summed over all the sliding grids with plastic strain $e''_{\alpha\beta_n}$.

In the grids where $\tau(x) = \pm\tau^{c}$, an incremental applied shear stress $\Delta\tau^{a}_{m}$, with $\Delta\tau_m = \Delta\tau = 0$, yields

$$\Delta\tau^{a}_{\alpha\beta_m} = -\sum_{n} C(m\,\alpha\beta; n, \alpha\beta)\,\Delta e''_{\alpha\beta_n}. \qquad (17)$$

Table 1. Resolved shear stresses in different slip systems caused by cyclic loading τ_{22} and τ_{zz} (α denotes a_2 direction)

Slip system	Normal to slip plane $\xi(m)$	Slip direction $\eta(m)$	Schmid factor $\tau_{\xi\eta}/\tau_{zz}$
a_1	$\left(-\frac{\sqrt{2}}{2}, \frac{\sqrt{2}}{2}, 0\right)$	$\left(-\frac{\sqrt{2}}{4}, -\frac{\sqrt{2}}{4}, -\frac{\sqrt{3}}{2}\right)$	0
a_2	$\left(-\frac{\sqrt{2}}{2}, \frac{\sqrt{2}}{2}, 0\right)$	$\left(\frac{\sqrt{2}}{2}, \frac{\sqrt{2}}{2}, 0\right)$	0
a_3	$\left(-\frac{\sqrt{2}}{2}, \frac{\sqrt{2}}{2}, 0\right)$	$\left(-\frac{\sqrt{2}}{4}, -\frac{\sqrt{2}}{4}, -\frac{\sqrt{3}}{2}\right)$	0
b_1	$\left(-\frac{\sqrt{2}}{6}, \frac{\sqrt{2}}{2}, -\frac{2\sqrt{2}}{6},\right)$	$\left(\frac{\sqrt{2}}{4}+\frac{\sqrt{3}}{3}, \frac{\sqrt{2}}{4}-\frac{\sqrt{3}}{3}, -\frac{\sqrt{3}}{6}\right)$	0
b_2	$\left(-\frac{\sqrt{2}}{6}, \frac{\sqrt{2}}{6}, -\frac{2\sqrt{2}}{3},\right)$	$\left(\frac{\sqrt{2}}{4}, \frac{\sqrt{3}}{3}, \frac{\sqrt{2}}{4}, +\frac{\sqrt{3}}{3}, \frac{\sqrt{3}}{6}\right)$	0
b_3	$\left(-\frac{\sqrt{2}}{6}, \frac{\sqrt{2}}{6}, -\frac{2\sqrt{2}}{3}\right)$	$\left(-\frac{\sqrt{2}}{2}, \frac{\sqrt{2}}{2}, 0\right)$	0
c_1	$\left(\frac{\sqrt{3}}{3}+\frac{\sqrt{2}}{6}, \frac{\sqrt{3}}{3}-\frac{\sqrt{2}}{6}, -\frac{\sqrt{2}}{3}\right)$	$\left(\frac{\sqrt{2}}{4}, \frac{\sqrt{2}}{4}, \frac{\sqrt{3}}{2}\right)$	0.408
c_2	$\left(\frac{\sqrt{3}}{3}+\frac{\sqrt{2}}{6}, \frac{\sqrt{3}}{3}-\frac{\sqrt{2}}{6}, -\frac{\sqrt{2}}{3}\right)$	$\left(-\frac{\sqrt{3}}{3}, \frac{\sqrt{3}}{3}, \frac{\sqrt{3}}{3}\right)$	0
c_3	$\left(\frac{\sqrt{3}}{3}+\frac{\sqrt{2}}{6}, \frac{\sqrt{3}}{3}-\frac{\sqrt{2}}{6}, -\frac{\sqrt{2}}{3}\right)$	$\left(-\frac{\sqrt{2}}{4}+\frac{\sqrt{3}}{3}, -\frac{\sqrt{2}}{4}, -\frac{\sqrt{3}}{3}, -\frac{\sqrt{3}}{6}\right)$	−0.408
d_1	$\left(\frac{\sqrt{3}}{3}-\frac{\sqrt{2}}{6}, \frac{\sqrt{3}}{3}+\frac{\sqrt{2}}{6}, \frac{\sqrt{2}}{6}\right)$	$\left(-\frac{\sqrt{2}}{4}-\frac{\sqrt{3}}{3}, -\frac{\sqrt{2}}{4}+\frac{\sqrt{3}}{3}, \frac{\sqrt{3}}{6}\right)$	−0.408
d_2	$\left(\frac{\sqrt{3}}{3}-\frac{\sqrt{2}}{6}, \frac{\sqrt{3}}{3}+\frac{\sqrt{2}}{6}, \frac{\sqrt{2}}{3}\right)$	$\left(-\frac{\sqrt{2}}{4}, \frac{\sqrt{2}}{4}, \frac{\sqrt{3}}{2}\right)$	0.408
d_3	$\left(\frac{\sqrt{3}}{3}-\frac{\sqrt{2}}{6}, \frac{\sqrt{3}}{3}+\frac{\sqrt{2}}{6}, \frac{\sqrt{2}}{3}\right)$	$\left(\frac{\sqrt{3}}{3}, \frac{\sqrt{3}}{3}, \frac{\sqrt{3}}{3}\right)$	0

There are as many unknown $\Delta e''_{\alpha\beta_n}$ as the number of the above equations. The plastic strain increments $\Delta e''_{\alpha\beta_n}$ in the sliding grids for an incremental loading $\Delta\tau^a$ can be readily calculated. Similarly, the stress components $\tau^r_{\alpha\alpha}$ and $\tau^r_{\beta\beta}$ in R can be calculated [14] and written as

$$\left.\begin{aligned} -\tau^r_{\alpha\alpha_m} &= \sum_n C(m, \alpha\alpha; n, \alpha\beta) e''_{\alpha\beta_n} \\ -\tau^r_{\beta\beta_m} &= \sum_n C(m, \beta\beta; n, \alpha\beta) e''_{\alpha\beta_n} \end{aligned}\right\}. \quad (18)$$

As discussed earlier, c_3 is the most likely second slip system to become active. The resolved shear stress in c_3 is denoted by $\tau_{\xi\eta}$. The initial resolved shear stress $\tau^i_{\xi\eta}$ varies with the initial stress components τ^i_{13}, τ^i_{23}, τ^i_{33}. For our numerical calculations, $\tau^i_{\xi\eta}$ is assumed to be zero. The incremental resolved shear stress in this second slip system

$$\Delta\tau_{\xi\eta} = 0.318\Delta\tau_{22} - 0.408\Delta\tau_{\alpha\alpha}. \quad (19)$$

When $\tau_{\xi\eta}$ increases to τ^c or decreases to $-\tau^c$, this slip system slides and causes $e''_{\xi\eta}$. Now we have slip in the $\alpha\beta$ slip system in P and Q and in $\xi\eta$ slip system in R.

Let the two slices P and Q be divided into $2N$ grids and R into M grids. The resolved shear stress in the $\alpha\beta$ and the $\xi\eta$ slip system of the ith grid is written as

$$\left.\begin{aligned} \tau^r_{\alpha\beta_i} &= -C(i, \alpha\beta; j, \alpha\beta) e''_{\alpha\beta_j} - C(i, \alpha\beta; k, \xi\eta) e''_{\xi\eta_k} \\ \tau^r_{\xi\eta_i} &= -C(i, \xi\eta; j, \alpha\beta) e''_{\alpha\beta_j} - C(i, \xi\eta; k, \xi\eta) e''_{\xi\eta_k} \end{aligned}\right\}. \quad (20)$$

The repetition of subscript j denotes summation from 1 to $2N$ and that of subscript k denotes summation from 1 to M. $C(i, \xi\eta; j, \alpha\beta)$ is the residual stress $\tau^r_{\xi\eta}$ in the ith grid due to a unit plastic strain $e''_{\alpha\beta}$ in the jth grid. The incremental plastic strain in all grids are calculated from equation (17).

With the method described, the extrusion growth of a single fatigue band with cycles of loading was calculated for the case with no slip in the second slip system, corresponding to an ordered superalloy and that with slip in the second slip system corresponding to a disordered compound. These results are shown in Fig. 3. It is seen that ordered intermetallic compound has a much lower rate of extrusion on intrusion growth.

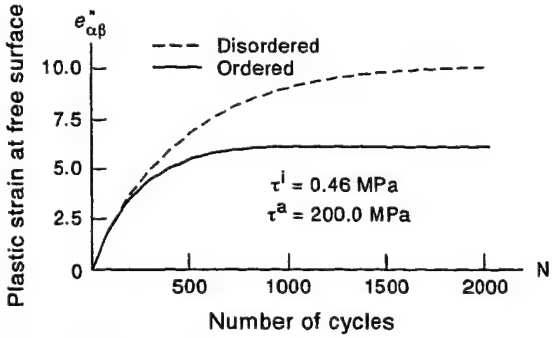

Fig. 3. Plastic shear strain $e''_{\alpha\beta}$ at free surface vs number of cycles, single fatigue band.

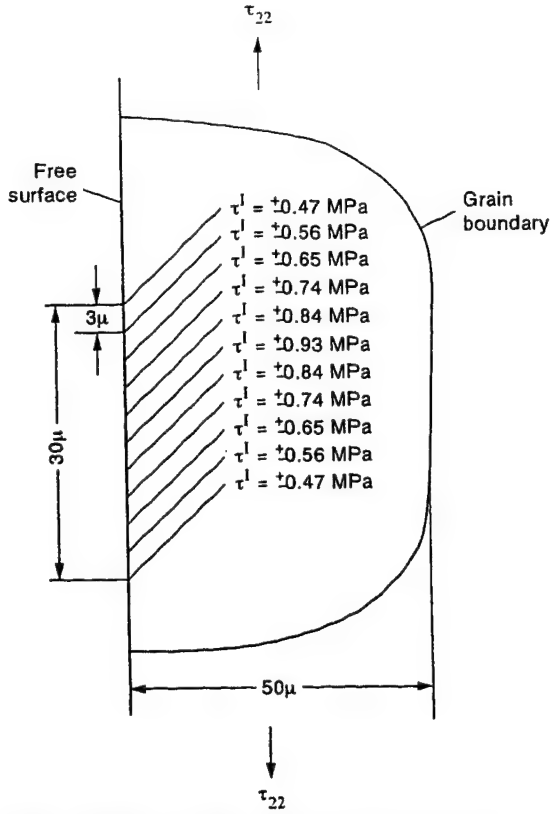

Fig. 4. Spacing of fatigue bands and their initial stress.

(b) Multiple fatigue bands

A number of slip bands have been observed in a most favorably oriented crystal in a polycrystal subject to cyclic loading [5]. The crystals surrounding this most favorably oriented crystal are less favorably oriented and hence have lower resolved shear stresses caused by the applied load. In the early stages of a high-cycle fatigue, the residual resolved shear stress in the neighboring crystals is small compared to the decrease of the applied resolved shear stress due to the difference in orientation. Hence, in the early stages of high-cycle fatigue, slip in the most favorably oriented crystal can develope to some extent without significant slip in the neighboring crystals. For numerical study, we consider the most favorable crystal to have eleven slip bands spaced at 3 microns apart as shown in Fig. 4. Each band is assumed to consist of three thin slices P, Q, and R as shown in Fig. 1. P and Q in each band are assumed to have equal and opposite uniform initial resolved shear stresses of the amounts as indicated in Fig. 4. The initial excessive shear stress τ^E is $\tau^i + \tau^a - \tau^c$. During loading this excessive shear stress τ^E is to be relieved with slip in the different slip bands. Slip distributions in these bands are readily calculated. Slip in one band not only relieves shear stress in this band but also in the other bands. This gives the interaction of slip bands.

Using the method described above, each thin slice P, Q and R of each band is divided along the α direction into three parallelogram grids, and the slip

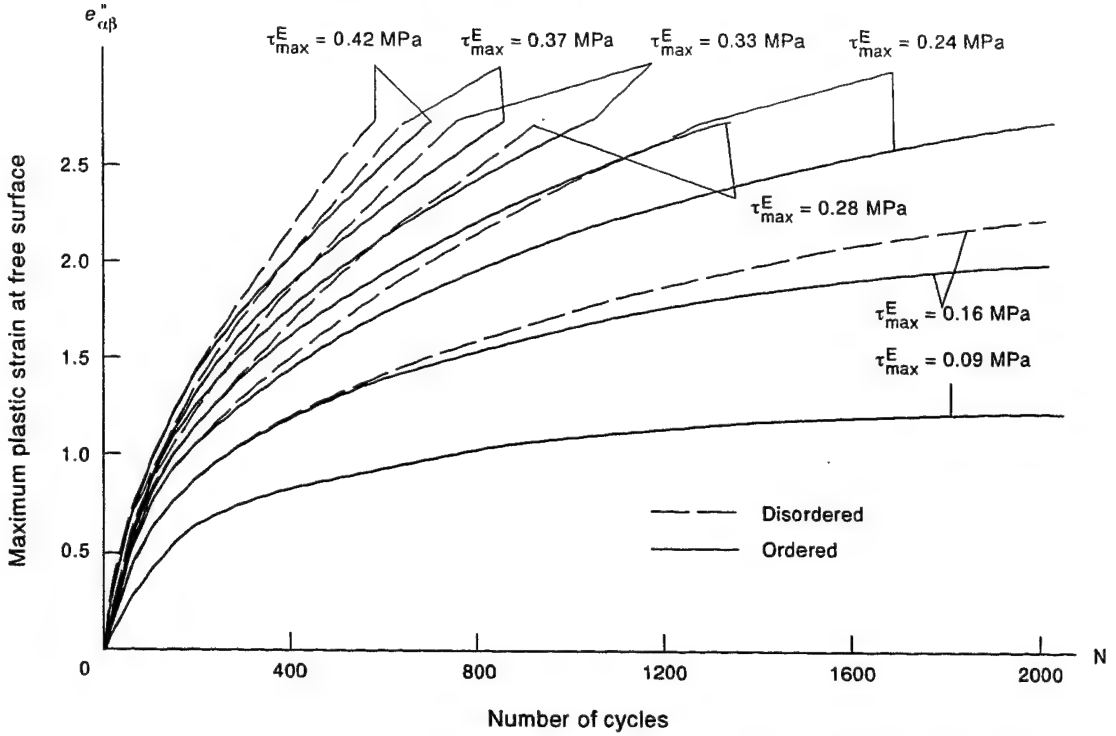

Fig. 5. Plastic strain $e''_{\alpha\beta}$ at free surface vs number of cycles at different applied excessive shear stresses.

distributions in the different slices of the slip bands were calculated. The center fatigue band has the maximum initial shear stress and has been found to give the maximum plastic shear strain at the free surface. This shear strain is considered to be a measure of the fatigue damage. The variation of this surface strain with the number of cycles of loading are plotted at different values of excessive resolved shear stresses for both ordered and disordered intermetallic compounds or alloys as shown in Fig. 5. For each value of this excessive shear stress, the number of active slip bands at different cycles of loading are shown in Fig. 6. From the curves in Fig. 5 we pick the number of cycles to yield the given value of the plastic resolved shear strain, $e''_{\alpha\beta}$ at the free surface, thus we obtain the excessive shear stress τ^E vs cycles

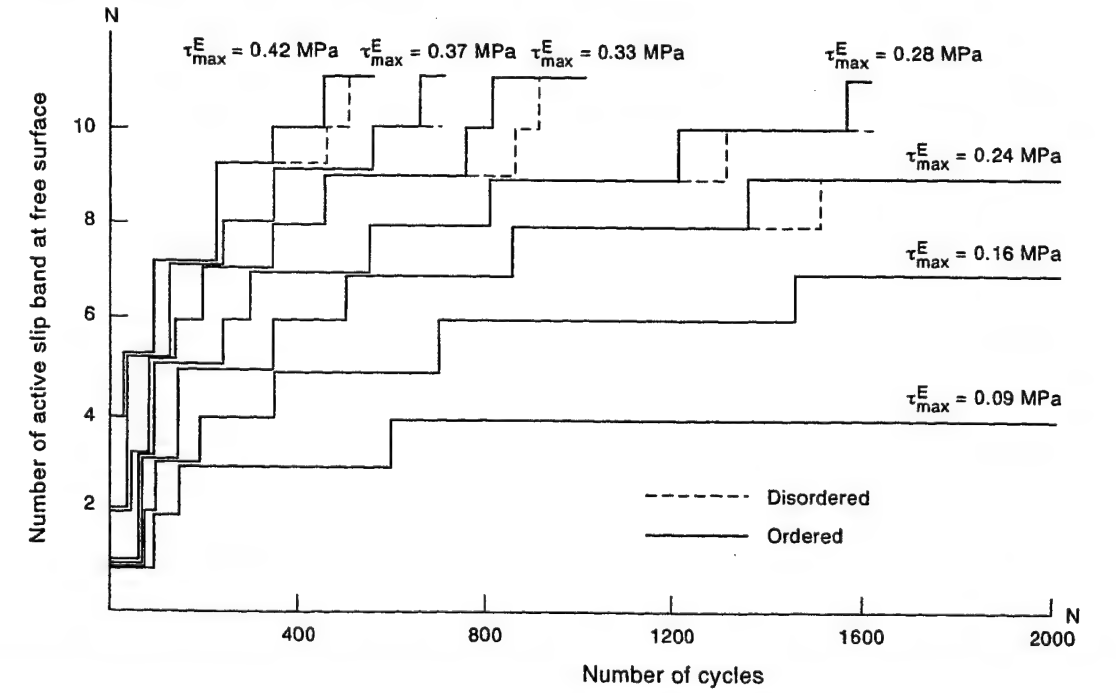

Fig. 6. Number of active fatigue bands at free surface vs number of cycles.

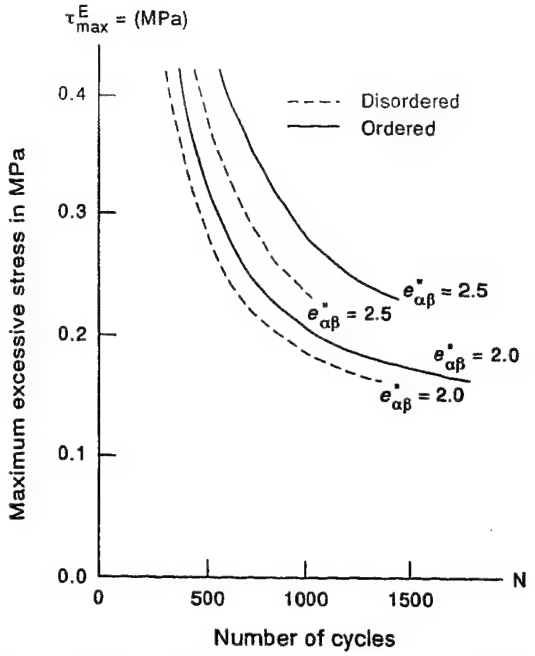

Fig. 7. Maximum initial excessive shear stress vs number of cycles τ–N curves at different levels of fatigue damage.

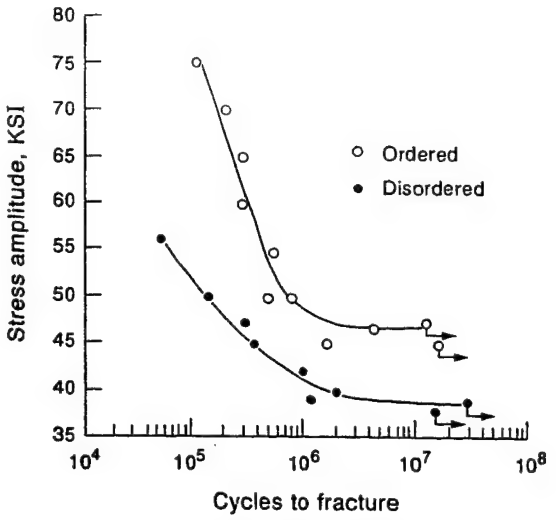

Fig. 8. Stress amplitude or cycles to failure for Ni_3Mn fatigued at 25°C reproduced from Trans. Metallurgical Society of AIME.

of loading to yield the given surface plastic strain, which is a measure of the extent of extrusion or intrusion and is taken as the extent of crack initiation. These τ^E vs N curves for both the ordered and disordered alloys are shown in Fig. 7. It is seen that the shape of these curves for different levels of fatigue damage is somewhat similar to a typical S–N curve.

At the initial stage of fatigue loading, the slip in a single band is directly proportional to the excessive shear stress. The rate of incremental slip in P and Q per cycle depends on the positive and negative resolved shear stresses $(\tau^i + \tau^r)$. As loading proceeds, extrusion grows and this shear stress $(\tau^i + \tau^r)$ decreases and reduces the growth rate of extrusion. This has the effect of decreasing the slope of the $e''_{\alpha\beta}$ at the free surface with N. It has been shown that this slope approaches zero when the extrusion approaches the "static extrusion" [17]. When more than one slip band becomes active, slip in one band relieves the shear stress not only in this band but also in other bands. This decreases the amount of slip in each band. This causes the curves $e''_{\alpha\beta}$ vs N to bend further down. This has the effect of causing the τ^A vs N curve to give a specified value of surface strain to become more flat.

Stress amplitude vs cycles to fatigue failure from tests by Boettner *et al.* [3] for ordered and quenched Ni_3Mn at 25°C is shown in Fig. 8. These test curves of Ni_3Mn instead of these of Ni_3Al are here used to compare the calculated results, since the corresponding test data of Ni_3Al is not found in the literature. The trend of these tests clearly agree to the calculated results as shown in Fig. 7. This explains why an ordered intermetallic compound or alloy has longer fatigue life than the disordered ones. Since the yield stress of ordered intermetallic alloys is lower than the disordered, the longer fatigue life is due to the longer life of crack initiation. This seems to explain well this observed longer high-cycle fatigue life of the ordered intermetallic compounds.

Acknowledgement—This research was supported by the office of Naval Research through Grant N00014-91-J-1923. The interest of Dr R. S. Barsoum and Dr Y. Rajapakse of ONR are gratefully acknowledged.

REFERENCES

1. L. M. Hsiung and N. S. Stoloff, *High-Temperature Ordered Intermetallic Alloys III* (edited by C. T. Liu, A. L. Taub, N. S. Stoloff and C. C. Koch) Vol. 133. Materials Research Society (1988).
2. N. S. Stoloff and R. E. Davies, *Progress in Material Science*, Vol. 13, (edited by B. Chalmers), pp. 1–84 Pergamon Press, Oxford (1966).
3. R. C. Boettner, N. S. Stoloff and H. G. Davies, *Trans. metall. Soc. AIME* **236**, 131 (1966).
4. C. Lall, S. Chin and D. P. Pope, *Metall. Trans.* **10A**, 1323 (1979).
5. N. S. Stoloff, G. E. Fuchs, A. K. Kuruvilla and S. J. Choe, *High-Temperature Ordered Intermetallic Alloys II* (edited by Stoloff, N. S., Koch, C. C., Liu, C. T. and O. Izumi), Vol. 81. Materials Research Society (1987).
6. P. J. E. Forsyth and C. A. Stubbington, *J. Inst. Metals* **83**, 395 (1955).
7. A. S. Kennedy, *Process of Creep and Fatigue of Metals*, p. 328. Wiley, New York (1963).
8. T. H. Lin, *Reviews of the Deformation Behavior of Materials*, (edited by P. Felham). Freund Publishing House, Tel-Aviv, Israel (1977).
9. T. H. Lin and Y. M. Ito, *J. Mech. Phys. Solids* **17**, 511 (1969).
10. T. H. Lin and Y. M. Ito, *Proc. U.S. Nat. Academy of Sciences* **62**, 631 (1969).
11. J. G. Antonopoulos, L. M. Brown and A. T. Winter, *Phil. Mag.* **34**, 549 (1967).
12. H. Mughrabi, R. Wang, K. Differet and V. Essmann, *Fatigue Mechanism, ASTM STP 811*, pp. 5–45 (1983).

13. T. H. Lin, *Theory of Inelastic Structures*, pp. 44–48. Wiley, New York (1968).
14. S. G. Lekhnitski, *Theory of Elasticity of an Anisotropic Body*, pp. 129–134. Holden-Day, San Francisco (1963).
15. S. R. Lin and T. H. Lin, *J. appl. Mech.* **50,** 367 (1983).
16. S. R. Lin and T. H. Lin, *J. Mech. Phys. Solids* **22,** 177 (1974).
17. T. H. Lin. *Adv. appl. Mech.* **29**, 1 (1992).
18. D. P. Pope and S. S. Ezz, *Int. Metal Rev.* **29,** 136 (1984).
19. S. M. Yang, *Metall. Trans.* **16A,** 661 (1985).

Materials Science and Engineering, A170 (1993) 103–110

Micromechanics of stress and strain-controlled, high cycle fatigue crack initiation of intermetallic compounds

T. H. Lin and Qiye Chen

Department of Civil Engineering, University of California, Los Angeles, CA 90024-1593 (USA)

Abstract

Tests have shown that ordered intermetallic compounds favor planar slip and tend to have no cross-slip or multislip. The yield stress of ordered compounds is less than that of disordered compounds. However, the stress-controlled, high cycle fatigue life of ordered compounds is appreciably more than that of disordered compounds. This is considered to be caused by a low rate of crack initiation. In contrast, strain-controlled tests show that ordering shortens life by crack initiation. In this paper, we attempt to explain these observed behaviors by the micromechanic theory of high cycle fatigue crack initiation developed by Lin and coworkers. The effect of ordering on crack initiation under cyclic combined axial and torsional loadings is also shown.

1. Introduction

Ordered intermetallic compounds are distinct from ordinary alloys according to their lattice structure and bonding. If the atoms of the two elements of the compounds segregate fairly completely to designated atomic sites, then it is called an ordered solution or superlattice.

At low and intermediate temperatures, nickel-based intermetallic compounds with $L1_2$ structures deform by $\langle 110\rangle\{111\}$ slip. If the slip occurs by the motion of $\frac{1}{2}\langle 110\rangle\{111\}$ dislocations, they will leave a plane of antiphase boundary in their wake. The energy required to create such a fault is high, which makes this slip difficult. In contrast, slip by the motion of $\langle 110\rangle\{111\}$ dislocations does not create such a fault, so occurs frequently. However, because the line energy of a dislocation is proportional to the square of the distance which the atom moves, this superdislocation $\langle 110\rangle\{111\}$ needs high energy to move. Nevertheless, if the superdislocation dissociates into two superpartial dislocations, this dislocation energy is reduced. Therefore, the energy of a superdislocation depends on the length of the Burgers vector and the antiphase boundary created by slip. Dislocations in a superlattice tend to move in a group, connected by a strip of antiphase boundary. The leading dislocation creates an antiphase boundary and the trailing dislocation eliminates it. It is unlikely that cross-slip of the associated pair can occur, since this requires the trailing dislocation to follow exactly in the wake of the leading dislocation. This causes cross-slip or multislip to be difficult in ordered intermetallic compounds.

Nickel-base intermetallic compounds with a long-range ordered structure have been found to exhibit an anomalous increase in flow stress with temperature. At a low temperature, these compounds deform by $\langle 110\rangle\{111\}$ slip; however, at elevated temperatures, slip occurred on the $\{010\}$ plane. Various theories have been advanced to explain the observed temperature dependence of the yield stress. Copley and Kear [1] proposed that, at low temperatures, the superpartial dislocations are dissocaited to Shockley partial dislocations, such that flow occurs by the easy $\frac{1}{6}\langle 112\rangle\{111\}$ shear of the crystal. At elevated temperatures, the superpartials are much less widely dissociated, leading to the difficult $\frac{1}{2}\langle 110\rangle\{111\}$ shear of the crystal and, hence, giving a high yield strength.

2. Experimental results

2.1. Stress-controlled fatigue

Tests have shown that long-range order substantially increases the high cycle fatigue lives of FeCo–V, Ni_3Mn (Fig. 1) and other intermetallic compounds, despite a decrease in yield stress [2]. The ratio of the fatigue limit to the yield strength exceeds 0.5 for most of the ordered alloys; in contrast, under the disordered condiion, the ratio decreases significantly. Since crack propagation is much more rapid in the ordered con-

0921-5093/93/$6.00

dition, it has been concluded by Stoloff *et al.* [3] that ordering substantially delays crack initiation.

2.2. *Strain-controlled fatigue*

Hsiung and Stoloff [4] have conducted experiments on fatigue crack initiation in two intermetallic compounds—Ni_3Al single crystals and FeCo–V polycrystal—under strain-controlled cycling. Strain-controlled tension–compression cyclic deformation tests, beginning in tension, were performed on a closed lop machine. The tests showed that order substantially decreases the strain-controlled fatigue resistance in this alloy (Fig. 2). However, there is little difference in the development of dislocation substructures and crack initiation sites [4]. Bundles of unit dislocations oriented crystallographically were found in the disordered material. Dislocation pairs were seen in the ordered alloy samples. Slip along ⟨110⟩ occurs in both ordered and disordered FeCo–V, and cracks initiated almost exclusively at slip bands, intrusions and extrusions. Tests carried out in high vacuum also have shown that slip bands are preferred sites for crack initiation and propagation in both the ordered and disordered conditions. The height of extrusion and the depth of intrusion are taken as measures of the fatigue crack initiation.

In short, the test results show that long-range ordered substantially increases the fatigue lives of intermetallic compounds in stress-controlled cycling but decreases the strain-controlled fatigue resistance (Figs. 1 and 2). Stoloff *et al.* [3] indicated that the least understood aspects of the cyclic behavior of intermetallic compounds are the processes leading to crack initiation. This paper is an attempt to explain the observed high cycle fatigue crack initiation characteristics of these intermetallic compounds.

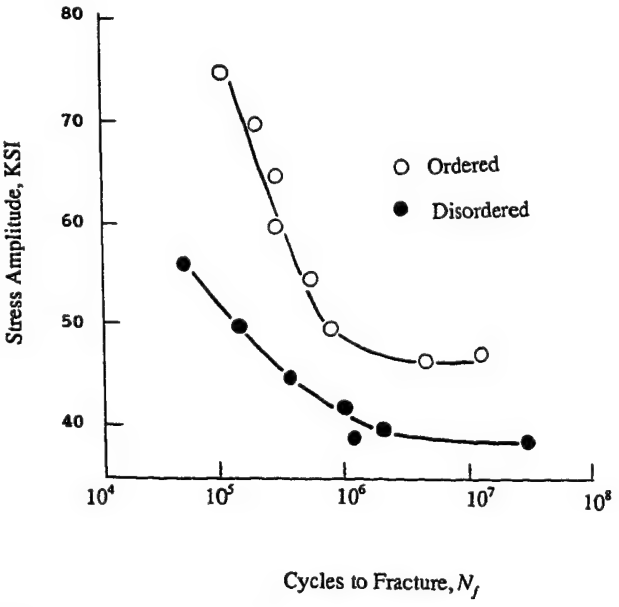

Fig. 1. Stress amplitude or cycles to failure for Ni_3Mn fatigued at 25 °C [2].

3. Micromechanic quantitative theory of fatigue crack initiation [5, 6]

Extrusion and intrusion were first discovered by Forsyth and Stubbington in 1955 [7]. For an extrusion to start, positive shear has to occur in a thin slice (P) and negative shear in a closely located slice (Q), as shown in Fig. 3. Initial defects exist in all metals and cause an initial stress field τ^i. An initial shear stress field favorable to positive shear in P and negative shear in Q is clearly one having a positive shear stress in P and a ngative shear stress in Q. Such an initial stress field can be provided by an initial tensile strain $e^i_{\alpha\alpha}$ in R. (The repetition of Greek letters does not denote summation.)

Let us consider a perfect crystal. If we cut a slit through a crystal and force a sheet of metal one atom thick into the slit, a pair of parallel edge dislocations (A and B) of opposite signs, forming an interstitial dipole, is produced, as shown in Fig. 4. If we cut a rectangular block along the dotted line, the free length of this block will be one atomic spacing more than the corresponding length of the hole. If there are n such dipoles in a length of atomic spacing N, this will give an initial strain $e^i_{\alpha\alpha}$ of n/N. Hence, this initial strain can be caused by an array of dislocation dipoles. This array of dipoles was suggested by Lin and Ito [8] in 1969 as a possible way of providing the initial strain to cause the favorable initial stress field.

It follows that this positive $e^i_{\alpha\alpha}$ can be caused by a row of interstitial dislocation dipoles and a negative $e^i_{\alpha\alpha}$ by vacancy dipoles [8]. It was shown by Mughrabi *et al.* [9] that the experimentally observed ladder structure in

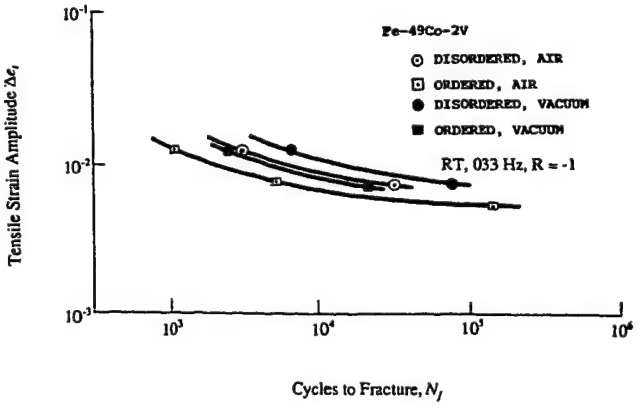

Fig. 2. Strain-controlled fatigue in FeCo–V [4].

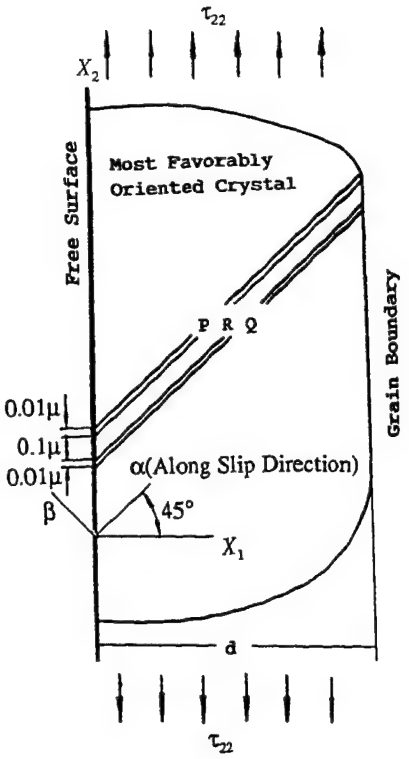

Fig. 3. Schematic diagram of most favorably oriented crystal at free surface.

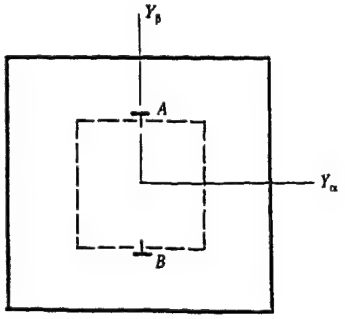

Fig. 4. Schematic diagram of a disloation interstitial dipole.

the persistent slip bands (PSBs) indicates dislocation dipoles. These cause such an initial resolved shear stresses at the interface between the PSB and the matrix.

If a metal specimen is loaded in cyclic tension and compression of low amplitude, the plastic deformation essentially occurs only in the most favorably oriented crystal. This crystal is considered to be at a free surface, with $\alpha\beta$ as the most favorably oriented slip system, as shown in Fig. 3. During loading, when the resolved shear stress in some region reaches the critical shear stress τ^c, slip occurs. After loading, this slip remains and causes a residual resolved shear stress τ^r. Then, we have the total shear stress equal to the sum of these stresses, such that

$$\tau = \tau^i + \tau^r + \tau^a \tag{1}$$

where τ^a is the applied shear stress.

3.1. Monotonic building of extrusion and intrusion [5, 6]

Tests show that the extrusions and intrusions increase monotonically with cyclic loading. For such an extrusion to build-up monotonically, slip in P (Fig. 3) during forward loading has to be irreversible during the reversed loading. This clearly needs a gating mechanism to prevent slip from reversing. It is interesting to see that the microstress field produced by slip supplies this gating mechanism.

Let us consider an initial stress field τ^i to be positive in P and negative in Q, as explained previously. A positive loading τ_{22} on the polycrystal (Fig. 3) causes a positive τ^a in the whole crystal. $\tau^i + \tau^a$ reaches the critical shear stress τ^c first in P and so this slides first. The plastic strain resulting from this slip is taken to be constant along the x_3 axis (Fig. 5). This gives

$$\frac{\partial \tau_{\alpha 3}}{\partial x_3} = 0$$

The equilibrium condition $\tau_{ij,j} = 0$ in rectangular coordinates x_1, x_2 and x_3 in terms of coordinates α, β and x_3 gives

$$\frac{\partial \tau_{\alpha\alpha}}{\partial \alpha} + \frac{\partial \tau_{\alpha\beta}}{\partial \beta} = 0$$

The first term here is finite. Since the sum of the two terms vanishes, the second term also must be finite. Hence, the change in $\tau_{\alpha\beta}$ along β, across the small distance from P to Q, owing to slip, is very small [5, 6].

Therefore, the slip in P relieves not only the positive shear stress in P but also that in its neighboring region including Q. This slip increases the negative resolved shear stress in Q, causing Q to slide more readily during the reverse loading [10]. Similarly, the negative slip in Q relieves the negative shear stress not only in Q but also in P, thus causing P to slide more readily during the second forward loading. This process is repeated for every cycle, thus providing a natural gating mechanism to cause the monotonic build-up of the local slip strain $e''_{\alpha\beta}$ in P and Q, as observed in experiments, pushing R out of the free surface to start an extrusion. Interchanging the signs of the initial stresses initiates an intrusion instead of an extrusion. This gating mechanism is briefly reviewed here for the readers' convenience. This gating mechanism was introduced by Lin and Ito [10] in 1969, was expressed

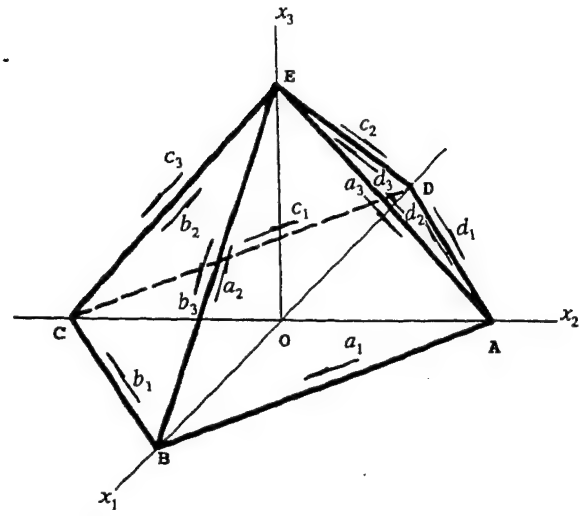

Fig. 5. Crystallographic directions of an f.c.c. crystal.

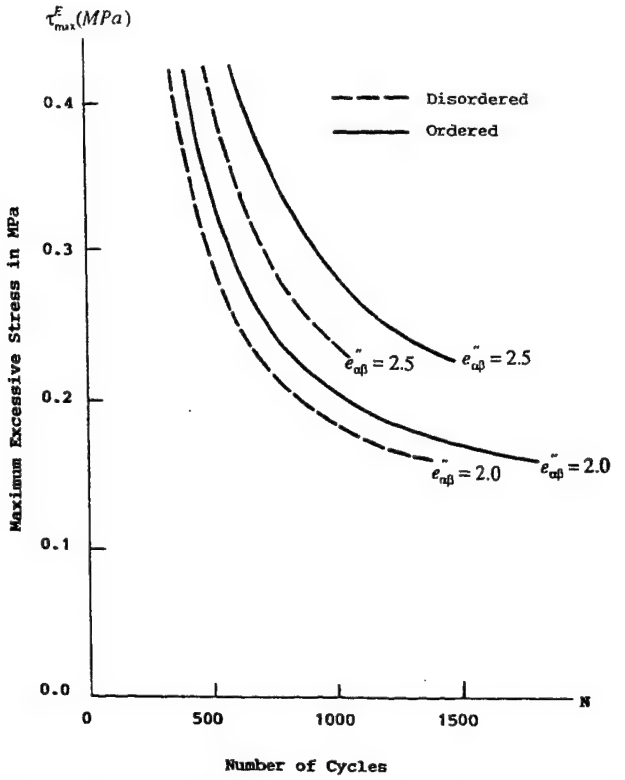

Fig. 6. Maximum initial excessive shear stress *vs.* number of cycles, *i.e.* τ–N curves, at different levels of fatigue damage.

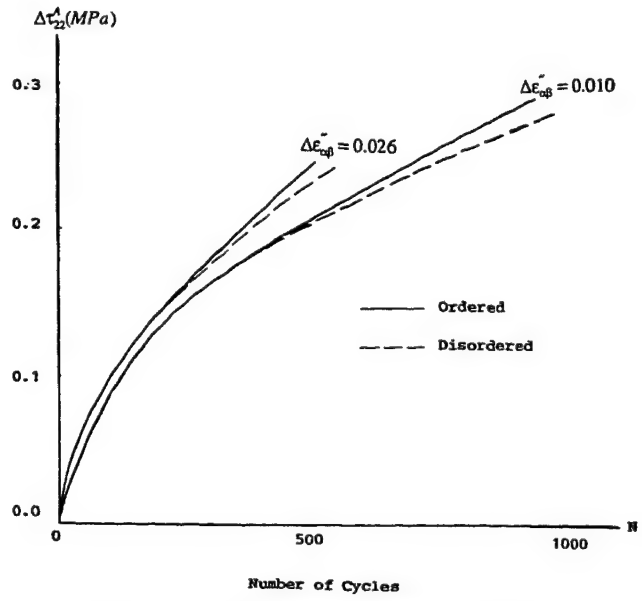

Fig. 7. Variation of cycle stress with cycles of loading in strain-controlled fatigue.

by dislocation arrays by Tanaka and Mura [11] in 1981 and is also discussed in Suresh's excellent book *Fatigue of Materials* [12]. This mechanism depends on the closeness of slid slices P and Q. This explains why the extrusions are very thin, as observed in fatigue specimens.

The governing condition for the initiation or continuation of slip is having the resolved shear stress τ equal to the critical shear stress τ^c. The residual stress τ^r is a component of the resolved shear stress τ. To calculate τ^r, the analogy of plastic strain and applied force developed by Lin [13] is used. Plastic strain is generally caused by the displacement of dislocations. As indicated by Hirth and Lothe in their excellent book *Theory of Dislocations* [14], most dislocation literature deals with dislocations in the isotropic approximation. They have given two good reasons for these approximations. "First, the mathematics becomes much more complicated when anisotropy is considered. Second, in many cases the errors involved in the isotropic approximation are about 20 to 30%, and these are submerged by other approximations in dislocation theory or by errors in experimental observation."

Hence, this isotropic approximation is not likely to change the general results, as shown in Figs. 6 and 7. To simplify the numerical calculation, this anisotropy of the intermetallic is neglected. Then, the residual stress resulting from a given plastic strain distribution e''_{ij} is given by

$$\tau^r_{ij} = \lambda\delta_{ij}e_{kk} + 2Ge_{ij} - \lambda\delta_{ij}e''_{kk} - 2Ge''_{ij} \qquad (2)$$

where e_{ij} is the strain caused by e'''_{ij}, δ_{ij} is the Kronecker delta, and λ and G are Lamé's constants. The length of slices P, Q and R along the x_3 direction are much larger than the thickness and their inclined lengths shown in Fig. 3.

Strains in the major central portion of the slices are taken to be of generalized plane strain. The displace-

ment along the x_i axis is denoted as

$$u_i = u_i(x_1, x_2) \qquad i = 1, 2, 3 \tag{3}$$

The stress–strain relationship is then [5, 6]

$$\tau_{ij} = 2G\left\{\frac{\nu}{1-2\nu}\,\delta_{ij}\theta + \frac{1}{2}\,(u_{i,j} + u_{j,i})\right\} \tag{4}$$

where $\theta = u_{1,1} + u_{2,2}$ and ν is Poisson's ratio.

Substituting eqn. (4) into the condition of equilibrium yields

$$\nabla^2 u_i + \frac{1}{1-2\nu}\frac{\partial\theta}{\partial x_i} + \frac{F_i}{G} = 0 \qquad i = 1, 2 \tag{5}$$

$$\nabla^2 u_3 + \frac{F_3}{G} = 0 \tag{6}$$

where

$$\nabla^2 = \frac{\partial^2}{\partial x_1^2} + \frac{\partial^2}{\partial x_2^2} \tag{7}$$

Equations (5) and (6) are not coupled and can be solved separately. The details of these solutions are given in refs. 5 and 6.

3.2. Effect of inhibition of cross-slip or multiple slip on fatigue crack

As indicated previously, cross-slip or multiple slip is inhibited in ordered intermetallic compounds. The build-up of local plastic strain $e''_{\alpha\beta}$ in P and Q depends on the initial stress τ^i, which is caused by $e^i_{\alpha\alpha}$ in R. This $e^i_{\alpha\alpha}$ is due to the extra initial length of R over that provided by the slot between P and Q. An extrusion grows at the expense of this extra length. When the extrusion equals this extra length—which is then called a static extrusion [9]—the growth may stop. However, the growth of an extrusion causes a residual tensile stress in R. This can cause changes in the resolved shear stress in all 12 slip systems of the f.c.c. crystal [5, 6]. The resolved shear stress in one slip system may reach the critical shear stress and slide. The plastic strain $e''_{\xi\eta}$ caused by this slip has a *tensor component* $e''_{\alpha\alpha}$, which is similar to $e^i_{\alpha\alpha}$ in causing the positive and negative $\tau^i_{\alpha\beta}$ in P and Q respectively. This $e''_{\xi\eta}$ has been shown to increase greatly the extent of an extrusion [5, 6].

The above gives the analytical method to calculate the growth of an extrusion and intrusion for the cases with secondary slip (corresponding to disordered) and without secondary slip (corresponding to ordered). These calculations were carried out for both stress-controlled and strain-controlled loadings.

4. Calculated results

The mechanical properties used in the present calculations were taken to correspond to Ni_3Al [15]. The critical resolved shear stress τ^c was taken to be 200 MPa [16]. The shear modulus G was obtained from the measured elastic compliance S_{1212} in ref. 17, giving $G = 29\,400$ MPa. Poisson's ratio ν was taken to be 0.3. The strain-hardening rate in the band is much less than that in the crystal. Hence, the strain hardening in the slip band is neglected.

The dimensions of the fatigue band in the most favorably oriented crystal at the free surface of an intermetallic compound polycrystal are shown in Fig. 3. The initial resolved shear stress τ^i in P and Q was taken to be ± 0.46 MPa. The applied shear stress $\tau^a = 200$ MPa. This gives an excessive shear stress τ^E, defined as $\tau^a + \tau^i - \tau^c$, of 0.46 MPa. The slip directions and slip planes of an f.c.c. crystal are indicated in Fig. 5. The most favorably oriented crystal of the polycrystal has a slip system with a slip direction and slip plane making an angle of 45° with the loading axis (Fig. 3). This slip system is identified as a_2 in Fig. 5 and is referred to as the primary slip system. During fatigue loading, an extrusion grows, causing a tensile stress in R. The Schmid factors of all 12 slip systems for the loadings τ_{22} and $\tau_{\alpha\alpha}$ have been calculated [5, 6]. It was found that four slip systems, *i.e.* c_1, c_3, d_1 and d_2, are equally favorable under $\tau_{\alpha\alpha}$. Of these four, c_3 is the most favorable under τ_{22}. Hence, c_3 is taken to be the active second slip system in R.

The slices P, Q and R are divided into a number of parallelogram grids along the length in the α direction. A constant plastic strain is assumed in each grid. The average stress in the grid is taken as the corresponding grid stress. From the plane strain solution of a semi-infinite medium, the stress field caused by the uniform plastic strain $e''_{\alpha\beta_n}$ in the nth grid was calculated. The average relieved stress over the mth grid is expressed as

$$\tau^r_{\alpha\beta_m} = -C(m, \alpha\beta; n, \alpha\beta)e_{\alpha\beta_n} \tag{8}$$

Here, the coefficient $C(m, \alpha\beta; n, \alpha\beta)$, for the stress $\tau_{\alpha\beta_m}$ relieved in the mth grid owing to a unit shear strain $e''_{\alpha\beta_n}$ equals $C(n, \alpha\beta; m, \alpha\beta)$ for the stress $\tau_{\alpha\beta_n}$ relieved in the nth grid owing to a unit shear strain $e''_{\alpha\beta_m}$. This reciprocal relationship facilitates numerical calculation.

In the grids where $\tau(x) = \tau^c$, an incremental applied shear stress is then

$$\Delta\tau^a_{\alpha\beta_m} = \Delta\tau^r_{\alpha\beta_m} = -\Sigma C(m, \alpha\beta; n, \alpha\beta)\Delta e''_{\alpha\beta_n} \tag{9}$$

This gives a set of equations to solve the unknown $\Delta e''_{\alpha\beta_n}$ values. The initial resolved shear stress in c_3, denoted by $\tau^i_{\xi\eta}$, is assumed to be zero. For each

unknown $\Delta e''_{\alpha\beta_n}$, there is one of the above equations. Hence, the plastic strain increments in the sliding grids for an incremental applied load are readily calculated. Indeed, the incremental shear stress in the second slip system c_3 is expressed as

$$\Delta\tau_{\xi\eta} = 0.318\Delta\tau_{22} - 0.408\Delta\tau_{\alpha\alpha} \tag{10}$$

When $\tau_{\xi\eta}$ reaches τ^c, this slip system slides and generates $e''_{\xi\eta}$. Slip then occurs both in the $\alpha\beta$ slip system in P and Q, and in the $\xi\eta$ system in R. The incremental resolved shear stresses are then

$$\Delta\tau^r_{\alpha\beta_m} = -C(m, \alpha\beta; n, \alpha\beta)\Delta e''_{\alpha\beta_n} - C(m, \alpha\beta; p, \xi\eta)\Delta e''_{\xi\eta_p} \tag{11}$$

$$\Delta\tau^r_{\xi\eta_m} = -C(m, \xi\eta; n, \alpha\beta)\Delta e''_{\alpha\beta_n} - C(m, \xi\eta; p, \xi\eta)\Delta e''_{\xi\eta_p} \tag{12}$$

(The repetitions of the subscript n and p denote summation.) Based on the method described above, the extrusion growth of a single fatigue band with loading cycles was calculated [5, 6, 16] for the case with no secondary slip, corresponding to an ordered superalloy, and that with second slip, corresponding to the disordered condition.

We have also considered the case where the most favorable crystal has 11 fatigue bands [5]. During loading, the excessive shear stress is relieved, owing to slip in the different slip bands. Slip in one band relieves the shear stress not only in this band but also in other bands. The center band has the maximum initial shear stress and gives the maximum plastic shear strain at the free surface. This shear strain is considered to be a measure of the fatigue damage. The excessive shear stress is defined as

$$\tau^E = \tau^i + \tau^a - \tau^c \tag{13}$$

The variation of the surface plastic strain with loading cycles for different values of excessive shear stress for both the ordered and disordered intermetallic compounds was calculated as shown in ref. 16. From these results, we pick the number of cycles to yield the given value of the surface plastic strain for different excessive shear stresses. This surface plastic strain is a measure of the extent of extrusion or intrusion and, hence, the extent of crack initiation. These τ^E *vs.* N curves for both the ordered and disordered superalloys for stress-controlled loadings are shown in Fig. 6. It can be seen that this high cycle fatigue crack initiation life in stress-controlled loading of the ordered intermetallic compounds is longer than that of the disordered case [15]. This explains the test results of Boettner *et al.* [2].

The rate of incremental slip in P and Q per cycle depends on the resolved shear stress $(\tau^i + \tau^r)$. As loading progresses, extrusion increases, causing $(\tau^i + \tau^r)$ to decrease and hence reducing the growth rate. This decreases the slope of $e'_{\alpha\beta}$ at the free surface with N. For the multiple fatigue bands, slip in one band relieves the shear stress not only in this band but also in other bands. This causes the $e'_{\alpha\beta}$ *vs.* N curve to bend further down.

4.1. Strain-controlled cyclic loading

Under strain-controlled fatigue, the incremental macroscopic plastic strain $\Delta E''$ per cycle is constant. $\Delta E''$ was taken to be proportional to the incremental surface shear strain $\Delta e''_{\alpha\beta}$ in the case of a single fatigue band in the most favorably oriented crystal and to be proportional to the sum of the incremental surface strains of all bands in the case of multiple fatigue bands. The method of calculation is the same as in the case of stress-controlled loadings [5, 6, 16]. The applied stress—also called the fatigue resistance—was varied to yield the given incremental palstic strain. Two values of $\Delta e''_{\alpha\beta}$ (second fatigue band) or the sum of $\Delta e''_{\alpha\beta}$ values (multiple fatigue bands), *i.e.* one of 0.010 and the other of 0.026, were analysed. The variation of this stress *vs.* loading cycles is shown in Fig. 7. It can be seen that this stress *vs.* loading cycles curve of the ordered case is higher than that of the disordered case. This agrees with the experimental results shown in Fig. 2.

4.2. Combined cyclic axial and torsional loadings

The above analysis of the effect of long-range order on fatigue crack initiation under cyclic axial loadings is here extended to combined cyclic axial and torsional loadings. Let us consider a circular shaft, with x along the axial, r along the radial and θ along the circumferential direction. Single-crystal tests [18] have shown that extrusions occurred on the slip plane along the most highly stressed slip direction and did not occur when the direction was parallel to the free surface. In cyclic torsion, the maximum shear stress occurs along the circumferential direction, parallel to the free surface, on a plane normal to the shaft axis. Hence, the extrusion or intrusion process will not occur in the slip system with maximum shear stress but may occur in

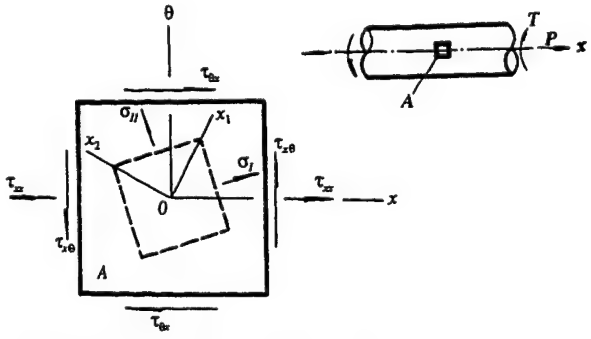

Fig. 8. Combined axial and shear loading.

some crystal with a slip plane normal to the shaft axis and a slip direction making an angle β with the circular boundary. Under combined axial and torsional loading, the maximum combined stresses occur in the outer layer of the shaft and gives two principal stresses σ_I and σ_{II}, as shown in Fig. 8. The third principal stress σ_{III} is along the radial direction and is zero. Referring to the x, r and θ coordinates, we have

$$\sigma_I, \sigma_{II} = \frac{\tau_{xx}+\tau_{\theta\theta}}{2} \pm \left\{\left(\frac{\tau_{xx}-\tau_{\theta\theta}}{2}\right)^2 + \tau_{x\theta}^2\right\}^{1/2} \tag{14}$$

The three extreme values of shear stresses are then

$$\tau_1 = \frac{\sigma_I - \sigma_{II}}{2} = \left\{\left(\frac{\tau_{xx}-\tau_{\theta\theta}}{2}\right)^2 + \tau_{x\theta}^2\right\}^{1/2} \tag{15}$$

$$\tau_2 = \frac{\sigma_{II}-\sigma_{III}}{2} = \frac{\tau_{\theta\theta}-\tau_{xx}}{4} - \frac{1}{2}\left\{\left(\frac{\tau_{xx}-\tau_{\theta\theta}}{2}\right)^2 + \tau_{x\theta}^2\right\}^{1/2} \tag{16}$$

$$\tau_3 = \frac{\sigma_{III}-\sigma_I}{2} = \frac{\tau_{\theta\theta}-\tau_{xx}}{4} - \frac{1}{2}\left\{\left(\frac{\tau_{xx}-\tau_{\theta\theta}}{2}\right)^2 + \tau_{x\theta}^2\right\}^{1/2} \tag{17}$$

where τ_2 and τ_3 have a shear direction making an angle of 45° with the free surface, and give the same inclination angle as specimens under cyclic tension and compression. Hence, the analysis for cyclic tension and compression is applicable to evaluate the fatigue crack initiation caused by τ_2 and τ_3. However, τ_1 has the maximum shear stress direction parallel to the free surface. The extrusion and intrusion process will not occur in this maximum shear stress direction. Nevertheless, this process can occur in some crystal with a slip direction making an angle β with the free surface (Fig. 9) as shown by Cooley and Lin [19].

Let us consider such a crystal which has a slip plane with a normal along the x_1 direction (Fig. 10). Thus, we have

$$\tau_{1\beta} = \tau_1 \cos\beta \tag{18}$$

Two closely located thin slices P and Q which have a slip direction that makes an angle β with the free surface are assumed to exist in a polycrystal, as shown in Fig. 9. As in the cases of cyclic tension and compression, positive slip in P and negative slip in Q increase monotonically with loading cycles to initiate an extrusion or intrusion. The displacement induced by the plastic strain $e''_{x\beta}$ is along the β direction. The component of the displacement normal to the free surface $u_\beta = te'_{1\beta}$ is taken as a measure of the amount of extrusion or intrusion and the crack initiation.

The radial component $u_r = u_\beta \sin\beta = te''_{\beta 1} \sin\beta$. This u_r at the free surface causes an extrusion and a stretch in R, and activates the secondary slip. This secondary slip in R will then increase the slip in P and Q. The surface plastic slip strain e''_{1r} with and without the secondary slip were calculated for different values of β. It was found that this surface plastic strain reaches a maximum at about $\beta = 25°$. At this β value, the surface strain e''_{1r} with secondary slip is 17% more than that with no secondary slip. The variation of this plastic strain with loading cycles in stress-controlled cycling is shown in Fig. 11. This gives the increase in surface plastic strain under cyclic loading of the disordered above that of the ordered intermetallic compounds.

Under combined axial and torsional loadings, the crack initation can be caused by τ_2 or τ_3, which has the

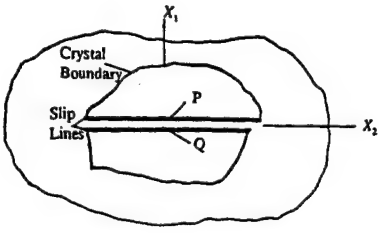

Fig. 9. Cross-section of the active glide plane. The slip direction β forms an angle β with the free surface [19].

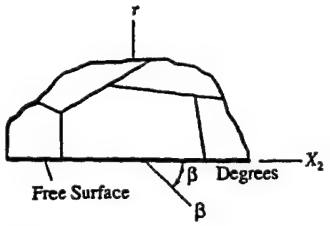

Fig. 10. Surface crystal with two slip lines P and Q [19].

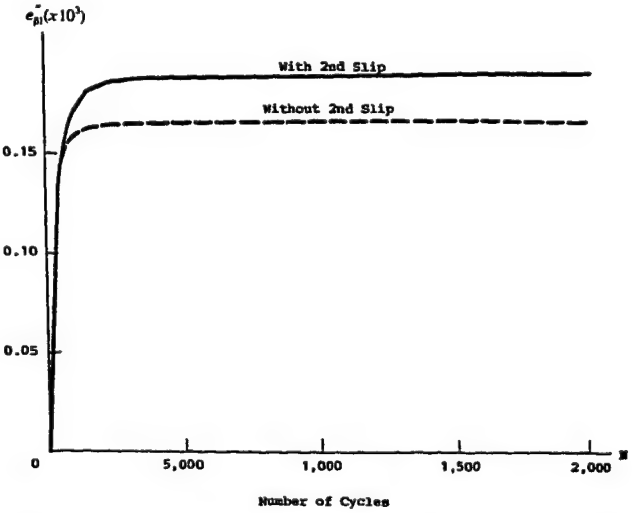

Fig. 11. Surface plastic strain *vs.* number of cycles of an intermetallic compound under a cyclic combined axal and shear loadings.

same extrusion characteristic as that under cyclic tension and compression, as shown in the first part of the paper, or that caused by τ_1, as shown in this section. The fatigue crack initiation is controlled by the highest extrusion or intrusion caused by these maximum shear stresses τ_1, τ_2 and τ_3.

5. Conclusion

This paper gives a method to analyse the effect of the long-range order of intermetallic compounds on high cycle fatigue crack initiation under axial stress-controlled and strain-controlled loadings. The effect of these intermetallic alloys under combined cyclic axial and torsional loadings subject to stress-controlled cycling is also shown. This seems to explain the experimental results.

Acknowledgments

This research was supported by the Office of Naval Research through Grant N00014-91-J-1923 and the Air Force Office of Scientific Research through Grant 89-0096.

References

1 S. M. Copley and B. H. Kear, Temperature and orientation dependence of the flow stress in off-stoichiometric Ni_3Al (γ' phase), *Trans. Metall. Soc. AIME, 239* (1967) 977.
2 R. C. Boettner, N. S. Stoloff and R. G. Davis, Effect of long-range order on fatigue, *Trans. Metall. Soc. AIME, 236* (1966) 131–133.
3 N. S. Stoloff, G. E. Fuchs, K. A. Kuruvilla and S. J. Choe, Fatigue of intermetallic compounds, in N. S. Stoloff, C. C. Koch, C. T. Liu and Oilzum (eds.), *High-Temperature Ordered Intermetallic Alloys II*, Materials Research Society, Pittsburgh, PA, 1986, p. 247.
4 L. M. Hsiung and N. S. Stoloff, in R. O. Kettunen, T. K. Lepistö and M. E. Lehtonen (eds.), Cyclic hardening and crack initiation on intermetallic compounds, *Strength of Metals and Alloys*, Pergamon, Oxford, Vol. 2, 1988, pp. 683–688.
5 T. H. Lin, Micromechanics of crack initiation in high-cycle fatigue, *Adv. Appl. Mech., 29* (1992) 1–68.
6 T. H. Lin, S. R. Lin and X. Q. Wu, Micromechanics of an extrusion in high-cycle fatigue, *Philos. Mag. A, 59* (6) (1989) 1263–1276.
7 P. J. E. Forsyth and C. A. Stubbington, The slip band extrusion effect observed in some aluminum alloys subjected to cyclic stresses, *J. Inst. Met., 83* (1955) 395–399.
8 T. H. Lin and Y. M. Ito, Fatigue crack nucleation in metals, *Proc. US Nat. Acad. Sci., 62* (1969) 631–635.
9 H. Mughrabi, R. Wang, K. Differet and U. Essmann, Fatigue crack initiation by cyclic slip irreversibilities in high-cycle fatigue, *Fatigue Mechanism, ASTM Spec. Tech. Publ., 811* (1983) 5–45.
10 T. H. Lin and Y. M. Ito, Micromechanics of a fatigue crack initiation mechanism, *J. Mech. Phys. Solids, 17* (1969) 511–523.
11 K. Tanaka and T. Mura, A dislocation model for fatigue crack initiation, *J. Appl. Mech., 48* (1981) 97–102.
12 S. Suresh, *Fatigue of Materials*, Cambridge University Press, Cambridge, 1991, Ch. 3.
13 T. H. Lin, *Theory of Inelastic Structures*, Wiley, New York, 1968, Ch. 2.
14 J. P. Hirth and J. Lothe, *Theory of Dislocations*, Wiley, New York, 1982, 2nd edn., p. 423.
15 D. P. Pope and S. S. Ezz, Mechanical properties of Ni_3Al and nickel-based alloys with high volume fraction of γ', *Int. Met. Rev., 29* (1984) 136–166.
16 T. H. Lin and Q. Y. Chen, Micromechanics of high-cycle fatigue crack initiation, *Acta Metall. Mater., 40* (12) (1992) 3255–3263.
17 S. W. Yang, Elastic constants of monocrystalline nickel-base superalloys, *Metall. Trans. A, 16* (1985) 661.
18 N. Thompson and N. J. Wadsworth, Metal fatigue, *Adv. Phys., London, 7* (1958) 72–170.
19 W. U. Cooley and T. H. Lin, Fatigue crack initiation under cyclic torsion, *J. Appl. Mech., 13* (1986) 550–554.

HIGH-CYCLE FATIGUE CRACK INITIATION OF INTERMETALLIC COMPOUNDS

Qiye Chen* and T.H. Lin*

Tests have shown that ordered intermatallic compounds favor planar slip and tend to have no cross-slip or multi-slip. The flow stress of the ordered is less than that of the disordered. However, the stress controlled high-cycle fatigue life of the ordered is considerably more than that of disordered. This is believed to be due to low rate of crack initiation. On the other hand, strain-controlled tests show that ordering shortens life in crack initiation. This paper is an attempt to explain these observed behaviors by the micromechanic theory of high-cycle fatigue crack initiation developed by Lin and his associates (1,2).

EXPERIMENTAL FATIGUE CHARACTERISTICS

Intermetallic compounds have been tested under stress-controlled and strain controlled cyclic loadings. It was found that long range order increases the stress-controlled high-cycle fatigue lives (3), in spite of a decrease in yield stress. The ratio of the fatigue limit to yield strength exceeds 0.5 for most of the ordered alloys, while in the disordered condition, this ratio decreases significantly. Since crack propagation is much more rapid in ordered condition, it has been concluded (4) that ordering substantially delays crack initiation.

Hsiung and Stoloff (5) have tested intermetallic compounds under strain-controlled cycling. Tests show that ordering substantially decreases the fatigue resistance in *FeCoV*. Stoloff et al. (5) indicated that the least understood aspects of cyclic behavior of intermetallic compounds are the processes leading to crack initiation. The present paper attempts to give these processes for both stress-controlled and strain-controlled loadings.

* Department of Civil Engineering, University of California, Los Angeles, CA 90024-1593.

A MICROMECHANIC QUANTITATIVE THEORY OF FATIGUE CRACK INITIATION IN INTERMETALLIC COMPOUNDS

Initial stress: slip along (110) occurred in both ordered and disordered *FeCoV* and crack initiated almost exclusively at slip bands, intrusions and extrusions. For an extrusion to start, positive shear has to occur in a thin slice P and negative shear in a closely located slice Q as shown in Fig. 1. Initial defects exist in all metals and cause an initial stress field τ^i. The initial shear stress field favorable to this shear is one having positive shear stress in P and negative one in Q. Such an initial stress field can be provided by an initial tensile strain $e^i_{\alpha\alpha}$ which may be caused by a row of interstitial dislocation dipoles and a negative $e^i_{\alpha\alpha}$ by vacancy dipoles (2). Recently it was shown (8) that the ladder structure in a persistent slip band (PSB) can be represented by an array of dislocation dipoles. These cause such an initial resolved shear stresses at the interface between the PSB and the matrix.

A metal specimen is loaded in cyclic tension and compression of low amplitude, so that plastic deformation essentially occurs only in the most favorably oriented crystal. This crystal is considered to be at a free surface with αβ as the most favorable slip system as shown in Fig. 1. when the resolved shear stress during loading reaches the critical shear stress τ^c in some region, slip occurs. This slip causes a residual shear stress τ^r. Denoting the shear stress caused by loading τ^a, we have the total shear stress equal to $\tau = \tau^i + \tau^r + \tau^a$.

Gating Mechanism: Tests show the extrusions and intrusions monotonically increasing with cyclic loadings. This indicates that slip in P during forward loading does not reverse during the reversed loading. This clearly needs a gating mechanism to prevent slip to reverse. This gating mechanism is here shown to be supplied by the microstress fields.

Consider an initial stress field τ^i to be positive in P and negative in Q. A positive loading τ_{22} (Fig. 3) causes a positive τ^a in the whole crystal. P has $\tau^i + \tau^a$ reaching τ^c first and slides. Due to the continuity of the resolved shear stress field across P and Q (1,2), the slip in P relieves not only the positive shear stress in P, but also in its neighboring region including Q. This is equivalent to increase the negative resolved shear stress in Q to cause Q more readily to slide negatively during the reverse loading. The negative slip in Q relieves the negative shear stress not only in Q, but also in P, thus causing P to slide more readily during the second forward loading. This process is repeated for every cycle thus providing a natural gating mechanism to cause the monotonic buildup of the local slip strain $\tilde{e}_{\alpha\beta}$ in P and Q as observed in experiments pushing R out of the free surface to start an extrusion. Interchanging the signs of the initial stresses initiates an intrusion instead of an extrusion. This mechanism has been published before and is here briefly revised for readers convenience.

The governing conditions for the initiation or continuation of slip is to have the resolved shear stress τ equal to the critical shear stress τ^c. To calculate τ, we need to calculate the residual stress τ^r. To calculate τ^r, we apply the analogy of plastic strain and applied force developed by Lin (2,7). Thus the stress fields caused by slip in P, Q and R are calculated.

Inhibition of Cross-Slip or Multislip: As indicated before, cross-slip or multiple slip is inhibited in ordered intermetallic compounds. The build-up of local strain $\tilde{e}_{\alpha\beta}$ in P and Q depends on the initial stress τ^i, which is caused by $e^i_{\alpha\alpha}$ in R. This $e^i_{\alpha\alpha}$ is due to the extra initial length of R over that provided by the slot between P and Q. Extrusion grows at the expense of this extra length. When the extrusion equals this extra length which is called the static extrusion by Mughrabi et al. (8), the growth may stop. However the growth of extrusion causes a residual tensile stress in R. This can cause changes of resolved shear stresses in all the 12 slip systems. The resolved shear stress in one slip system may reach the critical shear stress and slide. The plastic strain $\tilde{e}_{\phi\eta}$ caused by this slip has a tensor component $\tilde{e}_{\alpha\alpha}$ just like $e^i_{\alpha\alpha}$ in causing the positive and negative $\tau^i_{\alpha\beta}$ in P and Q respectively. This $e^i_{\phi\eta}$ has been shown to increase greatly the extent of an extrusion (1,2,6). An analytical method has been developed to calculate the growth of extrusion and intrusion for the cases with secondary slip corresponding to disordered and without secondary slip corresponding to ordered condition. This was carried out for both stress-controlled and strain-controlled loadings.

CALCULATED RESULTS AND CONCLUSIONS

Calculated Results: The mechanical properties used in the present calculations were taken to correspond to Ni_3Al. The critical resolved shear stress τ^c was taken to be 200 MPa (9). The shear modulus G was obtained from the measured S_{1212} of reference (10) giving G = 29,400 MPa (6). Poisson's ratio ν was taken to be 0.3. The strain-hardening rate in the band is much less than in the crystal. The strain-hardening in the slip band is neglected. Hence, $\Delta\tau^c = 0$.

The dimensions of the fatigue band in the most favorably oriented crystal at the free surface of an intermetallic compound are shown in Fig. 1. The initial resolved shear stress τ^i in P and Q was taken to be ± 0.46 MPa. The applied shear stress $\tau^a = 200.00$ MPa. This gives an excessive shear stress τ^E defined by $\tau^a + \tau^i - \tau^c$, of 0.46 MPa. The most favorably oriented crystal of the polycrystal has a slip system αβ. The extrusion grows during loading causing a tensile stress $\tau_{\alpha\alpha}$ in R. Among the 12 slip systems in the f.c.c. crystal, four have the same schmid factor under loading $\tau_{\alpha\alpha}$. Out of these four, one is most favorable under τ_{22}. Hence, this one is taken to be the active second slip system in R.

The slices P, Q and R are divided into grids along the length along α - direction. Constant plastic strain is assumed in each grid. The average stress of each grid is taken to correspond to the grid stress. Based on the condition that the sliding grid must have the resolved shear stress equal to the critical shear stress, the extrusion growth of a single fatigue band with loading cycles was calculated (6) for the case with no second slip corresponding to an ordered superalloy and that with second slip corresponding to the disordered state. The results are given in Fig. 2.

We have also considered the case where the most favorable crystal has eleven fatigue bands as shown in Fig. 3. During loading the excessive shear stress is relieved due to slip in the different slip bands. Slip in one band relieves the shear stress not only in this band, but also in other bands. This gives the interaction of slip bands. The center band has the maximum initial shear stress and gives the maximum plastic shear strain at the free surface. This shear strain is considered to be a measure of the fatigue damage. The excessive shear stress is defined as $\tau^E = \tau^i + \tau^a - \tau^c$. The variation of the surface plastic strain with loading cycles for different bands was calculated. Then the relation between the excessive shear stress τ^E and the cycles of loading to yield a given surface plastic strain, which is a measure of the extent of extrusion or intrusion was calculated. This extent represents the extent of crack initiation. These results for both ordered and disordered superalloys are shown in Fig. 4. Comparing these with test results of Boettner et al. (3), it is seen the trend of tests agrees with calculated results.

The rate of incremental slip in P and Q per cycle depends on the resolved shear stresses $(\tau^i + \tau^r)$. As loading progresses, extrusion grows and this $(\tau^i + \tau^r)$ decreases and hence reduces the growth rate. This decreases the slope of $e^{\sim}_{\alpha\beta}$ at the free surface with N. For the multiple fatigue bands, slip in one band relieves the shear stress not only in the band, but also in other bands. This causes the curve $e^{\sim}_{\alpha\beta}$ versus N curve to bend further down.

Strained Controlled Cyclic Loading: Under strain-controlled fatigue, the incremental macroscopic plastic strain $\Delta E^{\sim}$ per cycle is constant. The macroscopic plastic strain was assumed to be proportional to the surface plastic strains in the most favorably oriented crystal at the free surface. This $\Delta E^{\sim}$ was taken to be proportional to the incremental surface shear strain $\Delta e^{\sim}_{\alpha\beta}$ in the ease of single fatigue band (Fig. 1) and proportional to the sum of the incremental surface strains of all bands in the case of multiple fatigue bands (Fig. 4). The method of calculation is the same as in the case of stress-controlled loadings. The applied stress was varied to yield the given incremental plastic strain. Two values of $\Delta e^{\sim}_{\alpha\beta}$'s (single fatigue band) or the sum of $\Delta e^{\sim}_{\alpha\beta}$'s (multiple fatigue bands), one of 0.010 and the other of 0.026 were analyzed. This applied stress is also known as the fatigue resistance. The variations of this stress versus cycles of loading are shown in Fig.

5. It is seen that this stress versus cycles of loading of the ordered case is higher than that of disordered. This agrees with the experimental results shown in Fig. 4 of Ref. 5.

ACKNOWLEDGEMENTS

This research was supported by the Office of Naval Research through Grant N00014-91-J1923 and Air Force Office of Scientific Research through Grant 89-0096.

REFERENCES

1. Lin, T.H., Lin, S.R. and Wu, X.Q., "Micromechanics of an Extrusion in High-Cycle Fatigue", Phil. Magazine A., Vol. 59. No. 6, p. 1263-1276, 1989.
2. Lin, T.H., "Micromechanics of Crack Initiation in High-Cycle Fatigue", Advances in Applied Mechanics, Academic Press, Vol. 29, p. 1-68, 1992.
3. Boettner, R.C., Stoloff, N.S. and Davis, R.G., "Effect of Long-Range Order on Fatigue", Trans. Metallurigical Soc. AIME, Vol. 236, p. 136, 1966.
4. Stoloff, N.S., Fuchs, G.E., Kuruvilla, K.A. and Choe, S.J., "Fatigue of Intermetallic Compounds", High-Temperature Ordered Intermetallic Alloys II, edited by N.S. Stoloff, C.C. Koch, C.T. Liu and O. Izumi, published by Materials Research Society, Vol. 81, p. 247, 1986.
5. Hsiung, L.M. and Stoloff, N.S., "Cyclic Hardening of Crack Initiation in Intermetallic Compounds", Strength of Metals and Alloys (ICSMA), p. 638-688, 1988.
6. Lin, T.H. and Chen, Q.Y, "Micromechanics of High-Cycle Initiation of Fatigue Cracking Intermetallic Compounds", to be published in Acta Metall. Mater., 1992.
7. Lin, T.H., "Theory of Inelastic Structures", John Wiley & Sons, 1968.
8. Mughrabi, H., Wang, R., Differet, K. and Essmann, V., "Fatigue Crack Initiation of Cyclic Slip Irreversibilities in High-Cycle Fatigue", ASTM STP 811, Fatigue Mechanics, pp. 5-43, 1983.
9. Pope, D.P. and Ezz, S.S., "Mechanical Properties of Ni_3Al and Nickle-Base Alloys with High Volume Fraction of γ'", Int. Metals Reviews, Vol. 29, pp. 136-166, 1984.
10. Yang, S.W. "Plastic Constants of Monocrystalline Nickle-Base Superalloys", Metall. Trans. A, Vol. 16, pp. 661, 1985.

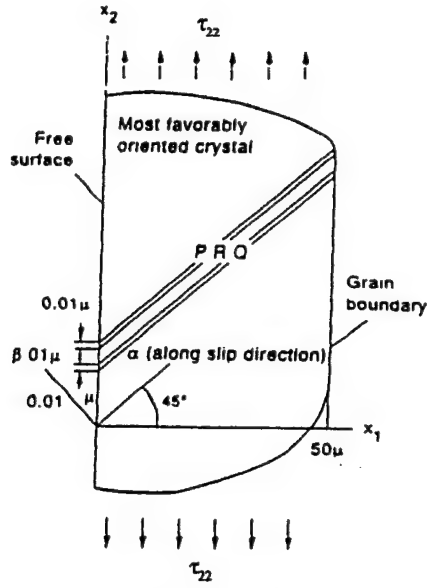

Fig. 1. Most favorably oriented crystal as free surface.

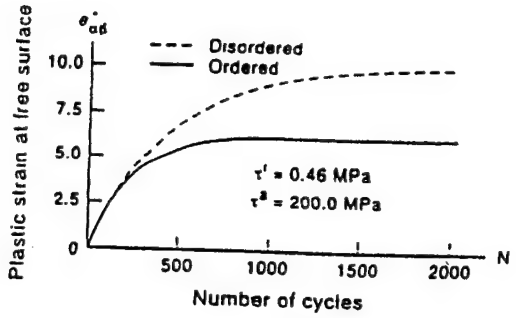

Fig. 2. Plastic shear strain $e^{*}_{\alpha\beta}$ at free surface vs number of cycles, single fatigue band.

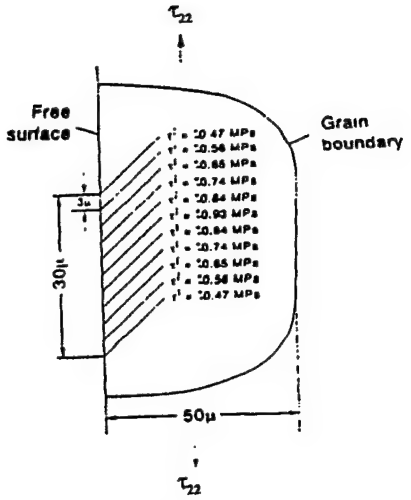

Fig. 3. Spacing of fatigue bands and their initial stress.

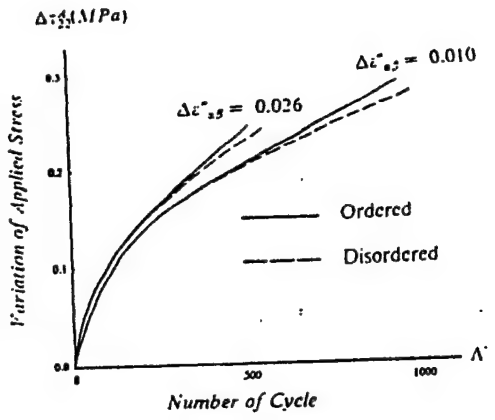

Fig. 5. Variation of applied stress corresponding to constant strain

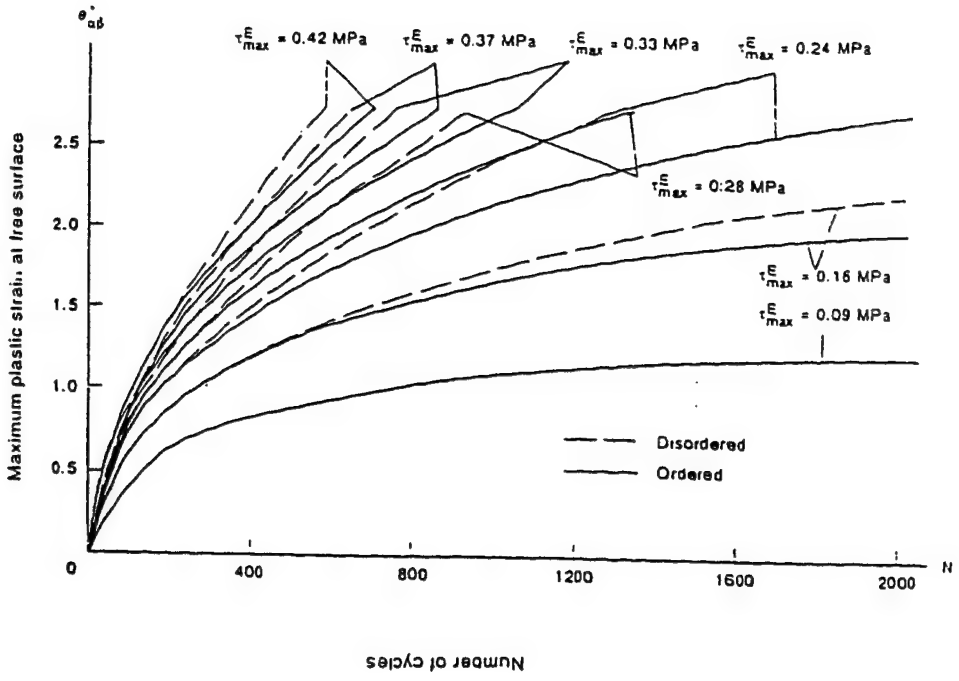

Fig. 4. Plastic strain $\dot{e}_{\alpha\beta}$ at free surface vs number of cycles at different applied excessive shear stresses.

AMD-Vol. 204, Numerical Methods in Structural Mechanics
ASME 1995

EFFECT OF ELASTIC ANISOTROPY ON FATIGUE BAND IN POLYCRYSTALLINE SOLIDS

N. J. Teng, T. H. Lin and K. F. Wong
Department of Civil and Environmental Engineering
University of California, Los Angeles
Los Angeles, California

ABSTRACT

Extrusions and intrusions in fatigue specimens are favorable sites for fatigue cracks. These extrusions and intrusions have been considered to be composed of three thin slices P, Q, and R in the surface crystal of a polycrystal. These thin slices are taken to be in the most favorably-oriented crystal at the free surface. Previous study (Lin and Ito, 1969, Lin, 1992) concerns mainly the fatigue bands in aluminum and its alloys. The anisotropy of the elastic constants of these alloys is insignificant and accordingly neglected. Then the polycrystal is considered as an elastically isotropic and homogeneous medium. However, the anisotropy of the elastic constants of some other metallic crystals, such as titanium and some intermetallic alloys, may not be negligible. In the present paper, the effect of anisotropy is analyzed.

The elastic anisotropy of the surface crystal is considered. Since the metal exterior to this surface crystal is composed of crystals with random orientations, it is assumed that the surface crystal is embedded in an elastically isotropic and homogeneous semi-infinite medium. Thus it is reduced to an inclusion problem. This heterogeneous solid is transformed into a homogeneous one by using Eshelby's Equivalent Inclusion Method (Eshelby, 1957, 1961, Mura, 1982). In this method, an extra set of eigenstrains, which are the same as the inelastic strains, is introduced. The eigenstrains explicitly depend on the applied stresses and plastic strains and thus can be implicitly incorporated in the formulation of solutions. The remaining calculation procedures are the same as those reviewed by Lin (1992). The anisotropic elastic constants of Ni_3Al monocrystalline intermetallic compound (Yang, 1985) are used. The isotropic elastic constants of the surrounding metal are taken from the conventional average method. The plastic strain distributions and the cumulative surface plastic strain in the fatigue band versus the number of loading cycles are calculated, and the effect of elastic anisotropy on the formation of extrusions and intrusions is examined in this paper.

INTRODUCTION

The process of fatigue failure in ductile metals can be classified into the following three stages: the crack initiation, the growth and coalescence of microcracks to form some macrocracks and the propagation of dominant cracks leading to the final catastrophic failure. In the high-cycle fatigue, most of fatigue life of materials is spent on crack initiation which starts with fatigue bands. Fatigue bands are the favorable sites for the formation of fatigue microcracks.

Fatigue bands consist of intensely localized plastic strains and have been observed in both monocrystalline and polycrystalline metals. Plastic strains are mainly induced by the displacement of dislocations. Under cyclic loadings, the localized plastic deformation accumulates with the increase of the number of loading cycles and causes extrusions and intrusions on the surface of materials. The extent of extrusions and intrusions is here taken as a measure of fatigue damage.

A ratchet mechanism has been proposed to model the fatigue band in polycrystals (Lin and Ito, 1969, Lin, 1992). It is assumed that a fatigue band composed of three thin slices P, Q and R is embedded near the free surface in an elastically isotropic and homogeneous semi-infinite medium. Since this model is concerned with the fatigue crack initiation of aluminum and its alloys, the elastic anisotropy of their constituent monocrystals is insignificant and accordingly neglected. For some other polycrystalline metals, such as titanium and some intermetallic alloys, however, the elastic anisotropy of crystals may not be negligible. Since the crystal orientations can vary, the local anisotropy and inhomogeneity of polycrystals will affect the formation of the fatigue band.

In this paper, the elastic anisotropy of the surface crystal is considered. Since the metal exterior to the surface crystal is composed of crystals with random orientations, the surface crystal is taken as being embedded in an elastically isotropic and homogeneous semi-infinite medium. Thus this analysis is reduced to an inclusion problem. This heterogeneous solid is transformed into a homogeneous one by using the Eshelby's Equivalent Inclusion Method (Eshelby, 1957, 1961, Mura, 1982). In this method, an extra set of eigentrains, which are the same as the inelastic strains, is introduced. These eigenstrains can be explicitly expressed in terms of applied stresses and plastic strains as well. After this transformation, the procedures of analysis are the same as those reviewed by Lin (1992). In the following numerical calculations, the anisotropic elastic constants of Ni_3Al monocrystalline intermetallic compound (Yang, 1985) are used. The isotropic elastic constants of the surrounding metal are taken from the conventional average method. The plastic strain distributions and the cumulative surface plastic strains in the fatigue band versus the number of loading cycles are calculated, and the effect of elastic anisotropy on the formation of extrusions and intrusions is examined.

CALCULATION OF RESIDUAL STRESS FIELD

The residual stress field due to a distribution of inelastic strains can be calculated by the analogy between inelastic strains and applied forces (Lin, 1969). It has been shown that the equivalent body force per unit volume along the x_i- axis due to inelastic strains ε^*_{ij} is

$$F_i = -C_{ijkl}\varepsilon^*_{kl,j} \tag{1}$$

where C_{ijkl} is the elastic modulus. The summation convention is used here and the subscript after a comma denotes the differentiation with respect to the coordinate variable. For isotropic elastic solids, the elastic constants are

$$C_{ijkl} = \lambda\delta_{ij}\delta_{kl} + \mu(\delta_{ik}\delta_{jl} + \delta_{il}\delta_{jk})$$

where λ and μ are Lame's constants and δ_{ij} is the Kronecker delta. The equivalent surface force per unit area along the x_i- axis has been shown as

$$S_i = C_{ijkl}\varepsilon''_{kl}\nu_j \tag{2}$$

where ν_j is the direction cosine of the normal to the area. The fictitious stresses $\sigma^s_{ij}(\mathbf{x})$ at point $\mathbf{x}$ caused by equivalent forces in domain Ω can be written by using the Green's function as

$$\begin{aligned}\sigma^s_{ij}(\mathbf{x}) &= \int_{\Omega} \tau^k_{ij}(\mathbf{x},\mathbf{x}')F_k(\mathbf{x}')d\Omega + \int_{\Gamma} \tau^k_{ij}(\mathbf{x},\mathbf{x}')S_k(\mathbf{x}')d\Gamma \\ &= -C_{klmn}\int_{\Omega} \tau^k_{ij}(\mathbf{x},\mathbf{x}')\varepsilon''_{mn,l}(\mathbf{x}')d\Omega + C_{klmn}\int_{\Gamma} \tau^k_{ij}(\mathbf{x},\mathbf{x}')\varepsilon''_{mn}(\mathbf{x}')\nu_l d\Gamma\end{aligned} \tag{3}$$

where $\tau^k_{ij}(\mathbf{x},\mathbf{x}')$ represents the stress component σ_{ij} at point $\mathbf{x}$ caused by a unit force acting at point $\mathbf{x}'$ along the x_k-axis. Γ is the boundary of domain Ω. The residual stress field is

$$\sigma^r_{ij}(\mathbf{x}) = \sigma^s_{ij}(\mathbf{x}) - C_{ijkl}\varepsilon''_{kl}(\mathbf{x}) \tag{4}$$

To calculate the residual stress field numerically, the discretization of a continuous problem is needed. In the following, the domain Ω in an extended solid is divided into a number of subdomains Ω_α. In each of them, it is assumed that the inelastic strains ε''_{ij} are uniform. After applying eqns (3) and (4) to Ω_α, the residual stress field due to $\varepsilon''_{mn}(\mathbf{x}')(\mathbf{x}' \in \Omega_\alpha)$ alone is

$$\sigma^r_{ij}(\mathbf{x}) = \{\int_{\Gamma_\alpha} C_{klmn}\tau^k_{ij}(\mathbf{x},\mathbf{x}')\nu_l d\Gamma_\alpha - H(\mathbf{x},\Omega_\alpha)C_{ijmn}\}\varepsilon''_{mn}(\Omega_\alpha)$$

where the function $H(\mathbf{x},\Omega_\alpha)$ is defined as

$$H(\mathbf{x},\Omega_\alpha) = \begin{cases} 1, & \mathbf{x} \in \Omega_\alpha \\ 0, & \mathbf{x} \notin \Omega_\alpha \end{cases}$$

Taking the average of $\sigma^r_{ij}(\mathbf{x})$ in subdomain Ω_β as

$$\sigma^r_{ij}(\Omega_\beta) = \frac{1}{V_\beta}\int_{\Omega_\beta} \sigma^r_{ij}(\mathbf{x})d\Omega$$

and letting $\sigma^r_{ij}(\Omega_\beta)$ represent the residual stresses in Ω_β due to ε''_{mn} in Ω_α, then we obtain

$$\sigma^r_{ij}(\Omega_\beta) = G_{ijmn}(\Omega_\beta,\Omega_\alpha)\varepsilon''_{mn}(\Omega_\alpha) \tag{5}$$

where $G_{ijmn}(\Omega_\beta,\Omega_\alpha)$ are called the residual stress influence coefficients, which represent the residual stresses in subdomain Ω_β caused by unit inelastic strain components in subdomain Ω_α.

GENERALIZATION OF EQUIVALENT INCLUSION METHOD

An elegant approach introduced by Eshelby (1957, 1961), which is now called the Eshelby's Equivalent Inclusion Method, can be used to transform an inhomogeneous problem into a homogeneous one by introducing a distribution of eigenstrains (Mura, 1982). Originally, this method was applied to solve the problems with an ellipsoidal inhomogeneity. In this study, this method is generalized to solve inhomogeneous problems of various shapes.

In the following, the matrix and vector notation will be used instead of tensor notation for convenience. Vectors are denoted by boldface lowercase Roman or Greek letters and matrices by boldface uppercase Roman letters. The Eshelby's equivalent equation is

$$\mathbf{C}^*(\mathbf{x})(\boldsymbol{\varepsilon}^\circ+\boldsymbol{\varepsilon}(\mathbf{x})-\boldsymbol{\varepsilon}^p(\mathbf{x}))=\mathbf{C}(\boldsymbol{\varepsilon}^\circ+\boldsymbol{\varepsilon}(\mathbf{x})-\boldsymbol{\varepsilon}^*(\mathbf{x})-\boldsymbol{\varepsilon}^p(\mathbf{x})) \quad , \ \mathbf{x}\in\Omega \tag{6}$$

where Ω is an inclusion or a subdomain with the elastic constant $\mathbf{C}^*(\mathbf{x})$ embedded in an extended body D with the isotropic elastic constant $\mathbf{C}$. $\boldsymbol{\varepsilon}(\mathbf{x})$ is the disturbance strain, $\boldsymbol{\varepsilon}^*(\mathbf{x})$ the eigenstrain, $\boldsymbol{\varepsilon}^p(\mathbf{x})$ the plastic strain and $\boldsymbol{\varepsilon}^\circ$ uniform strain from which $\boldsymbol{\sigma}^\circ=\mathbf{C}\boldsymbol{\varepsilon}^\circ$ where $\boldsymbol{\sigma}^\circ$ is the applied far-field stress. Eqn(6) shows that the eigenstrain $\boldsymbol{\varepsilon}^*(\mathbf{x})$ plays the same role as the plastic strain $\boldsymbol{\varepsilon}^p(\mathbf{x})$ does in the homogeneous materials.

When a continuous problem is discretized for the purpose of numerical analysis, the domain of Ω is further divided into N subdomains Ω_i $(1\le i\le N)$ called elements in which both of the eigenstrain $\boldsymbol{\varepsilon}^*$ and plastic strain $\boldsymbol{\varepsilon}^p$ are assumed to be uniform. The stresses in element Ω_i caused by the unit eigenstrain $\boldsymbol{\varepsilon}^*$ in element Ω_j are related by the residual stress influence coefficients, the same as caused by the plastic strain $\boldsymbol{\varepsilon}^p$. Thus the stress $\boldsymbol{\sigma}_i^r$ in Ω_i induced by both of the eigenstrains and plastic strains in all the elements concerned is

$$\boldsymbol{\sigma}_i^r=\sum_j \mathbf{G}_{ij}\boldsymbol{\varepsilon}_j^*+\sum_k \mathbf{G}_{ik}\boldsymbol{\varepsilon}_k^p \quad , \qquad 1\le i\le N \tag{7}$$

where

$$\boldsymbol{\varepsilon}_j^*=\left\{\varepsilon_{11}^*,\ \varepsilon_{22}^*,\ \varepsilon_{33}^*,\ \varepsilon_{23}^*,\ \varepsilon_{13}^*,\ \varepsilon_{12}^*\right\}_j^T$$

$$\boldsymbol{\varepsilon}_j^p=\left\{\varepsilon_{11}^p,\ \varepsilon_{22}^p,\ \varepsilon_{33}^p,\ \varepsilon_{23}^p,\ \varepsilon_{13}^p,\ \varepsilon_{12}^p\right\}_j^T$$

in Ω_j and $\mathbf{G}_{ij}$ are 6×6 matrices of the residual stress influence coefficients, which are contracted from $G_{klmn}(\Omega_i,\Omega_j)$. Notation $\{\cdots\}^T$ represents the transpose. Since the generalized plane strain problem is dealt with in this study, the following equation also holds

$$\boldsymbol{\sigma}_i^r=\overline{\mathbf{C}}\boldsymbol{\varepsilon}_i-\mathbf{C}(\boldsymbol{\varepsilon}_i^*+\boldsymbol{\varepsilon}_i^p) \tag{8}$$

where

$$\bar{\mathbf{C}}=\begin{bmatrix} \lambda+2\mu & \lambda & 0 & 0 & 0 \\ \lambda & \lambda+2\mu & 0 & 0 & 0 \\ \lambda & \lambda & 0 & 0 & 0 \\ 0 & 0 & 2\mu & 0 & 0 \\ 0 & 0 & 0 & 2\mu & 0 \\ 0 & 0 & 0 & 0 & 2\mu \end{bmatrix}, \quad \mathbf{C}=\begin{bmatrix} \lambda+2\mu & \lambda & \lambda & 0 & 0 & 0 \\ \lambda & \lambda+2\mu & \lambda & 0 & 0 & 0 \\ \lambda & \lambda & \lambda+2\mu & 0 & 0 & 0 \\ 0 & 0 & 0 & 2\mu & 0 & 0 \\ 0 & 0 & 0 & 0 & 2\mu & 0 \\ 0 & 0 & 0 & 0 & 0 & 2\mu \end{bmatrix}$$

and

$$\boldsymbol{\varepsilon}_i=\{\varepsilon_{11},\ \varepsilon_{22},\ \varepsilon_{23},\ \varepsilon_{13},\ \varepsilon_{12}\}_i^T \quad \text{with} \quad \varepsilon_{33}\equiv 0$$

From eqns(7) and (8), solving for disturbance strains $\boldsymbol{\varepsilon}_i$ in Ω_i in terms of $\boldsymbol{\varepsilon}_j^*$ and $\boldsymbol{\varepsilon}_k^p$, we obtain

$$\boldsymbol{\varepsilon}_i=\bar{\mathbf{C}}^{-1}\left[\mathbf{C}(\boldsymbol{\varepsilon}_i^*+\boldsymbol{\varepsilon}_i^p)+\sum_j \mathbf{G}_{ij}\boldsymbol{\varepsilon}_j^*+\sum_k \mathbf{G}_{ik}\boldsymbol{\varepsilon}_k^p\right] \quad , \quad 1\le i\le N \tag{9}$$

where

$$\bar{\mathbf{C}}^{-1}=\frac{1}{E}\begin{bmatrix} 1 & -\nu & -\nu & 0 & 0 & 0 \\ -\nu & 1 & -\nu & 0 & 0 & 0 \\ 0 & 0 & 0 & 1+\nu & 0 & 0 \\ 0 & 0 & 0 & 0 & 1+\nu & 0 \\ 0 & 0 & 0 & 0 & 0 & 1+\nu \end{bmatrix}$$

in which E is the Young's modulus and ν the Poisson's ratio.

The left-hand side of eqn(6) can also be written for the generalized plane strain problems as

$$\boldsymbol{\sigma}_i=\boldsymbol{\sigma}_i^*+\bar{\mathbf{C}}^*\boldsymbol{\varepsilon}_i-\mathbf{C}^*\boldsymbol{\varepsilon}_i^p \tag{10}$$

where $\mathbf{C}^*$ is a 6×6 anisotropic elastic stiffness matrix and $\bar{\mathbf{C}}^*$ a 6×5 matrix formed from matrix $\mathbf{C}^*$ by taking the third column away. And $\boldsymbol{\sigma}_i^*=\bar{\mathbf{C}}^*\boldsymbol{\varepsilon}^\circ$ in which

$$\boldsymbol{\varepsilon}^\circ=\{\varepsilon_{11}^\circ,\ \varepsilon_{22}^\circ,\ \varepsilon_{23}^\circ,\ \varepsilon_{13}^\circ,\ \varepsilon_{12}^\circ\}^T \quad \text{with} \quad \varepsilon_{33}^\circ\equiv 0$$

Substituting eqn(9) into eqn(10) and eqn(7), eqn(6) becomes

$$\mathbf{T}\boldsymbol{\varepsilon}_i^*+\sum_j \mathbf{S}_{ij}\boldsymbol{\varepsilon}_j^*=\mathbf{q}_i+(\mathbf{C}^*-\mathbf{T})\boldsymbol{\varepsilon}_i^p-\sum_k \mathbf{S}_{ik}\boldsymbol{\varepsilon}_k^p \qquad 1\le i\le N \tag{11}$$

where

$$\mathbf{T} = \overline{\mathbf{C}}^{*}\overline{\mathbf{C}}^{-1}\mathbf{C}$$

$$\mathbf{S}_{ij} = (\overline{\mathbf{C}}^{*}\overline{\mathbf{C}}^{-1} - \mathbf{I})\mathbf{G}_{ij}$$

$$\mathbf{q}_i = \sigma^{\circ} - \sigma_i^{*}$$

$$\sigma^{\circ} = \overline{\mathbf{C}}\varepsilon^{\circ}$$

and I is a 6×6 unit matrix.

It can be seen that eigenstrains ε_i^* depend on the applied load σ° and the distribution of plastic strains ε_k^p as well. Solving eqn(11) for ε_i^* in all elements Ω_i, we have

$$\varepsilon_i^{*} = \mathbf{p}_i + \sum_k \mathbf{R}_{ik}\varepsilon_k^{p} \quad , \ 1 \le i \le N \tag{12}$$

where $\mathbf{p}_i$ is a vector in terms of σ° in Ω_i. The total stress in Ω_i, obtained by substituting eqn(12) into eqn(7), is

$$\begin{aligned}\sigma_i &= \sigma^{\circ} + \sigma_i^{r} \\ &= \sigma^{\circ} + \sum_j \mathbf{G}_{ij}\mathbf{p}_j + \sum_k (\mathbf{G}_{ik} + \sum_j \mathbf{G}_{ij}\mathbf{R}_{jk})\varepsilon_k^{p}\end{aligned} \tag{13}$$

In the above equation, the term of $\sum \mathbf{G}_{ij}\mathbf{p}_j$ is a modification to the effect of the applied load σ° and $\sum \mathbf{G}_{ij}\mathbf{R}_{jk}$ the one to the matrix $\mathbf{G}_{ik}$ of the residual stress influence coefficients due to the inhomogeneity.

If there is only the stress component σ_{22}° applied, then it is denoted in eqn(13) that

$$\sigma^{\circ} + \sum_j \mathbf{G}_{ij}\mathbf{p}_j = \overline{\mathbf{p}}_i\sigma_{22}^{\circ}$$

and

$$\overline{\mathbf{G}}_{ik} = \mathbf{G}_{ik} + \sum_j \mathbf{G}_{ij}\mathbf{R}_{jk}$$

Eqn(13) becomes

$$\sigma_i = \overline{\mathbf{p}}_i\sigma_{22}^{\circ} + \sum_k \overline{\mathbf{G}}_{ik}\varepsilon_k^{p}$$

For slip system $\alpha\beta$ in element Ω_i, the following relations hold

$$\varepsilon_i^{p} = \mathbf{m}_{\alpha\beta}\mathrm{e}_{\alpha\beta i}^{p}$$

$$\tau_{\alpha\beta i} = \mathbf{n}_{\alpha\beta}^{T}\sigma_j$$

where $e^{p}_{\alpha\beta i}$ and $\tau_{\alpha\beta i}$ are the plastic shear strain and resolved shear stress, respectively, and

$$\mathbf{m}_{\alpha\beta} = \{m_{11},\ m_{22},\ m_{33},\ m_{23},\ m_{13},\ m_{12}\}^{T}_{\alpha\beta}$$

$$\mathbf{n}_{\alpha\beta} = \{n_{11},\ n_{22},\ n_{33},\ n_{23},\ n_{13},\ n_{12}\}^{T}_{\alpha\beta}$$

in which m_{ij} and n_{ij} are composed of direction cosines of slip system $\alpha\beta$. The total resolved shear stress in the slip system is

$$\tau_{\alpha\beta i} = \tau^{I}_{\alpha\beta i} + \tau^{A}_{\alpha\beta i} + \tau^{R}_{\alpha\beta i}$$

where

$$\tau^{A}_{\alpha\beta i} = \mathbf{n}^{T}_{\alpha\beta}\,\bar{\mathbf{p}}_i \sigma^{\circ}_{22} = s_{\alpha\beta i}\sigma^{\circ}_{22}$$

$$\tau^{R}_{\alpha\beta i} = \sum_{k}\sum_{\xi\eta} G(\alpha\beta,\Omega_j\ ;\ \xi\eta,\Omega_k)\, e^{p}_{\xi\eta k}$$

in which

$$G(\alpha\beta,\Omega_i\ ;\xi\eta,\Omega_k) = \mathbf{n}^{T}_{\alpha\beta}\bar{\mathbf{G}}_{ik}\mathbf{m}_{\xi\eta}$$

and the summation with regard to slip system $\xi\eta$ includes all the slip systems in k-th element in question.

$s_{\alpha\beta i}$ and $G(\alpha\beta,\Omega_i\,;\xi\eta,\Omega_j)$ are the modified Schmid factors and the residual stress influence coefficients , respectively, after transforming the inhomogeneous problem into a homogeneous one.

PHYSICAL MODEL AND NUMERICAL CALCULATION

A polycrystal model has been established to study the effect of crystal anisotropy and inhomogeneity on the fatigue crack initiation as shown in Fig. 1. An elastically anisotropic crystal is embedded near the free surface in a semi-infinite elastic medium. Since the orientations of surrounding crystals are random, it is assumed that the metal exterior to the surface crystal is isotropic and homogeneous. A fatigue band composed of three thin slices P, Q and R is in this surface crystal, which is taken as to be the most favorably-oriented with the primary slip system being 45° inclining to the load axis.

The elastic constants of a nickel-base superalloy Ni_3Al single crystal with cubic symmetry (Yang, 1985) are used in the numerical calculation. The elastic compliance moduli in $10^{-2}/GPa$ with respect to the crystal axes [001], [010] and [100] in the same notation as Yang's are

$$S_{11} = 1.01$$

$$S_{12} = -0.393$$

$$S_{44} = 0.848$$

The shear modulus for the isotropic and homogeneous material is 75 GPa, which is obtained by taking the average stress over a number of orientations of the single crystal corresponding to a given uniform strain, and the Poisson's ratio is 0.3.

In order to fit the geometry of the surface crystal and the fatigue band, a constant strain trapezoidal element in general and a linear strain element for the fatigue band in particular are developed to calculate the residual stress influence coefficients for the generalized plane strain problem. The area of

the surface crystal is divided into 50 constant strain elements and each slice of P, Q and R into 12 linear strain elements.

With the method described previously, the modified Schmid factor varying along slice P is shown in Fig. 2. Compared with the case without considering the crystal anisotropy where the Schmid factor is uniformly 0.5, the anisotropy and inhomogeneity lower this value. Since the slip theory is used in this study, the slip system in which the total resolved shear stress reaches the critical shear stress τ^c may slide first. Therefore, the sliding starts inside the band, where the modified Schmid factor takes the maximum value. The development of fatigue band depends upon the irreversibility of the plastic shear deformations in P and Q. This irreversibility of sliding in the fatigue band is caused by an initial stress field τ^I, which is induced by an initial strain field (Lin and Lin, 1983). In the numerical calculations, the initial stress τ^I is 0.5 MPa. The critical shear stress τ^c is taken as 200MPa and the applied loading magnitude τ^A is 480MPa. Since the sliding outside the fatigue band is reversible during the cyclic loading process, the plastic deformation concentrates in the fatigue band. Fig. 3 shows the extrusion growth of the fatigue band with cycles of loading. The plastic shear strain distributions in P and Q are plotted at various loading cycles in Fig. 4.

CONCLUDING REMARKS

A generalized Eshelby's Equivalent Inclusion Method is developed to study the effect of the elastic anisotropy of crystals on the crack initiation of polycrystalline metals. Since this is a local effect, the results depend on the elastic properties of both the surface crystal and the surrounding metal. In this study, the elastic constants for the surrounding metal are of the upper bound by nature. The selection of these elastic constants should reflect the average effect of the surrounding material on the surface crystal. A more realistic model which incorporates the surrounding crystals with different orientations is being developed to study this effect.

ACKNOWLEDGMENT

The research was supported by the U. S. Air Force Office of Scientific Research Grant F49620-92-0171. The interest of Dr. Jim Chang, Dr. Walter Jones and Dr. Spencer Wu is gratefully acknowledged.

REFERENCES

Eshelby, J. D., 1957, " The Determination of the Elastic Field of an Ellipsoidal, and Related Problems," *Proc. Roy. Soc.*, Vol. A241, pp. 376-396.

Eshelby, J. D., 1961, " Elastic Inclusions and Inhomogeneities," *Progress in Solid Mechanics* 2, I. N. Sneddon and R. Hill, ed., Horth-Holland, Amsterdam, pp. 89-140.

Lin, T. H., 1969, *Theory of Inelastic Structures,* Wiley, New York, pp. 44-48.

Lin, T. H., 1992, "Micromechanics of Crack Initiation in High-Cycle Fatigue," *Advances in Applied Mechanics,* Vol. 29, pp. 1-62.

Lin, T. H. and Ito, Y. M., 1969, " Micromechanics of a Fatigue Crack Nucleation Mechanism," *J. Mech. Phys. Solids*, Vol. 17, pp. 511-523.

Lin, S. R. and Lin, T. H., 1983, "Initial Strain Field and Fatigue Crack Initiation Mechanics," *ASME J. Appl. Mech.*, Vol. 50, pp. 367-372.

Mura, T., 1982, *Micromechanics of Defects in Solids,* Martinus Nijhoff Publishers.

Yang, S. M., 1985, "Elastic Constants of a Monocrystalline Nickel-Base Superalloy," *Metall. Trans.*, Vol. 16A, pp.661-665.

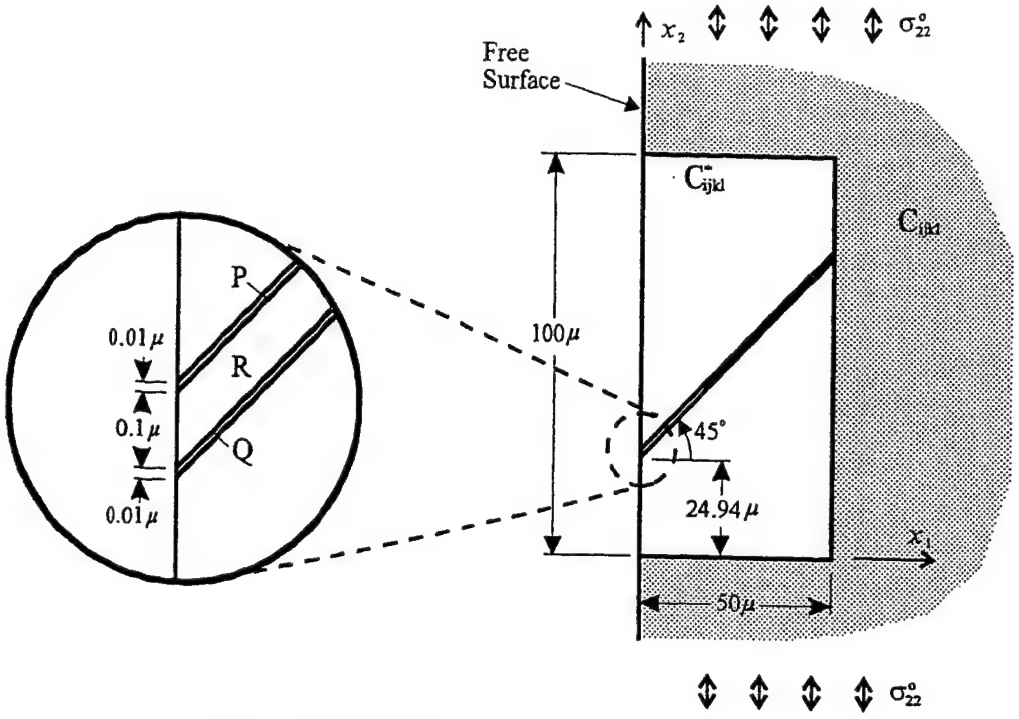

Fig. 1 Fatigue Band in an Anisotropic Surface Crystal

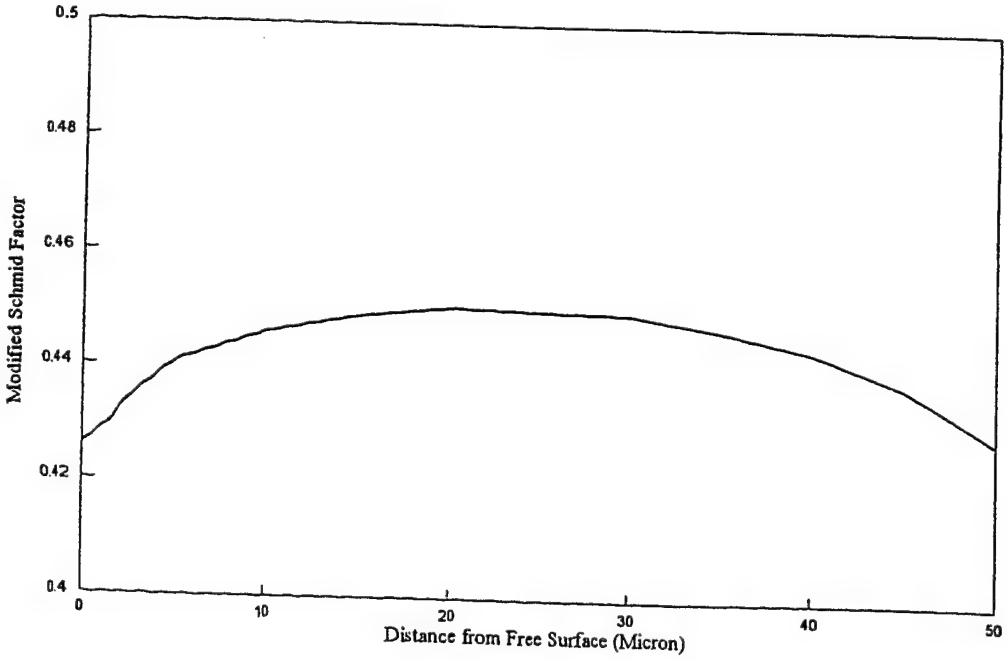

Fig. 2 Modified Schmid Factor Varying along P

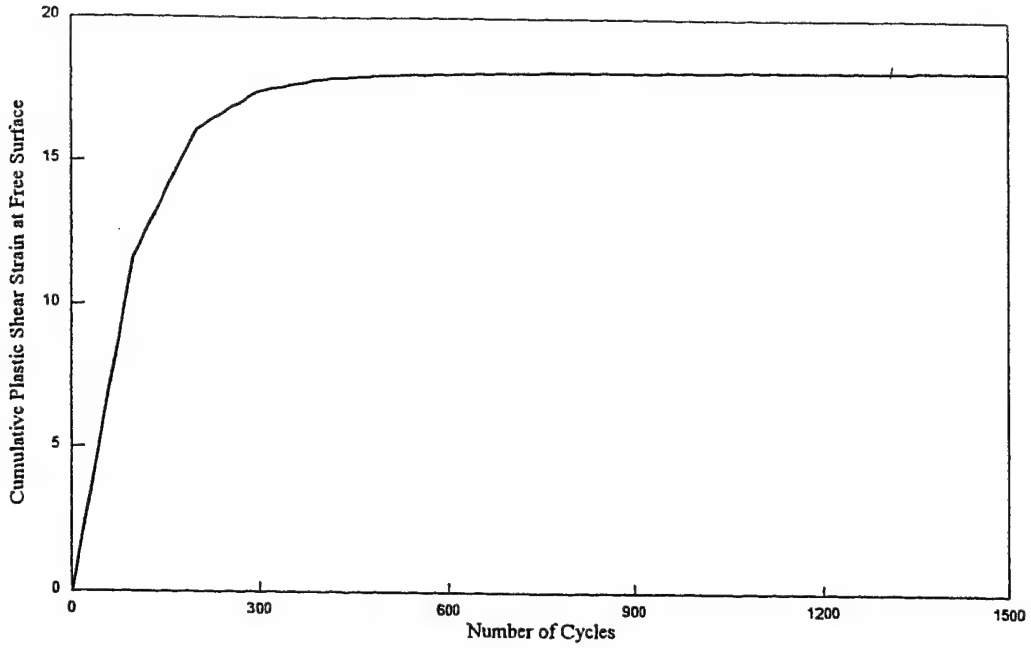

Fig. 3 Cumulative Plastic Shear Strain at the Free Surface in P vs. the Number of Cycles

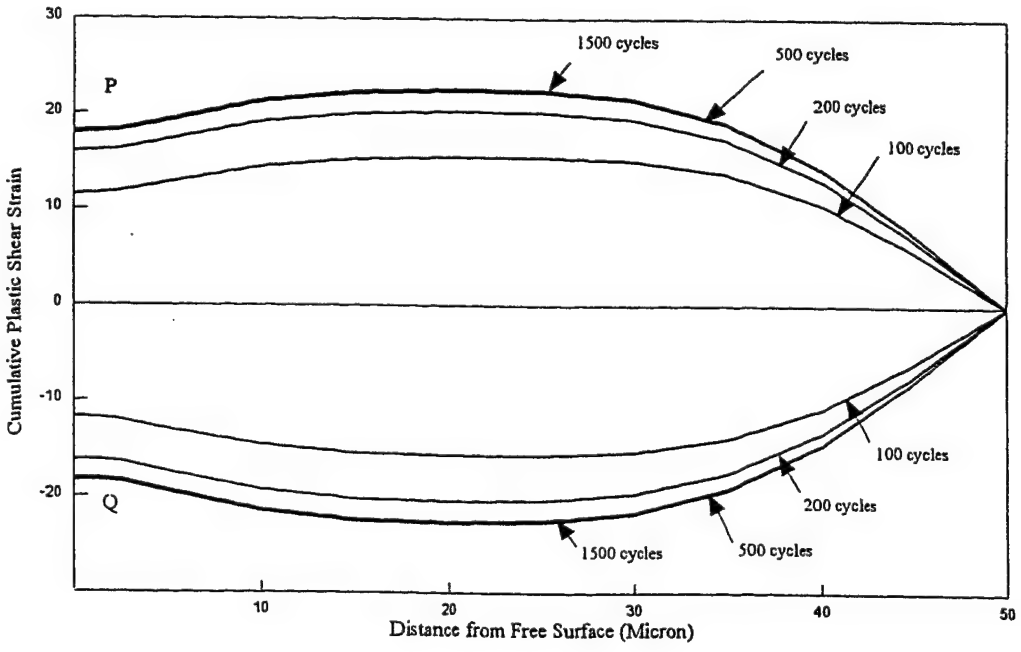

Fig. 4 Cumulative Plastic Strain Distributions in P and Q at Cycles of Loading

Elastic Anisotropy Effect of Crystals on Polycrystal Fatigue Crack Initiation

N. J. Teng

T. H. Lin

Department of Civil and Environmental Engineering,
University of California, Los Angeles,
Los Angeles, CA 90024

Fatigue bands have been observed in both monocrystalline and polycrystalline metals. Extrusions and intrusions at the free surface of fatigued specimens are favorable sites for fatigue crack nucleation. Previous studies (Lin and Ito, 1969; Lin, 1992) mainly concerned the fatigue crack initiation in aluminum and its alloys. The elastic anisotropy of individual crystals of these metals is insignificant and was accordingly neglected. However, the anisotropy of the elastic constants of some other metallic crystals, such as titanium and some intermetallic compounds, is not negligible. In this paper, the effect of crystal anisotropy is considered by using Eshelby's equivalent inclusion method. The polycrystal analyzed is Ni_3Al intermetallic compound. The plastic shear strain distributions and the cumulative surface plastic strain in the fatigue band versus the number of loading cycles were calculated, and the effect of crystal anisotropy on the growth of the extrusions was examined.

1 Introduction

The process of fatigue failure in ductile metals is divided into the following three stages: (1) the crack initiation, (2) the growth and coalescence of microcracks to form some macrocracks, and (3) the propagation of dominant cracks leading to the final catastrophic failure. In high-cycle fatigue, fatigue crack initiation predominates fatigue life. Fatigue bands are the favorable sites for the nucleation of fatigue microcracks.

Fatigue bands consist of highly localized plastic strains and have been observed in both single crystals and polycrystals. Plastic strains are mainly due to the movement of dislocations. Under the cyclic loading, the localized plastic deformation increases with the number of loading cycles and causes extrusions and intrusions at the free surface of metals. The height of extrusions or the depth of intrusions is here taken as a measure of fatigue damage.

A theory of micromechanics of fatigue crack initiation has been proposed to model the gating mechanism of fatigue bands in polycrystals (Lin and Ito, 1969; Lin, 1992). A fatigue band composed of three thin slices P, Q, and R in a most favorably oriented surface crystal was considered. Under cyclic tension and compression loading, the alternate monotonic build-up of plastic shear strains in both P and Q causes the growth of extrusions or intrusions at the free surface of polycrystals. Since this model is concerned mainly with the fatigue crack initiation of aluminum and its alloys, the elastic anisotropy of their individual crystals is insignificant and accordingly neglected. Hence the surface crystal is assumed to be embedded in an elastically isotropic and homogeneous semi-infinite medium. For some other polycrystalline metals, such as titanium and some intermetalic superalloys, however, the elastic anisotropy of crystals is not negligible. For such polycrystals, the local microstress field in a crystal depends not only on the applied stresses but also on the orientations of its surrounding crystals. Hence the elastic anisotropy of crystals will affect the fatigue crack initiation in these metals.

In this paper, the elastic anisotropy of individual grains in a polycrystal is considered. A fatigue band is assumed to occur in the most favorably oriented surface crystal. This crystal is surrounded by the crystals of various given orientations. The crystals outside the surrounding crystals are randomly oriented and assumed to be isotropic and homogeneous. Hence this surface crystal and the surrounding crystals of given orientations are considered to be embedded in a semi-infinite isotropic and homogeneous elastic medium. Thus it becomes an inclusion problem. This heterogeneous solid is transformed into a homogeneous one by using Eshelby's equivalent inclusion method (Eshelby, 1957, 1961; Mura, 1982). In this method, an extra set of eigenstrains is introduced. These eigenstrains can be explicitly expressed in terms of the applied stresses and plastic strains. After this transformation, the procedures for this micromechanical analysis are the same as those given by Lin (1992) for elastically isotropic polycrystals. In the following numerical calculation, the anisotropic elastic constants of Ni_3Al monocrystalline intermetallic compound (Yang, 1985) were used. The isotropic elastic constants of the surrounding metal were taken from the experimental data (Stoloff, 1989). The plastic strain distributions and the cumulative surface plastic strains in the fatigue band versus the number of loading cycles were calculated, and the effect of elastic anisotropy on the formation of extrusions and intrusions was examined.

2 Gating Mechanism Provided by Microstress Field

Single crystal tests show that slip occurs on certain crystallographic planes along certain directions. This slip depends on the resolved shear stress in the slip system and is independent of the normal stress on the sliding plane. The dependence of slip on the resolved shear stress is known as the Schmid law. It has been shown that the Schmid law also holds when crystalline solids are subjected to cyclic loading (Parker, 1961). For a face-centered cubic crystal (FCC), there are four slip planes, on each of which, there are three slip systems. These twelve slip systems are shown in Fig. 1.

All metals have initial defects, hence, have initial stresses. These initial stresses play an important role in fatigue crack initiation. Lin and Ito (1969) first point out that the initial stress field favorable to extrusions and intrusions can be caused by a row of dislocation dipoles. Later, these dislocation dipoles have been observed in the ladder structure in a persistent slip band (PSB) (Antonopoulos, 1976; Mughrabi, 1982). These dipoles induce initial resolved shear stresses at the interface between the PSB and the matrix.

Based on experimental observations, a micromechanic theory of fatigue crack initiation was proposed by Lin and Ito (1969).

Contributed by the Materials Division for Publication in the JOURNAL OF ENGINEERING MATERIALS AND TECHNOLOGY. Manuscript received by the Materials Division June 3, 1995. Associate Technical Editor: G. J. Weng.

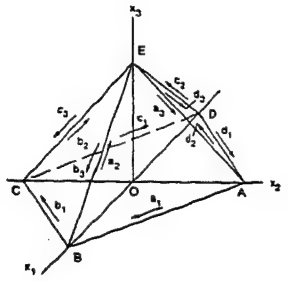

Slip Systems and Their Directions

Slip System	Slip Plane	Slip Directon
a_1		[1 $\bar{1}$ 0]
a_2	(1 1 1)	[$\bar{1}$ 0 1]
a_3		[0 1 $\bar{1}$]
b_1		[$\bar{1}$ $\bar{1}$ 0]
b_2	(1 $\bar{1}$ 1)	[0 1 1]
b_3		[1 0 $\bar{1}$]
c_1		[$\bar{1}$ 1 0]
c_2	($\bar{1}$ $\bar{1}$ 1)	[1 0 1]
c_3		[0 $\bar{1}$ $\bar{1}$]
d_1		[1 1 0]
d_2	($\bar{1}$ 1 1)	[0 $\bar{1}$ 1]
d_3		[$\bar{1}$ 0 $\bar{1}$]

Fig. 1 Crystallographic slip planes and directions of FCC crystals

In this model, a most-favorably oriented surface crystal containing a fatigue band composed of three thin slices P, Q, and R in a semi-infinite polycrystal shown in Fig. 2 is considered. The slip plane and slip direction of the primary slip system $\alpha\beta$ form an angle of 45 deg with the loading axis. Lin and Lin (1983) have calculated a uniform initial resolved shear stress field τ^I, positive in P and negative in Q, caused by a distribution of plastic strains. This initial stress field satisfies the conditions of both compatibility and equilibrium. During the cyclic loading, plastic strains occur in P, Q and R and cause a residual stress field. The total resolved shear stress τ in a slip system is the sum of three stresses as

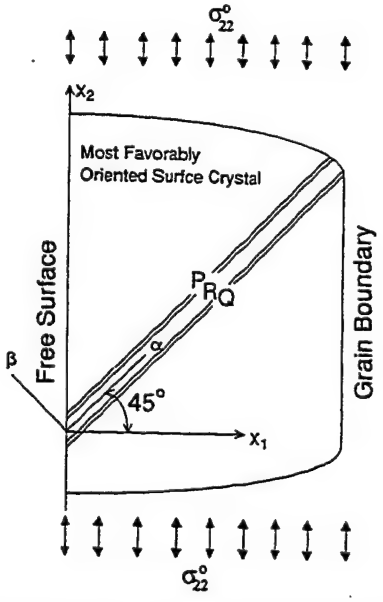

Fig. 2 Fatigue band in the most favorably oriented surface crystal

$$\tau = \tau^A + \tau^I + \tau^R$$

where τ^A is the resolved shear stress caused by the applied load and τ^R the residual resolved shear stress due to plastic strains.

A tensile loading σ^0_{22} on the polycrystal produces a positive τ^A in the entire surface crystal. Since τ^I in P is positive, the total resolved shear stress τ in P, which is $\tau^A + \tau^I$, reaches the critical shear stress τ^C first; and hence, according to Schmid law, P slides. The plastic shear strain caused by this slip in P produces a residual stress field τ^R, which has negative resolved shear stress in Q and makes Q to slide more readily in the reverse loading. The negative slip in Q induces in turn a positive residual resolved shear stress τ^R in P making P more readily to slide under the next tensile loading. This process is repeated during the cyclic loading for every cycle thus providing a natural gating mechanism for a monotonic buildup of local resolved plastic shear strain $\epsilon^p_{\alpha\beta}$ in both P and Q, pushing R out of the free surface and promoting an extrusion. The elongation of R may activate a secondary slip system to slide. The effect of slip in the secondary slip system enhances the extent of extrusion (Lin, et al., 1989). Interchanging the signs of the initial stresses in P and Q initiates an intrusion instead of an extrusion. This micromechanical theory on fatigue crack initiation has overwhelming metallurgical experimental evidences (Lin, 1977).

3 Calculation of Residual Stress Field

3.1 Residual Stress Field. The residual stress field due to a distribution of inelastic strains can be calculated by the analogy between inelastic strains and applied forces (Lin, 1969). It has been shown that the equivalent body force per unit volume along the x_i-axis due to inelastic strains ϵ''_{ij} is

$$\bar{F}_i = -C_{ijkl}\epsilon''_{kl,j} \tag{1}$$

where C_{ijkl} is the elastic modulus. The summation convention is used here and the subscript after a comma denotes the differentiation with respect to the coordinate variable. For isotropic elastic solids, the elastic constants are

$$C_{ijkl} = \lambda\delta_{ij}\delta_{kl} + \mu(\delta_{ik}\delta_{jl} + \delta_{il}\delta_{jk})$$

where λ and μ are Lame's constants and δ_{ij} is the Kronecker delta. The equivalent surface force per unit area along the x_i-axis has been shown as

$$\bar{S}_i = C_{ijkl}\epsilon''_{kl}\nu_j \tag{2}$$

where ν_j is the direction cosine of the normal to the area. The fictitious stresses $\sigma^s_{ij}(\mathbf{x})$ at point $\mathbf{x}$ caused by equivalent forces in domain Ω can be written by using the Green's function as

$$\sigma^s_{ij}(\mathbf{x}) = \int_\Omega \tau^k_{ij}(\mathbf{x}, \mathbf{x}')\bar{F}_k(\mathbf{x}')d\Omega + \int_\Gamma \tau^k_{ij}(\mathbf{x}, \mathbf{x}')\bar{S}_k(\mathbf{x}')d\Gamma$$

$$= -C_{klmn}\int_\Omega \tau^k_{ij}(\mathbf{x}, \mathbf{x}')\epsilon''_{mn,l}(\mathbf{x}')d\Omega$$

$$+ C_{klmn}\int_\Gamma \tau^k_{ij}(\mathbf{x}, \mathbf{x}')\epsilon''_{mn}(\mathbf{x}')\nu_l d\Gamma \tag{3}$$

where $\tau^k_{ij}(\mathbf{x}, \mathbf{x}')$ represents the stress component σ_{ij} at point $\mathbf{x}$ induced by a unit force acting at point $\mathbf{x}'$ along the x_k-axis. Γ is the boundary of domain Ω. If inelastic strain components of $\epsilon''_{mn}(\mathbf{x})$ are constant in Ω, eqn (3) is reduced to

$$\sigma^s_{ij}(\mathbf{x}) = C_{klmn}\left\{\int_\Gamma \tau^k_{ij}(\mathbf{x}, \mathbf{x}')\nu_l d\Gamma\right\}\epsilon''_{mn}(\Omega) \tag{4}$$

where $\epsilon''_{mn}(\Omega)$ is the constant inelastic strain in Ω. The residual stress field is

$$\sigma^r_{ij}(\mathbf{x}) = \sigma^s_{ij}(\mathbf{x}) - C_{ijkl}\epsilon''_{kl}(\mathbf{x}) \tag{5}$$

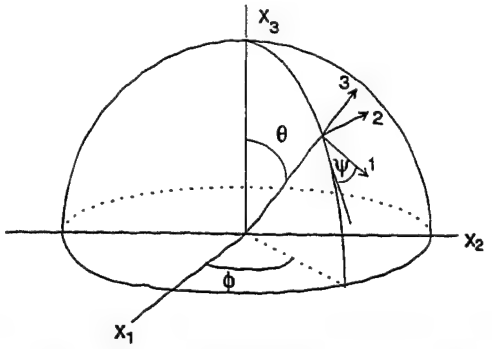

Fig. 3 Euler angles and representation of crystal orientations

3.2 Residual Stress Influence Coefficient. To calculate the residual stress field numerically, the discretization of a continuous problem is needed. In the following, the domain Ω in an extended solid is divided into a number of subdomains or elements Ω_q. In each of them, it is assumed that the inelastic strain ϵ''_{ij} is uniform. After applying Eqs. (4) and (5) to Ω_q, the residual stress field due to $\epsilon''_{mn}(\mathbf{x}')(\mathbf{x}' \in \Omega_q)$ is

$$\sigma^r_{ij}(\mathbf{x}) = \left\{ \int_{\Gamma_q} C_{klmn} \tau^k_{ij}(\mathbf{x}, \mathbf{x}') \nu_l d\Gamma_q - H(\mathbf{x}, \Omega_q) C_{ijmn} \right\} \epsilon''_{mn}(\Omega_q) \quad (6)$$

where the function $H(\mathbf{x}, \Omega_q)$ is defined as

$$H(\mathbf{x}, \Omega_q) = \begin{cases} 1, & \mathbf{x} \in \Omega_q \\ 0, & \mathbf{x} \notin \Omega_q \end{cases}$$

Generally, residual stress field $\sigma^r_{ij}(\mathbf{x})$ varies from one point to another. The volume average of $\sigma^r_{ij}(\mathbf{x})$ over subdomain Ω_p is taken to represent the residual stresses in element Ω_p. Letting $\sigma^r_{ij}(\Omega_p)$ represent the residual stresses in Ω_p due to ϵ''_{mn} in Ω_q, we have

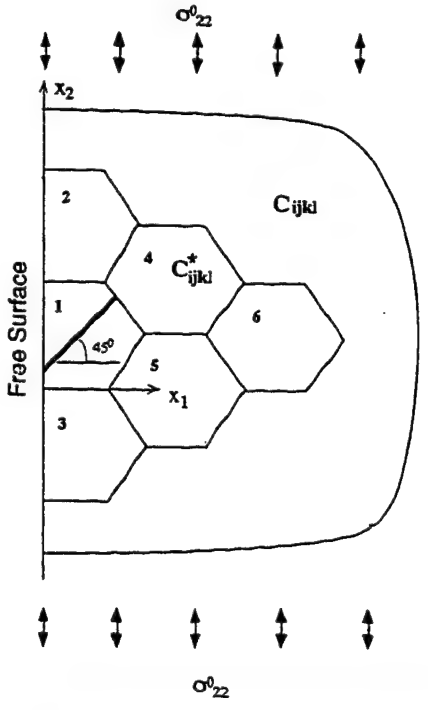

Fig. 4 Polycrystal model of fatigue crack initiation

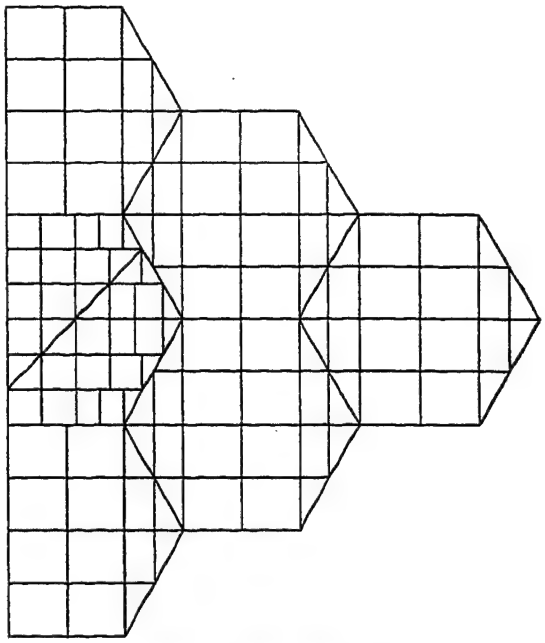

Fig. 5 Layout of elements

$$\sigma^r_{ij}(\Omega_p) = G_{ijmn}(\Omega_p, \Omega_q) \epsilon''_{mn}(\Omega_q) \quad (7)$$

where $G_{ijmn}(\Omega_p, \Omega_q)$ are called the residual stress influence coefficients, which represent the residual stresses in subdomain Ω_p caused by unit inelastic strain components in subdomain Ω_q.

For the resolved residual shear stress $\tau^r_{\alpha\beta}$ in slip system $\alpha\beta$ in Ω_p due to the resolved plastic shear strain $e^p_{\xi\eta}$ in slip system $\xi\eta$ in Ω_q, Eq. (7) can be rewritten by the tensor transformation as

$$\tau^r_{\alpha\beta}(\Omega_p) = G(\alpha\beta, \Omega_p; \xi\eta, \Omega_q) e^p_{\xi\eta}(\Omega_q) \quad (8)$$

where $G(\alpha\beta, \Omega_p; \xi\eta, \Omega_q)$ represents the residual resolved shear stress in slip system $\alpha\beta$ in Ω_p caused by a unit resolved plastic shear strain in slip system $\xi\eta$ in Ω_q. The total resolved shear stress $\tau_{\alpha\beta}$ in slip system $\alpha\beta$ in Ω_p is

$$\tau_{\alpha\beta}(\Omega_p) = \tau^I_{\alpha\beta} + \tau^{\wedge}_{\alpha\beta} + \sum_q \sum_{\xi\eta} G(\alpha\beta, \Omega_p; \xi\eta, \Omega_q) e^p_{\xi\eta} \quad (9)$$

The summation with regard to slip system $\xi\eta$ includes all the slip systems in Ω_q.

3.3 Generalized Plane Strain Problem. The thickness of fatigue bands is much smaller than the length (dimension along the x_3-axis) as observed at the free surface of metals. Therefore, the problem is considered under the plane strain deformation. The plastic strain due to slip in the secondary slip system is not confined to the x_1x_2 plane. This causes an equivalent force component F_3 acting along the x_3-direction. The existence of this F_3 requires a modification of the plane strain problem. Hence, the generalized plane strain problem is considered in the present study. A similar problem is shown in the analysis of prismatic anisotropic bars by Lekhnitski (1963). This generalized plane strain deformation is defined as

$$u_i = u_i(x_1, x_2), \quad i = 1, 2, 3$$

where u_i is the displacement component along x_i-axis. This gives

$$\sigma_{ij} = 2\mu \left\{ \frac{\nu}{1 - 2\nu} \delta_{ij} \theta + \frac{1}{2} (u_{i,j} + u_{j,i}) \right\}$$

where $\theta = u_{1,1} + u_{2,2}$ and ν is the Poisson's ratio. The equilib-

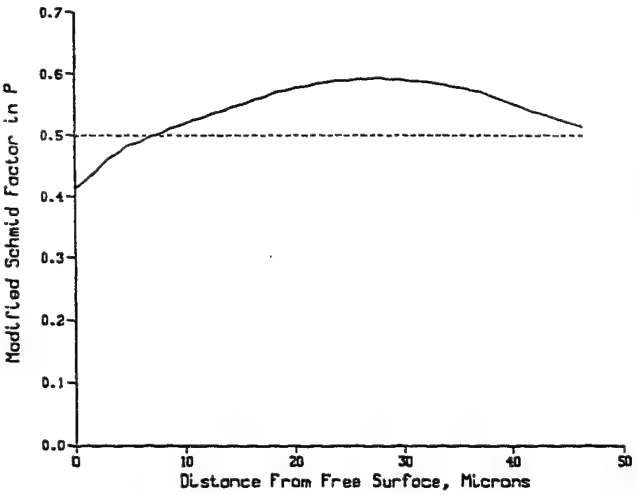

Fig. 6 Modified Schmid factor varying along slice P

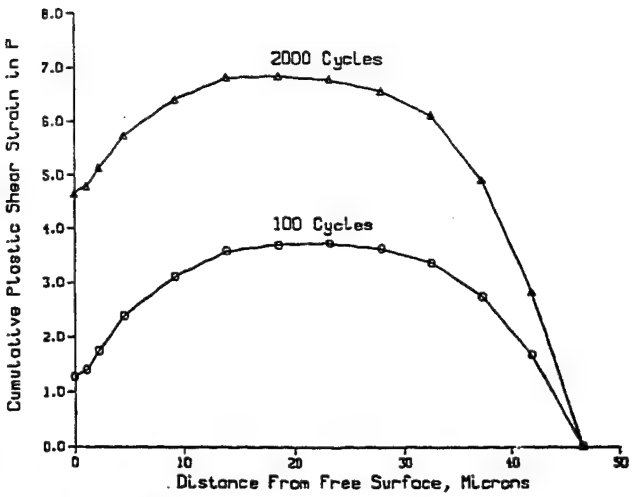

Fig. 8 Plastic shear strain distributions in P at 100 cycles and 2000 cycles

rium equations in terms of displacement components u_i can be expressed as

$$\nabla^2 u_i + \frac{1}{1-2\mu}\frac{\partial \theta}{\partial x_i} + \frac{F_i}{\mu} = 0, \quad i = 1, 2 \qquad (10)$$

and

$$\nabla^2 u_3 + \frac{F_3}{\mu} = 0 \qquad (11)$$

where

$$\nabla^2 = \frac{\partial^2}{\partial x_1^2} + \frac{\partial^2}{\partial x_2^2}$$

and F_i is the body force component. Equations (10) and (11) are not coupled and can be solved separately.

The stress components $\tau_{ij}^k(\mathbf{x}, \mathbf{x}')$ in Eq. (3) for the semi-infinite medium with the generalized plane strain deformation have been expressed in terms of the Airy's stress functions (Lin and Lin, 1974) as

$$\tau_{11}^k(\mathbf{x}, \mathbf{x}') = \frac{\partial^2 \phi_k}{\partial x_2^2}, \quad \tau_{22}^k(\mathbf{x}, \mathbf{x}') = \frac{\partial^2 \phi_k}{\partial x_1^2},$$

$$\tau_{12}^k(\mathbf{x}, \mathbf{x}') = -\frac{\partial^2 \phi_k}{\partial x_1 \partial x_2}, \tau_{33}^k(\mathbf{x}, \mathbf{x}') = \nu \nabla^2 \phi_k,$$

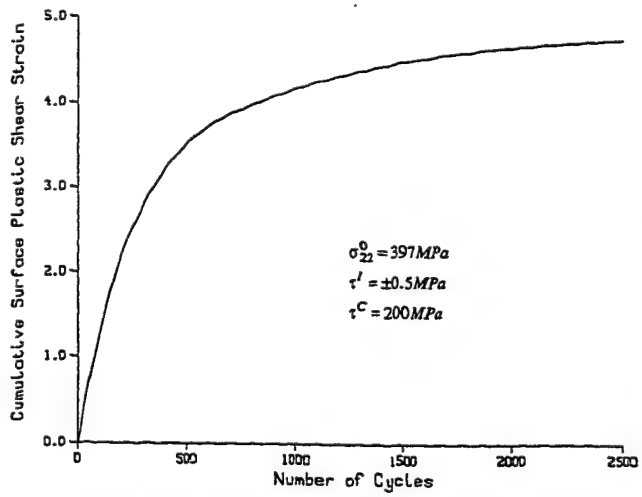

Fig. 7 Plastic shear strain at free surface versus number of cycles

$$\tau_{13}^k(\mathbf{x}, \mathbf{x}') = \tau_{23}^k(\mathbf{x}, \mathbf{x}') \equiv 0, \quad k = 1, 2 \qquad (12)$$

and

$$\tau_{13}^3(\mathbf{x}, \mathbf{x}') = \frac{\partial \phi_3}{\partial x_1}, \quad \tau_{23}^3(\mathbf{x}, \mathbf{x}') = \frac{\partial \phi_3}{\partial x_2},$$

$$\tau_{ij}^3(\mathbf{x}, \mathbf{x}') \equiv 0, \quad \text{for other } i \text{ and } j \qquad (13)$$

where the Airy's stress functions are

$$\phi_1(\mathbf{x}, \mathbf{x}') = -(p+q)(x_2 - x_2')(\theta_1 + \theta_2) + \tfrac{1}{2}q(x_1 - x_1')\ln(X_1/X_2) + 2px_1x_1'(x_1 + x_1')/X_2$$

$$\phi_2(\mathbf{x}, \mathbf{x}') = (p+q)(x_2 - x_2')(\theta_1 + \theta_2) + \tfrac{1}{2}q(x_2 - x_2')\ln(X_1/X_2) - 2px_1x_1'(x_2 - x_2')/X_2$$

$$\phi_3(\mathbf{x}, \mathbf{x}') = -\frac{1}{4\pi}(\ln X_1 + \ln X_2)$$

with

$$p = \frac{1}{4\pi(1-\nu)}, \quad q = p(1-2\nu)$$

$$\theta_1 = \arctan\left(\frac{x_2 - x_2'}{x_1 - x_1'}\right), \quad -\pi \le \theta_1 < \pi$$

$$\theta_2 = \arctan\left(\frac{x_2 - x_2'}{x_1 + x_1'}\right), \quad -\frac{\pi}{2} \le \theta_2 < \frac{\pi}{2}$$

$$X_1 = (x_1 - x_1')^2 + (x_2 - x_2')^2,$$

$$X_2 = (x_1 + x_1')^2 + (x_2 - x_2')^2$$

By using Eqs. (6), (12) and (13), the residual stresses as well as the residual stress influence coefficients due to the inelastic strains in the element of a specific shape can be readily calculated.

4 Generalization of Equivalent Inclusion Method

Eshelby's equivalent inclusion method (Eshelby, 1957, 1961) is here used to transform an inhomogeneous problem into a homogeneous one by introducing a distribution of eigenstrains (Mura, 1982). Originally, this method was applied to solve the problems with an ellipsoidal inhomogeneity. In the present study, this method is generalized to solve inhomogeneous problems of arbitrary shapes.

In the following, the matrix and vector notation will be used instead of tensor notation for convenience. It is easy to contract a second-order tensor with components G_{ijkl} into a matrix with entries G_{ij} by setting, for instance, $G_{11} = G_{1111}$, $G_{12} = G_{1122}$, $G_{16} = G_{1112} + G_{1121}$ and $G_{61} = G_{1211}$, etc. Vectors are denoted by boldface lowercase Roman or Greek letters and matrices by boldface uppercase Roman letters. The Eshelby's equivalent equation is

$$\mathbf{C}^*(\mathbf{x})[\boldsymbol{\epsilon}^0 + \boldsymbol{\epsilon}(\mathbf{x}) - \boldsymbol{\epsilon}^p(\mathbf{x})] = \mathbf{C}[\boldsymbol{\epsilon}^0 + \boldsymbol{\epsilon}(\mathbf{x}) - \boldsymbol{\epsilon}^*(\mathbf{x}) - \boldsymbol{\epsilon}^p(\mathbf{x})], \mathbf{x} \in \Omega \quad (14)$$

where Ω is an inclusion or a subdomain with the elastic constant $\mathbf{C}^*(\mathbf{x})$ embedded in an extended body D with the isotropic elastic constant $\mathbf{C}$. $\boldsymbol{\epsilon}(\mathbf{x})$ is the disturbance strain, $\boldsymbol{\epsilon}^*(\mathbf{x})$ the eigenstrain, $\boldsymbol{\epsilon}^p(\mathbf{x})$ the plastic strain and $\boldsymbol{\epsilon}^0$ uniform strain from which $\boldsymbol{\sigma}^0 = \mathbf{C}\boldsymbol{\epsilon}^0$ where $\boldsymbol{\sigma}^0$ is the applied far-field stress. The stress $\boldsymbol{\sigma}$ and strain $\boldsymbol{\epsilon}$ are vectors expressed as

$$\boldsymbol{\sigma} = \{\sigma_{11}, \sigma_{22}, \sigma_{33}, \sigma_{23}, \sigma_{13}, \sigma_{12}\}^T$$

$$\boldsymbol{\epsilon} = \{\epsilon_{11}, \epsilon_{22}, \epsilon_{33}, \epsilon_{23}, \epsilon_{13}, \epsilon_{12}\}^T$$

where notation $\{\cdot\ \cdot\ \cdot\}^T$ represents the transposition. Equation (14) shows that the eigenstrain $\boldsymbol{\epsilon}^*(\mathbf{x})$ plays the same role as the plastic strain $\boldsymbol{\epsilon}^p(\mathbf{x})$ does in the homogeneous materials.

When a continuous problem is discretized for the purpose of numerical analysis, the domain of Ω is further divided into N subdomains $\Omega_i (1 \le i \le N)$ called elements, in each of which both the eigenstrain $\boldsymbol{\epsilon}^*$ and plastic strain $\boldsymbol{\epsilon}^p$ are assumed to be uniform. The stresses in element Ω_i caused by the unit eigenstrain $\boldsymbol{\epsilon}^*$ in element Ω_j are the same as those caused by the unit plastic strain $\boldsymbol{\epsilon}^p$. Thus the stress $\boldsymbol{\sigma}_i^r$ in Ω_i induced by both of the eigenstrains and plastic strains in all the elements is

$$\boldsymbol{\sigma}_i^r = \sum_j \mathbf{G}_{ij}\boldsymbol{\epsilon}_j^* + \sum_k \mathbf{G}_{ik}\boldsymbol{\epsilon}_k^p, \quad 1 \le i \le N \quad (15)$$

where

$$\boldsymbol{\epsilon}_j^* = \{\epsilon_{11}^*, \epsilon_{22}^*, \epsilon_{33}^*, \epsilon_{23}^*, \epsilon_{13}^*, \epsilon_{12}^*\}_j^T$$

$$\boldsymbol{\epsilon}_j^p = \{\epsilon_{11}^p, \epsilon_{22}^p, \epsilon_{33}^p, \epsilon_{23}^p, \epsilon_{13}^p, \epsilon_{12}^p\}_j^T$$

in Ω_j and $\mathbf{G}_{ij}$ are 6×6 matrices of the residual stress influence coefficients, which are contracted from $G_{klmn}(\Omega_i, \Omega_j)$.

For the generalized plane strain problem, u_3 does not vary along the x_3-direction. The total normal strain component ϵ_{33}^T is equal to zero. The strain component ϵ_{33}^0 is here taken to be zero.

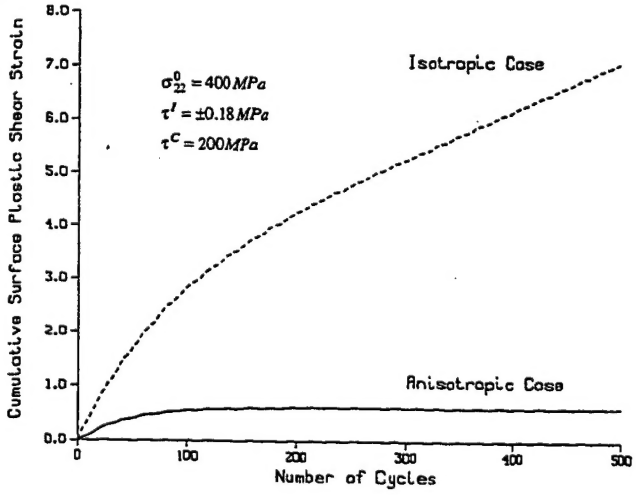

Fig. 9 Comparison of surface plastic strains with and without considering crystal anisotropy

Since the total strain ϵ_{33}^T is the sum of ϵ_{33}^0 and ϵ_{33}, hence $\epsilon_{33} \equiv 0$. The stress-strain relation may be given as

$$\boldsymbol{\sigma}_i^r = \bar{\mathbf{C}}\boldsymbol{\epsilon}_i - \mathbf{C}(\boldsymbol{\epsilon}_i^* + \boldsymbol{\epsilon}_i^p) \quad (16)$$

where

$$\bar{\mathbf{C}} = \begin{bmatrix} \lambda+2\mu & \lambda & 0 & 0 & 0 \\ \lambda & \lambda+2\mu & 0 & 0 & 0 \\ \lambda & \lambda & 0 & 0 & 0 \\ 0 & 0 & 2\mu & 0 & 0 \\ 0 & 0 & 0 & 2\mu & 0 \\ 0 & 0 & 0 & 0 & 2\mu \end{bmatrix},$$

$$\mathbf{C} = \begin{bmatrix} \lambda+2\mu & \lambda & \lambda & 0 & 0 & 0 \\ \lambda & \lambda+2\mu & \lambda & 0 & 0 & 0 \\ \lambda & \lambda & \lambda+2\mu & 0 & 0 & 0 \\ 0 & 0 & 0 & 2\mu & 0 & 0 \\ 0 & 0 & 0 & 0 & 2\mu & 0 \\ 0 & 0 & 0 & 0 & 0 & 2\mu \end{bmatrix}$$

and

$$\boldsymbol{\epsilon}_i = \{\epsilon_{11}, \epsilon_{22}, \epsilon_{23}, \epsilon_{13}, \epsilon_{12}\}_i^T \quad \text{with} \quad \epsilon_{33} \equiv 0$$

From Eqs. (15) and (16), expressing the disturbance strains $\boldsymbol{\epsilon}_i$ in Ω_i in terms of $\boldsymbol{\epsilon}_j^*$ and $\boldsymbol{\epsilon}_k^p$, we obtain

$$\boldsymbol{\epsilon}_i = \bar{\mathbf{C}}^{-1}[\mathbf{C}(\boldsymbol{\epsilon}_i^* + \boldsymbol{\epsilon}_i^p) + \sum_j \mathbf{G}_{ij}\boldsymbol{\epsilon}_j^* + \sum_k \mathbf{G}_{ik}\boldsymbol{\epsilon}_k^p], \quad 1 \le i \le N \quad (17)$$

where

$$\bar{\mathbf{C}}^{-1} = \frac{1}{\mathrm{E}} \begin{bmatrix} 1 & -\nu & -\nu & 0 & 0 & 0 \\ -\nu & 1 & -\nu & 0 & 0 & 0 \\ 0 & 0 & 0 & 1+\nu & 0 & 0 \\ 0 & 0 & 0 & 0 & 1+\nu & 0 \\ 0 & 0 & 0 & 0 & 0 & 1+\nu \end{bmatrix}$$

in which E is the Young's modulus.

The left-hand side of Eq. (14) can also be written for the generalized plane strain problems as

$$\boldsymbol{\sigma}_i = \boldsymbol{\sigma}_i^* + \bar{\mathbf{C}}^*\boldsymbol{\epsilon}_i - \mathbf{C}^*\boldsymbol{\epsilon}_i^p \quad (18)$$

where $\mathbf{C}^*$ is a 6×6 anisotropic elastic stiffness matrix and $\bar{\mathbf{C}}^*$ a 6×5 matrix formed from matrix $\mathbf{C}^*$ by taking the third column away. And $\boldsymbol{\sigma}_i^* = \bar{\mathbf{C}}^*\boldsymbol{\epsilon}^0$ in which

$$\epsilon^0 = \{\epsilon_{11}^0, \epsilon_{22}^0, \epsilon_{23}^0, \epsilon_{13}^0, \epsilon_{12}^0\}^T \quad \text{with} \quad \epsilon_{33}^0 \equiv 0$$

Substituting Eq. (17) into Eq. (18) and Eq. (15), Eq. (14) becomes

$$\mathbf{T}\boldsymbol{\epsilon}_i^* + \sum_j \mathbf{S}_{ij}\boldsymbol{\epsilon}_j^* = \mathbf{q}_i + (\mathbf{C}^* - \mathbf{T})\boldsymbol{\epsilon}_i^p - \sum_k \mathbf{S}_{ik}\boldsymbol{\epsilon}_k^p, \quad 1 \le i \le N \quad (19)$$

where

$$\mathbf{T} = \bar{\mathbf{C}}^*\bar{\mathbf{C}}^{-1}\mathbf{C}$$

$$\mathbf{S}_{ij} = (\bar{\mathbf{C}}^*\bar{\mathbf{C}}^{-1} - \mathbf{I})\mathbf{G}_{ij}$$

$$\mathbf{q}_i = \boldsymbol{\sigma}^0 - \boldsymbol{\sigma}_i^*$$

$$\boldsymbol{\sigma}^0 = \bar{\mathbf{C}}\boldsymbol{\epsilon}^0$$

and $\mathbf{I}$ is a 6×6 unit matrix.

It can be seen that eigenstrains $\boldsymbol{\epsilon}_i^*$ depend on the applied load $\boldsymbol{\sigma}^0$ and the distribution of plastic strains $\boldsymbol{\epsilon}_k^p$ as well. Equation (19) is a set of linear algebraic equations with unknowns

ϵ_i^*. Solving these equations for ϵ_i^* in all elements Ω_i, we can express ϵ_i^* as

$$\epsilon_i^* = \mathbf{p}_i + \sum_k \mathbf{R}_{ik}\epsilon_k^p, \quad 1 \le i \le N \tag{20}$$

where $\mathbf{p}_i$ is a vector in terms of σ^0 in Ω_i and $\mathbf{R}_{ik}$ is the matrix relating the plastic strains ϵ_k^p in Ω_k to the eigenstrains ϵ_i^* in Ω_i. The total stress in Ω_i, obtained by substituting Eq. (20) into Eq. (15), is

$$\sigma_i = \sigma^0 + \sigma_i^r$$
$$= \sigma^0 + \sum_j \mathbf{G}_{ij}\mathbf{p}_j + \sum_k (\mathbf{G}_{ik} + \sum_j \mathbf{G}_{ij}\mathbf{R}_{jk})\epsilon_k^p \tag{21}$$

In the above equation, the term of $\Sigma\, \mathbf{G}_{ij}\mathbf{p}_j$ is a modification to the effect of the applied load σ^0 and $\Sigma\, \mathbf{G}_{ij}\mathbf{R}_{jk}$ the one to the matrix $\mathbf{G}_{ik}$ of the residual stress influence coefficients due to the inhomogeneity.

Under the stress component σ_{22}^0 alone, Eq. (21) reduces to

$$\sigma_i = \bar{\mathbf{p}}_i\sigma_{22}^0 + \sum_k \bar{\mathbf{G}}_{ik}\epsilon_k^p$$

where

$$\bar{\mathbf{p}}_i\sigma_{22}^0 = \sigma^0 + \sum_j \mathbf{G}_{ij}\mathbf{p}_j$$

and

$$\bar{\mathbf{G}}_{ik} = \mathbf{G}_{ik} + \sum_j \mathbf{G}_{ij}\mathbf{R}_{jk}$$

For slip system $\alpha\beta$ in element Ω_i, we have

$$\epsilon_i^p = \mathbf{m}_{\alpha\beta}e_{\alpha\beta i}^p$$

forming the inhomogeneous problem into a homogeneous one. The summation with regard to slip system $\xi\eta$ includes all the slip systems in kth element. It can be seen that Eq. (22) corresponds to Eq. (9).

5 Effect of Crystal Elastic Anisotropy on Fatigue Crack Initiation in Polycrystals

5.1 Elastic Constants of Monocrystalline and Polycrystalline Crystals. In the present study, nickel-base superalloy polycrystals of FCC structure are taken for the numerical analysis. Fatigue crack initiation of other materials can be analyzed by the same approach.

There are many experimental data available for nickel-base superalloy single crystals in the literature. Since the alloy compositions vary with different materials tested, the elastic constants obtained may slightly differ from each other. In the following analysis, the elastic constants of a nickel-base superalloy Ni_3Al single crystal given by Yang (1985) are used. The elastic compliance moduli in $10^{-2}/GPa$ with respect to the crystal axes [001], [010] and [100] in the same notation as Yang's are

$$S_{11} = S_{1111} = 1.01$$

$$S_{12} = S_{1122} = -0.393$$

$$S_{44} = 4S_{1212} = 0.848$$

The crystal orientations with respect to the loading axes (fixed coordinates) are represented by the Euler angles (θ, ϕ, ψ) as shown in Fig. 3. The global elastic compliance in tensor notation is

$$\mathbf{L} = [l_{i\alpha}] = \begin{bmatrix} \cos\theta\cos\phi\cos\psi - \sin\phi\sin\psi, & -\cos\theta\cos\phi\sin\psi - \sin\phi\cos\psi, & \sin\theta\cos\phi \\ \cos\theta\sin\phi\cos\psi + \cos\phi\sin\psi, & -\cos\theta\sin\phi\sin\psi + \cos\phi\cos\psi, & \sin\theta\sin\phi \\ -\sin\theta\cos\psi, & \sin\theta\sin\psi & \cos\theta \end{bmatrix}$$

and

$$\tau_{\alpha\beta i} = \mathbf{n}_{\alpha\beta}^T\sigma_j$$

where $e_{\alpha\beta i}^p$ and $\tau_{\alpha\beta i}$ are the plastic shear strain and resolved shear stress, respectively, and

$$\mathbf{m}_{\alpha\beta} = \{m_{11}, m_{22}, m_{33}, m_{23}, m_{13}, m_{12}\}_{\alpha\beta}^T$$

$$\mathbf{n}_{\alpha\beta} = \{n_{11}, n_{22}, n_{33}, n_{23}, n_{13}, n_{12}\}_{\alpha\beta}^T$$

in which m_{ij} and n_{ij} are composed of direction cosines of slip system $\alpha\beta$. The total resolved shear stress in the slip system is

$$\tau_{\alpha\beta i} = \tau_{\alpha\beta i}^I + \tau_{\alpha\beta i}^A + \tau_{\alpha\beta i}^R \tag{22}$$

in which

$$\tau_{\alpha\beta i}^A = \mathbf{n}_{\alpha\beta}^T\bar{\mathbf{p}}_i\sigma_{22}^0 = s_{\alpha\beta i}\sigma_{22}^0$$

$$\tau_{\alpha\beta i}^R = \sum_k \sum_{\xi\eta} \bar{G}(\alpha\beta, \Omega_j; \xi\eta, \Omega_k)e_{\xi\eta k}^p$$

where $s_{\alpha\beta i}$ is the modified Schmid factor with the consideration of anisotropic elastic constants and $\bar{G}(\alpha\beta, \Omega_i; \xi\eta, \Omega_j)$ expressed as

$$\bar{G}(\alpha\beta, \Omega_i; \xi\eta, \Omega_k) = \mathbf{n}_{\alpha\beta}^T\bar{\mathbf{G}}_{ik}\mathbf{m}_{\xi\eta}$$

are the modified residual stress influence coefficients after trans-

$$\bar{S}_{ijkm} = l_{i\alpha}l_{j\beta}l_{k\lambda}l_{m\gamma}S_{\alpha\beta\lambda\gamma} \tag{23}$$

where

The inverse of $\bar{S}_{ijkm}$ is the elastic stiffness modulus. Equation (23) was used to obtain the elastic stiffness matrices of single crystals referring to the specimen axes.

A range of test data of the Young's modulus and shear modulus of Ni_3Al polycrystal and its alloys are found in the article by Stoloff (1989). The isotropic elastic constants of Poisson's ratio, $\nu = 0.3$, and shear modulus, $\mu = 65$ GPa, are here used for our analysis of Ni_3Al polycrystals.

5.2 Physical Model and Numerical Results. A physical model to study the elastic anisotropy and inhomogeneity of crystals on the fatigue crack initiation in a polycrystal is shown in Fig. 4. An aggregate of crystals with various crystallographic orientations is embedded near the free surface in a semi-infinite elastic medium. The cross-sections of these crystals are either whole or part of a hexagon. Since the crystals at some distance away from the surface crystal, in which a fatigue band is analyzed, are randomly oriented, these surrounding crystals are assumed to be isotropic and homogeneous. The fatigue band is composed of three thin slices P, Q, and R. The orientation of surface crystal #1 is determined by the orientation of the primary slip system, which is 45 deg inclining to x_2-axis. The elastic stiffness matrix of this crystal with respect to the loading axes is

$$\mathbf{C}^* = \begin{bmatrix} 244.33 & 118.19 & 83.91 & -27.42 & -82.29 & -13.71 \\ 118.19 & 244.33 & 83.91 & 82.29 & 27.43 & -13.71 \\ 83.91 & 83.91 & 278.61 & -54.86 & 54.86 & 27.43 \\ -13.71 & 41.14 & -27.43 & 153.56 & 27.43 & 27.43 \\ -41.14 & 13.71 & 27.43 & 27.43 & 153.56 & -27.43 \\ -6.86 & -6.86 & 13.71 & 27.43 & -27.43 & 222.13 \end{bmatrix} \; GPa$$

The surface crystal with the fatigue band and the surrounding crystals are shown in Fig. 4. The fatigue band is divided into parallelogram elements and the remaining parts of the crystals are divided into trapezoidal elements. The paralellogram elements are assumed to have linear inelastic strains and the trapezoidal elements to have constant inelastic strains. Fig. 5 shows the layout of these elements in the aggregate.

The local stresses in the surface crystal containing the fatigue band are affected not only by the applied load but also by the orientations of its surrounding grains. Plastic strains can develop both inside and outside the fatigue band and the residual stresses are affected by the orientations of the surrounding crystals. The global elastic stiffness matrix of crystals of the orientation (θ, ϕ, ψ) is denoted as $\mathbf{C}^*(\theta, \phi, \psi)$.

The surrounding crystals can have different sets of orientations. In the following, one set is calculated to illustrate the effect of anisotropy and inhomogeneity on the fatigue crack initiation. In this set, the orientation of crystals #2 and #3 is chosen to be (60, 30, 30 deg), crystals #4 and #5 to be (0, 0, 0 deg) and crystal #6 to be (30, 30, 60 deg). The global elastic stiffness matrices of crystals with these orientations are listed as follows

$$\mathbf{C}^*(60, 30, 30 \text{ deg}) = \begin{bmatrix} 279.50 & 79.49 & 87.44 & -75.16 & -29.89 & -4.18 \\ 79.49 & 300.71 & 66.23 & 19.49 & 26.04 & 20.88 \\ 87.44 & 66.23 & 292.76 & 55.67 & 3.86 & -16.70 \\ -37.58 & 9.74 & 27.84 & 118.20 & -16.70 & 26.04 \\ -14.95 & 13.02 & 1.93 & -16.70 & 160.63 & -75.16 \\ -2.09 & 10.44 & -8.35 & 26.04 & -75.16 & 144.72 \end{bmatrix} \; GPa$$

$$\mathbf{C}^*(0, 0, 0 \text{ deg}) = \begin{bmatrix} 196.33 & 125.05 & 125.05 & 0.0 & 0.0 & 0.0 \\ 125.05 & 196.33 & 125.05 & 0.0 & 0.0 & 0.0 \\ 125.05 & 125.05 & 196.33 & 0.0 & 0.0 & 0.0 \\ 0.0 & 0.0 & 0.0 & 235.85 & 0.0 & 0.0 \\ 0.0 & 0.0 & 0.0 & 0.0 & 235.85 & 0.0 \\ 0.0 & 0.0 & 0.0 & 0.0 & 0.0 & 235.85 \end{bmatrix} \; GPa$$

$$\mathbf{C}^*(30, 30, 60 \text{ deg}) = \begin{bmatrix} 247.36 & 122.16 & 76.91 & -19.78 & 80.57 & 7.28 \\ 122.16 & 216.65 & 107.62 & 69.81 & -11.74 & 15.07 \\ 76.91 & 107.62 & 261.90 & -50.03 & -68.83 & -22.35 \\ -9.89 & 34.91 & -25.01 & 201.00 & -22.35 & -11.74 \\ 40.29 & -5.87 & -34.42 & -22.35 & 139.56 & -19.78 \\ 3.64 & 7.54 & -11.17 & -11.74 & -19.78 & 230.06 \end{bmatrix} \; GPa$$

With the method described, the modified Schmid factor $s_{\alpha\beta}$ of the primary slip system varying along slice P is shown in Fig. 6. The Schmid factor varies from 0.42 at the free surface to the maximum value of 0.59. It is seen that the effect of this anisotropy on the response to the applied load makes the Schmid factor greater than 0.5 in a large part of the slice. The drop of the modified Schmid factor close to the free surface seems to be due to the less constraint on the deformation near the surface than in the interior. Without considering the crystal anisotropy, the Schmid factor is uniformly 0.5. The increase of the Schmid factor decreases the applied load required to activate the plastic slip in the band in comparison with the isotropic and homogeneous case. The region in which the total resolved shear stress reaches the critical shear stress τ^c will slide first. Therefore, the sliding starts inside the band, where the Schmid factor takes the maximum value. The case, in which $\sigma_{22}^0 = 397 MPa$, $\tau^I = \pm 0.5 MPa$ and $\tau^c = 200 MPa$, was analyzed. The surface plastic resolved shear strain vs. the number of cycles is shown in Fig. 7. If crystal anisotropy is neglected, the fatigue band will not develop in the surface crystal under the applied load. Therefore, the threshold of fatigue crack initiation is lowered with the consideration of crystal anisotropy. Fig. 8 shows the plastic resolved shear strain distributions in P at 100 cycles and 2000 cycles, respectively.

The cumulative surface plastic shear strains versus the number of loading cycles for two cases, one with the consideration of crystal anisotropy and one without, were calculated and plotted in Fig. 9. It is seen that the neglect of the crystal anisotropy in a polycrystal may cause significant error in calculating the slip distribution and in estimating the fatigue crack initiation.

Acknowledgment

This research is supported by the U. S. Air Force Office of Scientific Research Grant F49620-92-0171. The interest of Dr. Jim Chang, Dr. Walter Jones and Dr. Spencer Wu is gratefully acknowledged.

References

Antonopoulos, J. G., Brown, L. M., and Winter, A. T., 1976, "Vacancy Dipoles in Fatigued Copper," *Philosophical Magazine*, Vol. A34, pp. 549–563.

Charsley, P., and Thompson, N., 1963, "The Behavior of Slip Lines on Aluminum Crystals under Reversed Stresses in Tension and Compression," *Philosophical Magazine*, Vol. 8, pp. 77–85.

Eshelby, J. D., 1957, "The Determination of the Elastic Field of an Ellipsoid, and related Problems," *Proc. Roy. Soc.*, Vol. A241, pp. 376–396.

Eshelby, J. D., 1961, "Elastic Inclusions and Inhomogeneities," *Progress in Solid Mechanics 2*, I. N. Snedden and R. Hill, eds., North-Holland, Amsterdam, pp. 89–140.

Forsyth, P. J. E., 1954, "Some Further Observations on the Fatigue Process in Pure Aluminum," *J. Inst. Met.*, Vol. 82, pp. 449–454.

Lekhnitski, S. G., 1963, *Theory of Elasticity of an Anisotropic Body,* Holden-Day, San Francisco, pp. 129–134.

Lin, S. R., and Lin, T. H., 1983, "Initial Strain Field and Fatigue Crack Initiation Mechanics," ASME *Journal of Applied Mechanics,* Vol. 50, pp. 367–372.

Lin, T. H., 1969, *Theory of Inelastic Structures,* Wiley, New York, pp. 44–48.

Lin, T. H., 1977, "Micromechanics of Deformation of Slip Bands under Monotonic and Cyclic Loading," *Reviews of the Deformation Behavior of Materials,* P. Felham, ed., Freund Publishing House, Tel-Aviv, Israel, pp. 263–316.

Lin, T. H., 1992, "Micromechanics of Crack Initiation in High-Cycle Fatigue," *Advances in Applied Mechanics,* Vol. 29, pp. 1–62.

Lin, T. H., and Ito, Y. M., 1969, "Mechanics of Fatigue Crack Nucleation Mechanism," *J. Mech. Phys. Solids,* Vol. 17, pp. 511–523.

Lin, T. H., and Lin, S. R., 1974, "Effect of Secondary Slip Systems on Early Fatigue Damage," *J. Mech. and Phys. Solids,* Vol. 22, pp. 177–192.

Lin, T. H., Lin, S. R., and Wu, X. Q., 1989, "Micromechanics of an Extrusion in High-Cycle Fatigue," *Philosophical Magazine,* Vol. A59, pp. 1263–1276.

Mughrabi, H., Wang, R., Differt, K., and Essmann, V., 1982, "Fatigue Crack Initiation by Cyclic Slip Irreversibilities in High-Cycle Fatigue," *Fatigue Mechanisms: Advances in Quantitative Measurement of Physical Damage,* ASTM STP 811, J. Lankford, D. J. Davidson, W. L. Morris, and R. P. Wei, eds., pp. 5–45.

Mura, T., 1982, *Micromechanics of Defects in Solids,* Martinus Nijhoff Publishers. pp. 150–159.

Parker, E. R., 1961, *Mechanical Behavior of Materials at Elevated Temperatures,* J. E. Dorn, ed., McGraw-Hill, New York, pp. 129–148.

Stoloff, N. S., 1989, "Physical and Mechanical Metallurgy of Ni_3Al and its Alloys," *Int. Mater. Res.,* Vol. 34, pp. 153–183.

Yang, S. W., 1985, "Elastic Constants of a Monocrystalline Nickel-Base Superalloy," *Metallurgical Transactions A,* Vol. 16A, pp. 661–665.